INFORMATION TO USERS

This manuscript has been reproduced from the microfilm master. UMI films the text directly from the original or copy submitted. Thus, some thesis and dissertation copies are in typewriter face, while others may be from any type of computer printer.

The quality of this reproduction is dependent upon the quality of the copy submitted. Broken or indistinct print, colored or poor quality illustrations and photographs, print bleedthrough, substandard margins, and improper alignment can adversely affect reproduction.

In the unlikely event that the author did not send UMI a complete manuscript and there are missing pages, these will be noted. Also, if unauthorized copyright material had to be removed, a note will indicate the deletion.

Oversize materials (e.g., maps, drawings, charts) are reproduced by sectioning the original, beginning at the upper left-hand corner and continuing from left to right in equal sections with small overlaps.

Photographs included in the original manuscript have been reproduced xerographically in this copy. Higher quality 6" x 9" black and white photographic prints are available for any photographs or illustrations appearing in this copy for an additional charge. Contact UMI directly to order.

Bell & Howell Information and Learning
300 North Zeeb Road, Ann Arbor, MI 48106-1346 USA

UMI®
800-521-0600

DISSERTATION

PEAK FLOW ANALYSIS USING A TWO-DIMENSIONAL WATERSHED MODEL WITH RADAR PRECIPITATION DATA

Submitted By

Jeffrey D. Jorgeson

Department of Civil Engineering

In partial fulfillment of the requirements

for the Degree of Doctor of Philosophy

Colorado State University

Fort Collins, Colorado

Summer 1999

COLORADO STATE UNIVERSITY

May 26, 1999

WE HEREBY RECOMMEND THAT THE DISSERTATION PREPARED UNDER OUR SUPERVISION BY JEFFREY D. JORGESON ENTITLED PEAK FLOW ANALYSIS USING A TWO-DIMENSIONAL WATERSHED MODEL WITH RADAR PRECIPITATION DATA BE ACCEPTED AS FULFILLING IN PART REQUIREMENTS FOR THE DEGREE OF DOCTOR OF PHILOSOPHY.

Committee on Graduate Work

Advisor

Department Head

ABSTRACT OF DISSERTATION

PEAK FLOW ANALYSIS USING A TWO-DIMENSIONAL

WATERSHED MODEL WITH RADAR PRECIPITATION DATA

The computational speed of computers and availability of spatial hydrologic data make distributed watershed models a viable approach for many applications including peak flow and storm motion analysis. A study is presented that couples distributed watershed modeling with radar rainfall estimates to analyze peak flow with the following objectives: 1) demonstrate the coupling of radar data with a distributed hydrologic model; 2) analyze conditions of storm size, velocity and intensity that produce peak discharge exceeding a specified threshold; and 3) examine the potential for increasing forecast lead-time using radar data and distributed modeling.

The CASC2D watershed model is applied on two watersheds in central Arizona, the Cave Creek and Hassyampa River basins. WSR-88D radar data for four rainfall events is analyzed, and uncalibrated radar data are shown to underestimate precipitation intensities. Calibration of the radar Z-R relationship based on ground observations is used, and these calibrated radar data compare well with rain gauge data and are used with the CASC2D model to successfully reproduce two runoff events on the Hassyampa River. Analysis of moving storm characteristics based on radar observations is also presented.

A parametric analysis is conducted to analyze the relationship between peak runoff and storm size, velocity, and intensity. A test matrix of moving storms with various velocities, sizes and intensities is applied to the Cave Creek and Hassyampa River models. Results show that for a given peak discharge there exists a nearly linear relationship between the storm length (L_s) and the storm velocity divided by the storm excess intensity (V_s / i_e). Changes in this linear relationship are demonstrated for different values of peak flow, different watersheds, and different soil moisture conditions.

An application of radar rainfall data as input to the CASC2D model is presented in which precipitation forecasts are generated by extrapolation of precipitation patterns from radar images. Forecast lead-time was increased for two events by 6 hours and 3 hours, respectively, through the inclusion of these precipitation forecasts. Finally, application of the parametric analysis results is demonstrated where peak flow estimates are determined based solely on radar observations of storm size, velocity and intensity.

Jeffrey D. Jorgeson
Civil Engineering Department
Colorado State University
Fort Collins, CO 80523
Summer 1999

ACKNOWLEDGMENTS

There are many that deserve my recognition and gratitude for their support and guidance as I have pursued this mission in life. High on that list is my advisor, Dr. Pierre Julien, whose encouragement, guidance and support has been limitless and without which this journey would have much less enjoyable. The other members of my committee, Dr. Jorge Ramirez, Dr. Chester Watson and Dr. Bill Doe, also are greatly appreciated for their support, insight, and guidance. My wife, Leah, deserves special recognition for her unending love and support during this long process, and my sons, Will and Adam, also have been an inspiration during this journey.

The financial support of the U.S. Army through their Long Term Training program and ILIR Research program has allowed me to devote much of my working time to this endeavor over the past three years, and without this support I likely would never have been able to pursue this goal. Finally, my colleagues at the U.S. Army Engineer Research and Development Center, Coastal and Hydraulics Laboratory have been particularly supportive of my efforts, and for that I am eternally grateful.

TABLE OF CONTENTS

LIST OF TABLES

LIST OF FIGURES

LIST OF SYMBOLS

Symbol	Description
a	transform coefficient
A	cross-sectional area of channel flow
A_s	area of storm
A_w	area of watershed
c	transform exponent
e	average excess precipitation rate
E	elevation
f	infiltration rate
F	cumulative infiltration depth
g	acceleration due to gravity
h	surface water depth
H_f	capillary pressure head at the wetting front
i	rainfall intensity
i_e	excess precipitation rate
K_p	constant defined by $i_e L_s/V_s$
K_s	hydraulic conductivity at normal saturation
L	length of runoff plane
L_R	radar resolution
L_s	length of storm
L_S	rainfall correlation length
L_W	watershed characteristic length
M_d	soil moisture deficit
n	Manning resistance coefficient
P_e	excess precipitation
q	unit discharge
q_l	lateral inflow/outflow to channel per unit length
q_p	peak unit discharge
q_x	unit flow rate in the x direction
q_y	unit flow rate in the y direction
Q	total channel discharge
Q_p	peak discharge
R	hydraulic radius
S_f	friction slope
S_{fx}	friction slope in the x direction
S_{fy}	friction slope in the y direction
S_{0x}	bed slope in the x direction
S_{0y}	bed slope in the y direction

t	time
t_e	time to equilibrium
t_p	time to peak
t_r	rainfall duration
T_c	time of concentration
u	average velocity in the x direction
U	storm speed
v	average velocity in the y direction
V_s	velocity of storm
W	cell size
Z	radar reflectivity
α	reflectivity-rainfall parameter
α	coefficient relating flow depth to discharge
β	exponent relating flow depth to discharge
β	reflectivity-rainfall parameter
Δt	computational time interval
κ	constant defined by $S^{1/2}/n$
λ_1	rainfall intensity parameter
ϕ	reduced variable obtained by dividing a variable by its mean value
Π	double logarithm of exceedance probability

Chapter 1

INTRODUCTION

1.1 Introduction

Forecasting the peak flow in a stream or river that results from the runoff of excess precipitation over a watershed is a very complex process. There are many variables that impact the ability to generate reliable and useful forecasts. Those variables include the amount of precipitation that falls over a watershed, the temporal and spatial distribution of that rainfall, the characteristics of a watershed that affect overland runoff, and the characteristics of stream channels that influence the flow of water through the channels. Of these variables, those that have a significant impact on the accuracy of a flow forecast and have traditionally been most difficult to capture for a specific storm event are the temporal and spatial characteristics of the precipitation. Intense rainfall that drops a given amount of water during a few minutes will result in a much different flow than a gentle rainfall that drops the exact same volume of precipitation over several hours or days. Also, very localized rainfall events, such as convective systems, will produce different runoff patterns from a watershed than rainfall from a slow moving frontal system that produces widespread precipitation over a region. The velocity and direction of travel of a precipitation event also influence the resultant runoff. Thus, knowledge of

the spatial and temporal characteristics of a precipitation event in as much detail as possible are among the most important pieces of data used in forecasting peak runoff.

1.2 Background

Historically, the spatial distribution of precipitation over a watershed has been estimated from a sparse network of precipitation gauges located in or near the watershed. These gauges provide point measurements of precipitation that are then extrapolated via a number of interpolation methods to estimate the overall spatial distribution of precipitation over the watershed. As an alternative to precipitation gauges, real-time weather radar provides rainfall estimates at a spatial and temporal scale that have been previously unavailable. The National Weather Service (NWS) has recently installed a series of WSR-88D (Weather Surveillance Radar - 1988 Doppler) weather radar units throughout the United States that have the potential to provide rainfall estimates at approximately 6 minute intervals on a grid base with roughly 4x4 kilometer spatial resolution. Weather radar units with similar capabilities also exist in other regions of the world. This level of detail can make a significant difference in the ability to provide reliable and more accurate forecasts of peak runoff.

Other relatively recent and significant developments in operational hydrology include the availability of detailed digital elevation data, the availability of soil and land use/land cover data in digital formats, and the development of Geographic Information Systems (GIS) with which these vast amounts of data can be analyzed and managed. In the application of deterministic models for flow forecasting, Garrote and Bras (1995) observed that the only viable option to incorporate these detailed precipitation and watershed data is through the use of a distributed modeling approach. Watershed models

have traditionally been "lumped" models that employ average values of hydrologic parameters over relatively large sub-areas of a watershed. The sub-areas are sometimes so large that the spatial detail of precipitation is lost when it is averaged over them. The current computational speed of computers and increased availability of spatial hydrologic data have made distributed watershed models a more feasible approach in real time forecasting. In a distributed model, the watershed is subdivided into a grid or elemental structure, and hydrologic characteristics are assigned to each grid cell based on the physical characteristics of soil and vegetation or land use that exist in that cell. Precipitation is then applied over each cell in the watershed, and the resultant overland runoff is computed and routed in two dimensions to the collecting channel. Once in the channel, traditional hydraulic routing methods are employed to route the flow to the outlet or point of interest in the watershed. The strengths of such a distributed watershed model are that the model parameters are largely physically based and that it allows the spatial variability of the land, soil, and precipitation to be captured with much greater detail than has previously been practical in watershed modeling.

There are situations where a distributed model may not be the best approach, but the distributed and physically based nature of distributed models make it attractive in some situations. One such situation is where the spatial scale of a storm is smaller than the basin and it is important that the exact location of the precipitation in the basin be captured. Another scenario, which is likely in overseas military operations, is a case where little or no flow data are available and for which some estimate of basin response is required. Lumped parameter models may perform well where adequate data are available for calibration, but where little or no such data are available a physically based model

provides a good alternative. GIS databases of elevation, soil type, and land use exist for much of the world, and these data can provide the physical basis for establishing the necessary model parameters in a distributed model that can then be used to provide the best solution given the available information and time. Thus, the distributed approach may not be the answer in all situations, but there are certainly situations when it is a desirable approach.

This proposed study is an examination of the coupling of these technologies to use radar generated precipitation data with a physically based distributed watershed model for analyzing peak runoff from a watershed. Of particular interest are the ability of a distributed model to capture precipitation at scales smaller than that of the watershed and the relationships between the storm parameters of size, intensity and velocity on peak runoff. The results of this study are anticipated to provide a greater understanding of the practical applicability of using a distributed watershed model for real time forecasting as well as greater insight into the spatial and temporal characteristics of radar precipitation observations for such forecasting operations. Potential applications of this information are widespread and include flood warning, flood control, reservoir operations, hydroelectric power generation, and military operations.

1.3 Study Objectives

The main objectives of this research are to investigate and demonstrate the applicability of a two-dimensional physically based watershed model for peak flow analysis using radar rainfall estimates and to investigate the relationships between the storm parameters of size, intensity and velocity and peak runoff. To accomplish these, the following specific objectives are defined:

1. Demonstrate the use of WSR-88D radar precipitation data coupled with a distributed hydrologic model (CASC2D).
2. Analyze the conditions of storm size, velocity and intensity required to produce peak discharge from a watershed exceeding a specified threshold.
3. Examine the potential for increasing forecast lead-time in predicting peak runoff through the combined use of radar and distributed modeling technologies with radar-based precipitation forecasts.

1.4 Approach

The intent of this study is to evaluate the feasibility of using a distributed watershed model such as CASC2D for peak flow forecasting. One of the strengths of distributed models is the ability to capture the spatial detail of precipitation, and the form of precipitation measurement that currently provides the best level of spatial detail is radar. This study will focus on the basic characteristics of precipitation that may be estimated from radar, including storm size, storm velocity, and precipitation intensity. Analysis of these parameters and how they effect peak runoff with a distributed model is one of the primary issues addressed in this study. In addition, the feasibility of using a distributed watershed model in a real-time scenario and how well radar rainfall measurements and rainfall forecasts can perform in such an application are also addressed.

The following requirements are set forth as the scope of this study:

- Data collection for two study watersheds on which elevation, land use, soil, and channel data are available and for which observed stream flow, rain gauge and radar data are available for a series of precipitation events.
- Develop, calibrate and verify models of the study watersheds using the CASC2D model.
- Analyze radar and rain gauge data to determine the correlation between the radar and rain gauge measurements and to provide a basis for estimating typical ranges of values for storm size, precipitation intensity and storm velocity.
- Perform a parametric analysis relating the storm size, precipitation intensity and storm velocity to peak flow.
- Demonstrate the CASC2D model in a simulated real-time mode using radar rainfall observations and precipitation forecasts generated from radar observations as the model input. Comparisons of the hydrographs generated with and without precipitation forecasts will be made to see how the incorporation of precipitation forecasts influences the forecast lead-time.
- Use the results from the storm parametric analysis to estimate peak runoff based solely on storm parameters as estimated from radar rainfall data.

The objectives of this study are met in the following manner. In Chapter 1 the scope of the research has been introduced, the study objectives defined, and the research approach outlined. Chapter 2 provides a summary of relevant literature covering the

topics addressed in this research, and in Chapter 3 the CASC2D model is presented with a brief discussion of the model formulation and data requirements. Chapter 4 presents the watersheds chosen for this study and details the data collection, data processing, model construction, and model calibration and verification using the CASC2D model. Chapter 5 contains analysis of the radar and rain gauge data including calibration of the radar data and analysis of the radar data to estimate typical ranges of storm size, precipitation intensity and storm velocity in the region near the study watersheds. In Chapter 6 a test matrix of moving storms is developed and the calibrated models are run using each of the storms in the test matrix. The results of these model runs provide a basis for completion of the parametric analysis. A practical example of the use of CASC2D with radar data for peak forecasting and a practical application of the parametric analysis results are presented in Chapter 7. Finally, Chapter 8 contains a summary of this study along with the conclusions that were reached. Appendices are provided that include a listing of the computer source code for the CASC2D model, the computer source code for a program that was written to generate CASC2D precipitation input files from WSR-88D radar data, and input data required for the CASC2D model.

Chapter 2

LITERATURE REVIEW

2.1 INTRODUCTION

Many studies have been conducted that are related to computerized modeling of watersheds for the purpose of flow forecasting, although few of those have involved the use of a distributed watershed model. In addition, studies on the use of radar rainfall estimates for flow forecasting are plentiful, but again these have typically involved lumped parameter runoff models. Review of the major research areas involved in this dissertation has been conducted, with emphasis on the use of radar rainfall data, distributed modeling for forecasting, and the effects of storm parameters on runoff. The following sections contain a review of watershed models used for short term flow forecasts, applications of flow forecasting using radar data, the WSR-88D radar system, generation of precipitation forecasts from radar data, other precipitation forecast methods, distributed modeling, and relations between storm parameters and runoff.

2.2 FLOW FORECASTING WITH WATERSHED MODELS

A variety of flow forecasting models and model applications are presented in the literature. These range from well established "industry standard" models such as those used in daily operations by the National Weather Service, to models that have been adapted or developed for one specific project or location, to more research oriented

approaches using new and developing techniques. The vast majority of these watershed models are lumped parameter models, although some more recent applications involve a distributed modeling approach. Since the focus of this research is to use a distributed model with radar data, examples of similar work with distributed models are presented first, followed by a review more standard approaches using lumped parameter models.

2.2.1 Forecasting with Distributed Models

One of the most recent studies using a distributed watershed model is presented by Vieux and Jones (1997) in which the use of a finite element model for flood forecasting is detailed. The model is known as *r.water.fea* and is integrated with the Geographic Resources Analysis Support System (GRASS) GIS system. This model uses a finite element approach, although it is limited to only rectangular elements. The kinematic wave approximation is used for both overland and channel routing, the Green-Ampt method is used to compute infiltration, and surface roughness values are derived from land use/land cover data. The specific application of the model presented uses 1x1 kilometer (km) grid resolution for the overland elements with hourly WSR-88D radar data at 4 x 4 km resolution as precipitation input. A real time methodology is outlined and is demonstrated on a 645 km^2 basin using archival radar data, but no precipitation forecasts were employed. Adjustment of model parameters in real time is proposed but not demonstrated. The proposed approach is for infiltration parameters to be adjusted to correct for runoff volume and for roughness parameters to be adjusted for hydrograph timing and peak. Future proposed research topics include how to adjust model parameters in real time, how to better ingest radar data, and coupling the model with a decision support system.

Garrote and Bras (1995) present another distributed watershed model for flow forecasting called the Distributed Basin Simulator (DBSIM). The model consists of two major components, a runoff generation module and a flow routing module. The surface flow routing is performed using a distributed convolution equation where the hydrograph at the outlet of the basin is based on the instantaneous response function of each elemental area. Travel times are obtained by estimating hillslope and stream velocities, and the model was tested on an 840 km^2 watershed using a grid cell size of 400 x 400 meters (m). Initial calibration and forecasting was done using a limited number of recording rain gauges and one stage gauge at the outlet. No radar rainfall estimates were used in the work described in this paper. Overall results were encouraging, but two issues were raised which would greatly enhance the model performance. One was that distributed rainfall data from radar maps is crucial to evaluate the response of the different areas of the basin to irregularly distributed rainfall, and the other was the importance of accurately estimating the initial soil moisture state in the watershed.

Schultz (1987) presents an earlier study using a distributed approach with radar data for forecasting. This approach uses radar rainfall measurements as input to the runoff model, a distributed system type runoff model, an optimization technique to update model parameters on the basis of observed data each hour, and a stochastic real-time quantitative precipitation forecast (QPF) method to forecast future rainfall until the end of an event while it is still raining. The runoff model uses 1 x 1 km elements and runoff is computed from each cell based on a time of concentration formula and a storage attenuation effect which transforms the excess precipitation into a runoff hydrograph.

A relatively recent development by the U.S. Army Hydrologic Engineering Center (HEC) is the modClark method which uses WSR-88D radar data as distributed input to rainfall-runoff modeling (U.S. Army Corps of Engineers, 1996). The modClark approach is an adaptation of Clark's unit hydrograph technique to accommodate spatially distributed rainfall data. To apply this model, raster digital elevation data for the watershed are obtained, and the travel distance from each elevation cell to the basin outlet is determined via GIS processing. The grid cells are registered and aggregated into 4 x 4 km cells used for the radar and the average travel length from each aggregated cell to the outlet is then found. The Clark time of concentration, T_c, and storage attenuation coefficient for the watershed are obtained from previous studies or through established calibration methods. The travel time from each cell is calculated by prorating the basin T_c according to the travel length from the cell to the outlet. The spatial processing in modClark then applies the radar rainfall data to each cell, the rainfall excess at each cell is computed and lagged to the basin outlet according to the cell's travel time, individual lagged cell outflows are routed through a linear reservoir, and finally the lagged and routed outflows are summed, baseflow is added, and the watershed's outlet hydrograph is produced (Kull and Feldman, 1995).

2.2.2 Forecasting with Lumped Models

Although the research presented herein specifically uses a distributed modeling approach, there is a long tradition of using lumped parameter watershed models for flow forecasting. In fact, with the exception of stochastic approaches, virtually all watershed scale forecast methods commonly used in operational environments today are lumped parameter models. No attempt will be made to review every lumped model that is or has

been used, but an overview of two of the most common and well accepted modeling systems is worthy of inclusion. These two modeling systems are employed by the National Weather Service and the U.S. Army Corps of Engineers, who together are responsible for forecasting flows at a large number of locations throughout the country on a daily basis. First, an overview of the current modeling methods and ongoing research at the National Weather Service is presented, followed by a brief discussion of the Corps of Engineers HEC1F flood forecast model.

Producing river forecasts on large river systems within the United States is primarily the function of the National Weather Service (NWS), and the forecast modeling system utilized by the NWS is probably responsible for generating more forecasts on a routine basis than any other model currently in use. The NWS generates flow forecasts using the National Weather Service River Forecast System (NWSRFS), which is an extensive system consisting of many models and components. NWSRFS includes techniques and programs for developing river forecasts from the initial processing of historical data to the preparation of forecasts. There are three major systems that comprise the NWSRFS. The Calibration System is used to generate time series based on historical data and to determine model parameters, the Operational Forecast System uses calibrated parameters to generate short term forecasts and maintain state variables, and the Extended Streamflow Prediction System uses current model states, calibrated parameters, and historical time series to generate probabilistic forecasts extending weeks or months into the future. Included in the NWSRFS are a number of rainfall-runoff models from which a forecaster may choose. Among these is an Antecedent Precipitation Index (API) model in which the API value at the beginning of the storm is related to time

of the year, storm duration, and storm rainfall to compute runoff, and the Sacramento Soil Moisture Accounting Model in which runoff is computed based on a detailed accounting of such processes as interflow, percolation, and subsurface drainage. The basic structure of the NWSRFS is lumped and forecasts are typically done at six-hour time intervals (National Weather Service, 1996).

Most flow forecasting performed by the National Weather Service River Forecast Centers is for mainstem rivers, and the NWSRFS is used for this purpose. Forecasting on smaller creeks and streams in headwater basins has historically been the responsibility of the Weather Forecast Offices (WFO). To support WFO hydrologic needs, the NWS Office of Hydrology is developing the WFO Hydrologic Forecast System (WHFS) which uses basin average precipitation and a unit hydrograph approach. Most existing models used in the NWS use a time step of 6 hours, but headwater basins must be modeled with greater temporal detail. Also, model parameters have been developed for large basin models and the effects of using these same parameters at much smaller spatial scales is being addressed. Issues related to deriving mean areal precipitation values from radar data is also the focus of ongoing research (Glaudemans, 1997). Historically, the NWS forecasts are prepared using 6-hour mean areal precipitation (MAP) estimates derived from rain gauge networks, but 1 and 6 hour MAPs derived from radar are now possible. At the one hour time step, radar MAPs capture more of the variability in the precipitation field than the gauge MAPs (Finnerty and Johnson, 1997).

With the advent of WSR-88D radar data, the NWS is preparing to move from current lumped parameter modeling approaches to more of a distributed parameter approach for river forecasting. Current procedures at the River Forecast Centers (RFC)

usually involve generation of mean areal precipitation values of large basins at 6-hour time increments. Calibration of the model parameters is done with historical precipitation and stream flow data at these coarse scales, and as such the model parameters are inherently related to the spatial and temporal scale of calibration. WSR-88D radar provides precipitation data at 1 hour time intervals with much greater spatial resolution that has typically been used (Smith et al., 1996). The NWS is studying how the hydrologic parameters from their large basin models will change as they move towards greater spatial and temporal detail. Using the Sacramento model, they show that surface runoff increases with smaller spatial scale. Basically this is because averaging precipitation over a very large area "washes" out localized intense rainfall and produces light precipitation over the entire area. Using smaller spatial scale, the areas of very intense rainfall are captured and the resultant runoff produced is also not lost (Finnerty et al., 1995).

The flood forecast model commonly used within the U.S. Army Corps of Engineers is the HEC1F model developed by the Hydrologic Engineering Center (Peters and Ely, 1985). The HEC1F model is an adaptation of the HEC1 model for the specific purpose of forecasting. The model is a lumped parameter model with various unit hydrograph, loss rate, and hydrologic routing options. HEC1F is a single event model that includes user selection of runoff parameters to best-fit observed flow conditions up to the time of the forecast. The capability exists for parameter optimization, but only for individual gauged basins (U.S. Army Corps of Engineers, 1985). Numerous applications of the HEC1F model exist in the literature. Lovell et al., (1993) detail an HEC1F study for reservoir operations and Mimikou et al., (1993) applied HEC1F to a basin in Greece.

Their findings were that HEC1F was adequate, but that better spatial distribution of precipitation, such as would be available from radar, would improve the forecasts.

2.2.3 Watershed Model Summary

Despite the abundance of modeling schemes, flood forecasting remains one of the unsolved problems of operational hydrology. Deterministic modeling of basin response can benefit greatly from recent developments in data availability and real time measurement of spatial precipitation in the form of radar generated rainfall maps. The only viable option to incorporate this detailed topographic and distributed rainfall data into the modeling process is through the use of a distributed model. Many other models than those presented above can be found in the literature which have been developed for forecasts in specific cases, virtually all of which are traditional lumped parameter models. Nearly all authors discussing forecast models indicate the need for greater spatial resolution in modeling in order to generate better forecasts and take advantage of the spatial detail provided by radar.

2.3 FLOW FORECASTING WITH RADAR DATA

The use of radar precipitation estimates for flow forecasting operations is extremely appealing due to the real time nature of radar data and the level of spatial detail in the precipitation field that radar provides. In a survey of forecasters at a National Weather Service River Forecast Center, Johnson (1995) found that the information most used by forecasters was that on radar reflectivity and radar rainfall that provided the temporal and spatial detail needed by the forecasters to issue useful flash flood warnings. The use of radar rainfall estimates in flow forecast modeling is not a new approach, and there are many applications of this approach detailed in the literature that almost

invariably involve a spatial average of radar rainfall data over sub-basins in lumped parameter models. Some examples of flow forecasting with radar rainfall estimates are presented below.

Mimikou and Baltas (1996) detailed a unit hydrograph based approach to modeling a 2,763 km^2 basin in Greece using radar data. They first used mean areal precipitation from rain gauges and then applied the same model using radar rainfall estimates. They found that the model performed better when using radar data, and when short-term rainfall forecasts were incorporated the results were encouraging. Another application of radar rainfall estimates to a flow forecast model is presented by Bell et al. (1989). They used a single event watershed model and found that they could produce better forecasts using radar than rain gauge data because radar allowed them to simulate the movement of a storm over a watershed before it actually arrived, thus increasing the forecast lead time, and provided better spatial resolution for the precipitation. Charley (1987) describes a system developed by HEC that retrieves real-time radar data and rain gauge data. The radar data is "calibrated" with the rain gauge data using a Kriging technique. From this, sub-basin average precipitation is computed for use by the flow-forecasting model. Other applications of radar data to watershed models for flow forecasting are those by Johnson (1986) who describes a flash flood warning system and by Bell and James (1985) who used the Texas A&M lumped parameter model and attempted to calibrate model output to observed flow data in real time and calibrate radar rainfall estimates to gauge data in real time. In additional to these specific applications, Wall and Shedd (1989) studied the effects on hydrologic forecasts of varying the resolution of radar rainfall estimates in both time and space. A definite relationship was

found between the standard error of the hydrograph peaks and both the spatial resolution and temporal resolution of the radar data. As finer spatial and temporal resolutions are used, forecast results improve, thus supporting the notion that every attempt should be made to take full advantage of the spatial and temporal detail provided by radar through the use of a runoff model which can adequately represent that level of detail.

2.4 WSR-88D (NEXRAD) RADAR

The U.S. National Weather Service has updated its weather radar capabilities with the deployment of over 120 WSR-88D (**W**eather **S**urveillance **R**adar - 19**88** **D**oppler) radars, sometimes known as NEXRAD (Klazura and Imy, 1993). Development and installation of the WSR-88D system is a combined effort by the U.S. Departments of Commerce, Defense and Transportation. The WSR-88D radar provides the 48 contiguous United States with nearly continuous radar coverage below 3,000 m above sea level, except where rising terrain occludes low elevation angle scans. With this capability to provide virtually complete spatial detail of precipitation, the WSR-88D system represents a significant advance in the field of operational hydrology (Hudlow, 1988). These radar systems employ linearly-polarized coherent microwaves at 2.750 gigahertz (GHz), corresponding to a wavelength of 10.7 centimeters (cm) in the S band. The beam width of the 8 m diameter antenna is approximately 1.0 degree. Attenuation does not affect S-band weather radar, even in the heaviest rainfall, making them ideal for weather observation. The WSR-88D radar measures the radar reflectivity factor Z , Doppler velocity, and Doppler spectral width. The radar reflectivity factor Z is an integrated measure of the sixth power of the raindrop size distribution (RSD) over the volume of a radar pulse. The rainfall rate is estimated from observations of Z by assuming the form

and parameters of the RSD, and a raindrop fall speed relation. Reflectivity-rainfall relations are often empirically derived and are of the form:

$Z = \alpha R^{\beta}$

where, R is the rainfall rate (length / time) and α and β are parameters.

From these base measurements, a wide variety of products are generated by the system for aviation, meteorological, and hydrologic applications. Among the products generated by the WSR-88D are several which have potential use for operational hydrology. These include one-hour rainfall estimates, three-hour rainfall estimates, storm total accumulations, which are all graphical products, and an hourly digital precipitation array. Each of these products is updated at time intervals ranging from 6 to 15 minutes depending upon the meteorological conditions being observed. The range of the radar is approximately 230 km.

The particular product generated by the WSR-88D radar that is most applicable for hydrologic modeling and forecasting is the hourly digital precipitation array (DPA). There are three stages of precipitation processing that occur with the DPA product. The first stage, or Stage I processing, occurs in the WSR-88D radar product generator (RPG). This processing includes automated quality control such as corrections for reflectivity outliers, beam blockages, and isolated bins of reflectivity echoes. The resultant hybrid scan of reflectivity is then converted to precipitation rates using a rainfall-reflectivity relationship, and rainfall rates are then accumulated over time to produce hourly accumulations. The next level of processing is called Stage II and it occurs at the WFO associated with the particular radar location. During this processing, various satellite and

ground observations are compared with the radar data to identify and correct error caused by anomalous propagation and other spurious radar echoes. This processing level also incorporates additional rain gauge data to generate a better mean field adjustment than is used during the Stage I processing, and Stage II products are generated at one-hour intervals. The final level of processing is Stage III processing which is performed at the RFC associated with the radar. During this stage of processing, data from a number of radar sites are merged together to form a mosaic over the complete area of responsibility for the RFC. At this point, forecasters have the ability to modify and edit the radar and gauge data based upon their expertise such that any identifiable errors not previously eliminated can be corrected. The Stage III products are generated on an hourly basis. This is the final step in a complex process to generate the best possible quantitative estimates of precipitation that have the potential to be used as input to hydrologic models (Shedd et al., 1992).

The radar data used in this research were Stage I DPA data. Each DPA file is a binary file that contains a series of header information followed by a 131x131 array of data values. The grid coordinate system used for data is the Hydrologic Rainfall Analysis Project (HRAP) grid. The HRAP grid is based on a polar stereographic projection with a standard longitude of 105 degrees West. The grid is positioned such that the HRAP coordinates of the North Pole are (401,1601), and all grid coordinates over the United States are positive. The grid resolution for WSR-88D radar data is often described as being on a "4 x 4 km grid." In reality, the mesh length for the HRAP system at 60 degrees North latitude is 4.7625 km, and depending upon the latitude, the grid spacing varies between approximately 3.5 and 4.5 km within the contiguous United States.

Additionally, the orientation and mesh length of the grid is such that it contains the National Meteorological Center Limited Fine Mesh I (LFM I) and the National Weather Service Manually Digitized Radar (MDR) grids as subsets of the HRAP grid. This universal grid system, although somewhat awkward to adjust to, makes the process of creating mosaics and correlating information between several radars much more feasible than if more localized coordinate systems were employed. (Shedd et al., 1992). When using radar rainfall data in a distributed hydrologic modeling application, the radar data must be properly georeferenced such that the precipitation is applied at the correct locations over the watershed. To do so, the data are typically converted from the HRAP coordinate system to the coordinate system within which the model was created. There are standard equations that transform the HRAP coordinates to the corresponding Latitude and Longitude, from which further conversion to the desired coordinate system, such as Universal Transverse Mercator (UTM) or Albers Equal Area, can be done. A program was written for this research to read the binary DPA files, perform the coordinate transformation from HRAP to UTM, and produce output files of various formats, one of which is the precipitation input file format for the CASC2D model. The source code for this program is provided as Appendix B.

In theory, radar data could be used for estimation of rainfall intensity without consideration of concurrent rain gauge measurements. It has, however, been repeatedly demonstrated in the literature that the accuracy of rainfall estimates from radar is substantially increased when rain gauge data are incorporated (Krajewski, 1987; Seo et al., 1990; Krajewski, 1997; and Ciach et al., 1997). A number of studies have been conducted to learn more about the accuracy and reliability of WSR-88D radar rainfall

estimates. Finnerty and Johnson (1997) performed analysis of 7 months of precipitation data from WSR-88D radar and from a rain gauge network. They generated mean areal precipitation (MAP) estimates from radar and rain gauges over nine watersheds using 1 and 6 hour rainfall accumulations. They found long term differences between the radar and gauge data in that the 7-month radar accumulations were 10% to 25% less than the gauges. For short term, the 6-hour radar and gauge MAPs had similar estimates for timing of individual runoff events, but the 1-hour radar and gauge MAPs showed discrepancies in the timing. Radar MAPs captured more of the spatial variability in the precipitation field at the 1 hour time step while the spatial variability at the 6 hour step was nearly equal for radar and gauge MAPs. Comparison of rainfall at point locations with radar and gauges is a more difficult problem due to the inherent differences in the way that rainfall is measured by the two. Gauges obviously measure at a single point at ground level while radar rainfall estimates represent an average volume of precipitation measured at several elevations over a 4 x 4 km area. Work at improving the ability to derive point estimates from radar is presented by Seliga and Chen (1996).

From the literature, there appears to be consensus that WSR-88D radar rainfall estimates have the potential to provide an unprecedented level of spatial and temporal detail for hydrologic modeling applications. However, since the system is still relatively new, only initial analyses have been performed on many of the issues related to the use of these rainfall data for operational hydrology. Issues such as the accuracy and uncertainty of the radar rainfall estimates, correlation of radar and gauge data, and use of radar data in runoff models continue to be actively explored by many researchers (Anagnostou et al., 1999, Ciach and Krajewski, 1999).

2.5 PRECIPITATION FORECASTS FROM RADAR

Given a known amount of precipitation and the spatial and temporal distribution of that precipitation, many runoff models are capable of producing adequate forecasts of the flow that will result from that precipitation. When longer lead times are needed for a flow forecast, some form of precipitation forecast must be coupled with the observed precipitation data to provide a look further into the future. Although there are many methods of producing precipitation forecasts, including numerical weather models and stochastic procedures, the method chosen for this research is the use of radar images to produce short-term precipitation forecasts. Although this method cannot provide long-term forecasts, the short-term forecasts that are produced do maintain the same level of spatial detail that the radar data provides. It is that level of spatial detail that makes such radar based forecasts desirable for use with a distributed watershed model.

A term that is often used to describe real time generation of precipitation forecasts from radar data is "nowcasting." Browning and Collier (1989) present a review of several nowcasting techniques in which they state that weather prediction models can provide precipitation forecast data, and although these models are improving in spatial resolution, they operationally may not be able to provide the level of detail that is desired for hydrologic forecasting in real time. For short-term forecasts, a simpler and perhaps better way is to simply extrapolate the existing weather pattern by assuming that it will continue to travel without significant change over the very short-term period of concern. Since extrapolation is the basis for this forecasting method, the quality of the forecast depends on the time ahead for which the linear extrapolation is valid. This may be different for different types of weather patterns, i.e., frontal systems may be able to be

extrapolated for several hours while convective activity may not be able to be forecast with this method beyond an hour. Accurate short-term precipitation forecasts can have significant benefits, particularly for flood forecasting, and precipitation forecasts for up to three hours ahead may be generated by linear extrapolation of areas of rain as derived from radar. Several objective methods of describing radar echoes or cloud areas have been proposed, primarily for the purpose of using such an objective description in the process of extrapolating the rainfall pattern forward in time. These methods include contouring where several intensity thresholds are used to extract a digital description of the echo or cloud including the centroid (Duda and Blackmer, 1972); clustering which is a type of contouring where a threshold is used to derive the centroids of features that are then divided into subcategories depending on how close they are (Haralick and Kelly, 1969); Fourier analysis where an echo or cloud shape is Fourier-analyzed such that the feature is described by the minimum number of harmonics (Duda and Blackmer, 1972); and bivariate normal distribution which employs a distribution having contours consisting of ellipses and cross sections that are normal distributions, and one that can be used to define the centroid and area of the echo or cloud (Ebert, 1987). Descriptions of rain at successive time intervals can be matched or correlated to extract the movement of the precipitation from one time interval to the next, and thus use this velocity vector to extrapolate the forecast. If compact and distinct regions of rainfall can be easily isolated, then the simplest procedure is to match the centroids of the rainfall. Some sort of limitation is usually applied when this procedure is used. For example it is not normal for echoes to move faster than 120 km/hr (Bond et al., 1981). Another method is to use cross-correlation techniques to match portions of one radar picture with portions of

another (Wilson, 1966). This procedure uses only one threshold level at a time and it has the advantage of taking into account the detailed shape of the rain area being tracked. Additionally, it decreases the chances of mismatching. If all of the features at a particular threshold tend to move together and if there are no significant changes in the size, shape or intensity, then the good method is to cross-correlate one entire radar image with another at a later time (Zawadski, 1973; Austin and Bellon, 1974). This works well for widespread rain over lowland areas, but not so well when convective activity is developing or when orographic effects exist. Of course, when the velocity of the rain varies in space or time such as is often the case over large areas, then this method may not perform particularly well.

2.6 OTHER PRECIPITATION FORECAST METHODS

Utilizing radar images to forecast precipitation is but one of many approaches. A wide variety of methods for forecasting precipitation based on such things as stochastic techniques, satellite observations and orographic models have been presented in the literature. Johnson and Bras (1980) present a multivariate stochastic precipitation forecast model that makes forecasts at multiple points to provide some spatial detail and at multiple lead times to provide some temporal detail. The model used is non-stationary, i.e., the mean and variance change in space and time, and they do produce estimates of storm velocity. All model parameters are derived from telemetered precipitation gauges for the event being predicted. The most critical issue is the ability to predict storm arrival times. Except for very short lead times (5-10 minutes) it is not possible to capture the fine structure of rainfall variability. Early in an event, little data is available and default model parameters must be used. As the storm progresses and more data are available, the

parameters are better estimated and results improve. Other statistical methods are presented by Lattermann and Ubald (1981) and Oganesyan and Snitkovskii (1987), while Georgakakos (1986), Krzysztofowicz (1993, 1996) and Krzysztofowicz et al. (1993) detail methods for generating probabilistic quantitative precipitation forecasts. Rhea and Hartzell (1993) describe a study by the U.S. Bureau of Reclamation to produce improved precipitation forecasts for use in hydrologic runoff models to improve reservoir operations by combining an orographic precipitation model with a runoff model. Howes (1988) describes the use of satellite and radar data for nowcasting precipitation, and Harrison et al. (1995) present a system which integrates radar, satellite, weather reports, and a mesoscale weather prediction model to generate precipitation forecasts. Wind fields from the mesoscale model are taken into account to advect the rain and forecasts are generated for up to six hours into the future. A one-dimensional physically based precipitation model using readily available meteorological data such as ground temperature, pressure and atmospheric moisture is presented by Georgakakos and Bras (1984). This model is able to predict spatially averaged ground surface precipitation on a scale determined by the spatial scale of the input data and they achieved good results for lead times up to six hours.

2.7 DISTRIBUTED WATERSHED MODELS

The use of a two-dimensional runoff model offers the ability to capture the spatial variability of precipitation input with greater detail than typical lumped parameter models. One of the earliest reports of a two-dimensional model is presented by Kuchment (1980) in which a rainfall runoff model using the two-dimensional kinematic wave approach for overland flow and Chezy roughness coefficient to describe surface

roughness is presented. The model used a one-dimensional kinematic wave approach for channel routing, and infiltration computations were based on a solution to the one-dimensional form of Richard's equation. Taylor et al. (1974) detail an even earlier finite element model that was tested on a series of simplified domains consisting of only a few elements. James and Kim (1990) developed a distributed watershed model using a finite difference solution on rectangular grid elements, two-dimensional diffusive wave overland routing, one-dimensional dynamic wave channel routing, and a Green-Ampt infiltration routine. More recent distributed models include the finite element approach using GIS by Vieux and Gaur (1994) that was discussed in Section 2.1.1 and the CASC2D model which originated with a two-dimensional overland flow routing algorithm developed at Colorado State University. Since the CASC2D model was used extensively in this research, a chapter has been devoted exclusively to CASC2D, and Chapter 3 presents an overview of the model.

2.8 ANALYSIS OF MOVING STORM PARAMETERS

Many studies have been performed related to the effects of storm parameters and rainfall characteristics on watershed runoff. Some early studies in this field involved the use of physical laboratory apparatus that documented storm motion effects on runoff (Yen and Chow, 1969; Roberts and Klingeman, 1970; Black, 1972). More recent studies have used numerical methods to analyze storm motion effects on runoff. Studies with a conceptual model of an urban area (Niemczynowicz, 1984), a distributed time-area model (Foroud et al., 1984), and a conceptual catchment model (Watts and Calver, 1991) all indicated that maximum peak discharge results from storms moving downstream at approximately the same velocity as the average channel velocity. Julien and Moglen

(1990) presented an investigation of the effects spatial variability using a one-dimensional model and their findings were further expanded using two-dimensional simulations by Ogden and Julien (1993). They performed an investigation on runoff sensitivity to temporal and spatial rainfall variability using the CASC2D model on two watersheds where infiltration and channel routing were neglected and surface roughness held constant. Using a precipitation generating model, 50 precipitation fields with similar characteristics were generated, each with an average intensity of 30 mm/hr. Rainfall duration, t_r, was varied with the duration being expressed as a function of the time to equilibrium, t_e. Values of t_r/t_e ranged from 0.1 to 5.0. With respect to the effects of spatial rainfall variability, they found that the shortest time to peak was just more than half of the time to equilibrium, the variability in the hydrograph timing is larger for short duration events ($t_r/t_e < 0.3$) than is the variability in peak flow, the variability in peak flow increases and variability in timing decreases as rainfall duration increases from $t_r/t_e = 0.3$ to 0.6, as duration increases to $0.8t_e$, variability in timing and peak decrease, and for $t_r > t_e$ variability in peak and timing is very small. With respect to the effects of temporal rainfall variability, relative sensitivity was found to increase with both rainfall duration and rainfall temporal resolution. Most of this increase occurs by $t_r/t_e = 2.0$ with little increase in sensitivity for longer durations. Ogden and Julien (1994) also conducted a study of model sensitivity to radar rainfall resolution. The used 1 x 1 km radar data from a research radar facility at Colorado State University (CSU) as the base data and aggregated this to coarser resolutions of 2, 3, 4, 6, and 8 km. The parameter L_R/L_S (radar resolution over rainfall correlation length) was used to describe "storm smearing" and L_R/L_W (radar resolution over watershed characteristic length) described "watershed

smearing." Storm smearing occurs when the rainfall data length (radar resolution) approaches or exceeds the rainfall correlation length, which tends to decrease rain rates in high intensity regions and increase rain rates in adjacent low intensity areas, effectively reducing rain rate gradients. Watershed smearing occurs when the rainfall data length approaches the watershed characteristic length and increases the uncertainty of the location of rainfall. Results with infiltration confirm that peak flow decreases with increasing L_R/L_W thus indicating a decrease in volume of excess rainfall due to rainfall data aggregation. For soil moisture deficits of 0.0, 0.1 and 0.3, the percentage of rainfall infiltrating increases as L_R/L_W increases since the increased spatial averaging of precipitation data results in overall lower intensities over the increasingly large areas. Finally, Ogden et al. (1995) studied similarities in catchment response with moving rainstorms. The objectives of this work were to identify a dimensionless hydrologic similarity parameter which relates storm speed to the influence of storm motion on the peak hydrograph for a one-dimensional plane, to determine the suitability of the 1-D results in describing the storm motion effect on a 2-D geometry, and to ascertain the sensitivity of a 2-D surface to storm speed and direction. Equivalent storms were used which have the same volume of rainfall, the same physical size, and whose intensities vary in proportion with speed such that total volume is preserved. The 2-D portion of the study was done at 125 m resolution, and the basin was assumed to be impervious with a constant surface roughness over the basin and no channel routing. The basin characteristic length was taken as the length of the longest flow path. A rectangular block storm pattern was used with varying sizes and the storm direction was varied. Storms moving downstream showed maximum effect of storm motion. The storm speed of

maximum effect was approximately $U = L_p/2t_e$, which is very small compared to typical storm speeds.

Singh (1997, 1998) studied the effects of storm direction and velocity of planar flow and the effect of spatial and temporal variability in rainfall on watershed runoff. Among his conclusions were that higher peaks resulted from storms moving in the direction of flow, peak and time to peak are dependent on storm velocity, and spatial variability of rainfall affects time to peak but has relatively small effect on the peak.

Chapter 3

THE CASC2D MODEL

3.1 BACKGROUND

CASC2D is a physically based hydrologic model using square grid cells with an explicit finite difference diffusive wave formulation to solve for overland flow. The Green-Ampt equation is used to compute infiltration and the one-dimensional diffusive wave formulation is used to compute channel flow. With its grid-based structure, the CASC2D model is ideally suited for use with precipitation estimates from weather radar, although the model has not yet been used for flow forecasting applications. The CASC2D model originated with a two-dimensional overland flow algorithm developed at Colorado State University, and the model was enhanced with the addition of Green-Ampt infiltration and diffusive wave channel routing capabilities (Julien and Saghafian, 1991; Saghafian, 1992; Julien et al., 1995). Further additions to the CASC2D model include a soil moisture redistribution routine and implicit channel routing (Ogden, 1994) along with more recent work to couple the model with a graphical interface (Ogden, 1997). The CASC2D model has been used with radar data (Ogden, 1992), it has been used to analyze runoff sensitivity to spatial and temporal variability in precipitation (Ogden and Julien, 1993), it has been used to study the effects of grid size resolution (Molnar, 1997), and it has been used to perform upland erosion modeling (Johnson, 1997).

3.2 MODEL DESCRIPTION

CASC2D is a physically based distributed watershed model that uses square grid elements to provide a spatially distributed representation of the watershed and precipitation domains. The model consists of several major components, including, infiltration, overland routing, and channel routing. Overland flow routing of excess precipitation and channel routing is based on an explicit solution of the diffusive wave form of the de St. Venant equations with the overland routing being performed in two dimensions and the channel routing in one dimension. Basic input requirements of the model are elevation, surface roughness, soil parameters, channel network, channel cross sections, channel roughness, and precipitation. Output from CASC2D includes outflow hydrographs and time series maps of surface water depth, infiltration rate, infiltration depth, soil moisture content, and distributed precipitation.

The model is formulated using the de St. Venant equations of continuity and momentum to simulate the mechanics of the flow for both overland and channel flow. The diffusive wave approximation of these equations is used due to its ability to model regions of small slope, high roughness, and stored water. A square grid structure is superimposed on the watershed and the numerical solution to the continuity and momentum equations is evaluated for each grid cell within the watershed. Precipitation, soil parameters, and surface roughness are assumed to be constant within each grid cell, but can vary from one cell to another. Figure 3.1 shows a typical grid mesh as used in the CASC2D model with the grid size W, x-coordinate k and y-coordinate j.

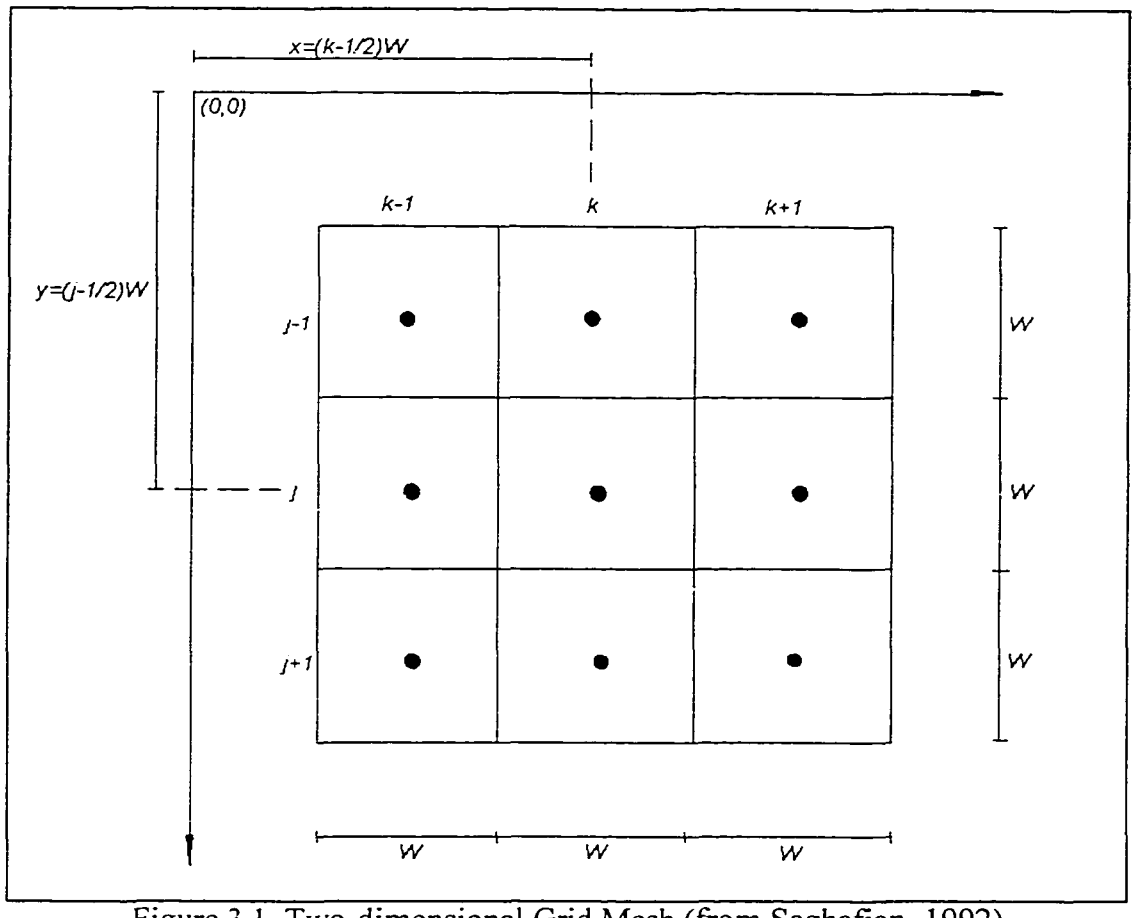

Figure 3.1 Two-dimensional Grid Mesh (from Saghafian, 1992)

There are several basic assumptions in the CASC2D model that are worthy of note. These key assumptions include:

- Surface runoff is a Hortonian process.
- Once water is lost from the surface to infiltration, it does not reappear.
- Parameters within each cell are homogeneous.
- Flow depth and discharge rate are considered uniform on individual cells.

3.3 GOVERNING EQUATIONS

There are four major components of the CASC2D model which are detailed in this section. Those model components include infiltration, overland routing, channel routing, and precipitation. Infiltration involves the movement of surface water into the soil through the effects of gravity and capillary forces. That portion of the precipitation that does not become subject to infiltration or other losses is considered excess precipitation, becomes surface runoff, and is routed as overland flow in the model. When that overland flow reaches a defined channel, it becomes channel flow and is routed in the model by the channel routing algorithm to the outlet of the watershed. Each of these four processes reacts to a specific spatial and temporal distribution of precipitation over the watershed, and the algorithms that compute infiltration, overland flow, and channel flow are executed based upon the intensity and duration of precipitation over each grid element in the model. The combination of all of these components provides a complete model of the watershed beginning with precipitation and ending with the runoff hydrograph at the watershed outlet.

3.3.1 Infiltration

The process through which water penetrates or is pulled into the ground surface is called infiltration. In the CASC2D model, a method developed by Green and Ampt (1911) is used to approximate the infiltration rate and cumulative infiltration depth for each grid element in the watershed. Applying the Green-Ampt method requires estimates of soil hydraulic conductivity, capillary suction head, and initial soil moisture deficit for each grid cell. Rawls et al. (1983) analyzed approximately 5,000 soil horizons throughout the United States and determined some average values for the Green-Ampt

parameters for different soil classes, and these average values are shown in Table C.1 in Appendix C. For the CASC2D model, values for the Green-Ampt parameters are generally obtained through reclassification of a soil texture map. With these parameters assigned to each cell, the infiltration rate is calculated as:

$$f^{t+\Delta t} = K_s\left(1 + \frac{H_f M_d}{F^t + \frac{\Delta t}{2} f^{t+\Delta t}}\right) \tag{3.1}$$

where,

f = infiltration rate

t = time

Δt = computational time interval

K_s = hydraulic conductivity at normal saturation (m/s)

H_f = capillary pressure head at the wetting front (m)

M_d = soil moisture deficit

F = cumulative infiltration depth

Water which does not infiltrate on a cell during a given time step is then surface water on the cell and is routed as overland flow to the next cell downslope.

3.3.2 Overland Flow Routing

If the rainfall intensity is large enough to satisfy the infiltration capacity of the soil, then there is excess precipitation which is routed as overland flow and subsequently as channel flow through the watershed. Routing of the overland flow proceeds in a two-dimensional cascading manner from each cell to the cell or cells downstream as depicted in Figure 3.2.

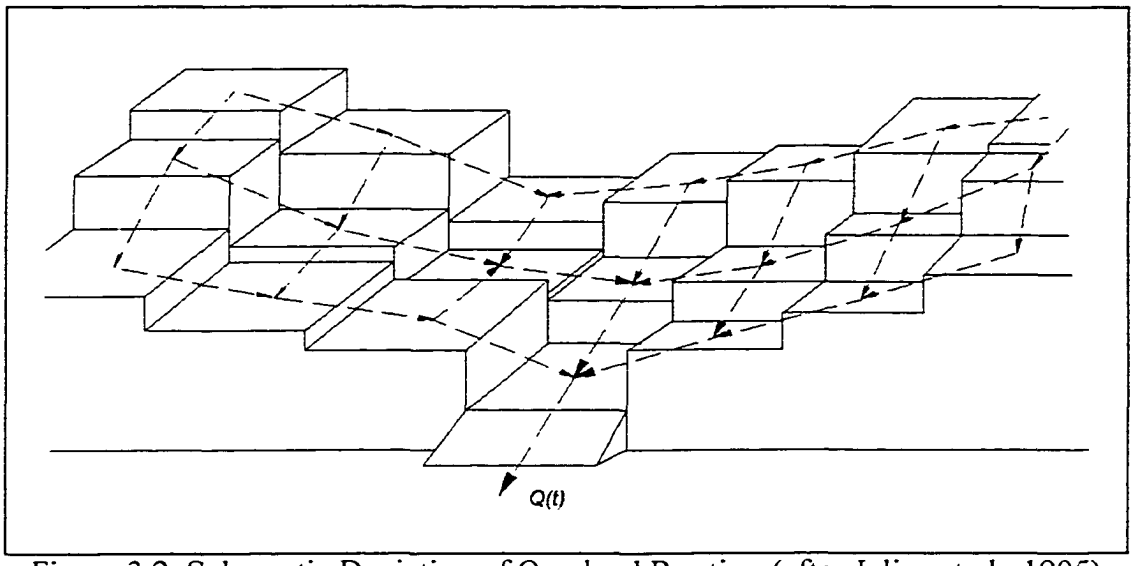

Figure 3.2 Schematic Depiction of Overland Routing (after Julien et al., 1995)

This routing is based upon the de Saint Venant equations of continuity and momentum. The two-dimensional continuity equation in partial differential form is expressed as:

$$\frac{\partial h}{\partial t} + \frac{\partial q_x}{\partial x} + \frac{\partial q_y}{\partial y} = P_e \qquad (3.2)$$

where,

h = surface water depth

t = time

q_x = unit flow rate in the x direction

q_y = unit flow rate in the y direction

P_e = excess precipitation (rainfall intensity - infiltration rate)

The momentum equation is derived by equating the net forces per unit mass to the acceleration of flow. The differential form of the momentum equation in the x and y directions is expressed as:

$$\frac{\partial u}{\partial t} + u\frac{\partial u}{\partial x} + v\frac{\partial u}{\partial y} = g\left(S_{0_x} - S_{f_x} - \frac{\partial h}{\partial x}\right) \quad (3.3)$$

$$\frac{\partial v}{\partial t} + u\frac{\partial v}{\partial x} + v\frac{\partial v}{\partial y} = g\left(S_{0_y} - S_{f_y} - \frac{\partial h}{\partial y}\right) \quad (3.4)$$

where,

h = surface flow depth

t = time

u, v = average velocities in the x and y directions, respectively

S_{0x}, S_{0y} = bed slopes in the x and y directions, respectively

S_{fx}, S_{fy} = friction slopes in the x and y directions, respectively

g = acceleration due to gravity

The left side of equations (3.3) and (3.4) describe the local and convective acceleration of the fluid, and the right side of the equations represent the net forces in the x and y directions.

In the CASC2D model, the diffusive wave approximation of these governing equations is used. This approximation is considered to be applicable for overland flow over rough surfaces and can be used to simulate backwater effects due to downstream disturbances that may be important when simulating floods (Beven, 1985). In the diffusive wave approximation, the acceleration terms on the left side of equations (3.3) and (3.4) are assumed to be negligible, and those equations are reduced to the following:

$$\frac{\partial h}{\partial x} = S_{0_x} - S_{f_x} \quad (3.5)$$

$$\frac{\partial h}{\partial y} = S_{0_y} - S_{f_y} \quad (3.6)$$

where,

h = flow depth

S_{0x}, S_{0y} = bed slopes in the x and y directions, respectively

S_{fx}, S_{fy} = friction slopes in the x and y directions, respectively

From the equations of continuity and momentum there are five hydraulic variables which need to be determined. Thus, a resistance law is required through which flow rate can be related to depth. In the CASC2D model, turbulent flow over a rough boundary is assumed for the overland flow and the Manning resistance equation is used:

$$q = \frac{S_f^{1/2}}{n} h^{5/3} \tag{3.7}$$

where,

q = unit discharge

S_f = friction slope

n = Manning resistance coefficient

h = surface flow depth

Overland flow is routed from cell to cell in the model following the mass conservation principle by solving the differential forms of the continuity and momentum equations using a finite difference representation of the watershed. Assuming an incompressible fluid, the net volume of fluid entering a cell is proportional to the change in volume of fluid within the cell over a short time period. For a given cell (j,k) at time t, the following first order approximation of the continuity equation for two-dimensional flow is applied:

$$h^{t+\Delta t}(j,k) = h^{t}(j,k) + \left\{ \bar{e} - \left[\frac{q_x^t(k \to k+1) - q_x^t(k-1 \to k)}{W} \right] - \left[\frac{q_y^t(j \to j+1) - q_y^t(j-1 \to j)}{W} \right] \right\} \Delta t \tag{3.8}$$

where,

$h^{t+\Delta t}(j,k)$ = flow depth at cell (j,k) at time $t+\Delta t$

$h^{t}(j,k)$ = flow depth at cell (j,k) at time t

Δt = computational time step

$\bar{e}$ = average excess precipitation rate

$q_x^t(k \to k+1)$ = unit flow rate in x-direction at time t from cell (j,k) to (j,k+1)

$q_x^t(k-1 \to k)$ = unit flow rate in x-direction at time t from cell (j,k-1) to (j,k)

$q_y^t(j \to j+1)$ = unit flow rate in y-direction at time t from cell (j,k) to (j+1,k)

$q_y^t(j-1 \to j)$ = unit flow rate in y-direction at time t from cell (j-1,k) to (j,k)

W = cell size

The unit flow rate at a grid cell is dependent upon the flow direction at a given time step, and the flow direction is determined by the sign of the friction slope. The friction slope in the x and y directions is computed from the diffusive wave approximation of the momentum equation as:

$$S_{fx}^t(k-1 \to k) = S_{0x}(k-1 \to k) - \frac{h^t(j,k) - h^t(j,k-1)}{W} \tag{3.9}$$

$$S_{fy}^t(j-1 \to j) = S_{0y}(j-1 \to j) - \frac{h^t(j,k) - h^t(j-1,k)}{W} \tag{3.10}$$

The bed slope, S_0, at each cell is evaluated from the elevation data as:

$$S_{0x}(k-1 \rightarrow k) = \frac{E(j,k) - E(j,k-1)}{W} \tag{3.11}$$

$$S_{0y}(j-1 \rightarrow j) = \frac{E(j,k) - E(j-1,k)}{W} \tag{3.12}$$

where E(j,k) = elevation of grid cell (j,k).

Finally, after the friction slope and flow direction have been determined, the unit discharge is computed from the following formulation of the Manning equation:

$$q_x'(k-1 \rightarrow k) = \frac{\left[S_{fx}'(k-1 \rightarrow k)\right]^{1/2}}{n(j,k-1)}\left[h'(j,k-1)\right]^{5/3} \quad \text{if} \quad S_{fx}'(k-1 \rightarrow k) \geq 0 \tag{3.13a}$$

or

$$q_x'(k-1 \rightarrow k) = -\frac{\left[-S_{fx}'(k-1 \rightarrow k)\right]^{1/2}}{n(j,k)}\left[h'(j,k)\right]^{5/3} \quad \text{if } S_{fx}'(k-1 \rightarrow k) < 0 \tag{3.13b}$$

The above represent the calculation of the flow rate in the x direction from cell (j,k-1) to cell (j,k). These equations are also used to evaluate the flow rate in the y direction from cell (j-1,k) to (j,k), in the x direction from cell (j,k) to (j+1,k), and in the y direction from cell (j,k) to (j,k+1). These calculations are carried out for every cell in the computational mesh that falls within the watershed.

3.3.3 Channel Routing

Overland flow in a watershed will generally make its way to a defined channel where it will continue its flow to the outlet of the watershed. In CASC2D the channel routing is performed using the diffusive wave approximation similar to the overland routing, although the channel routing is a one-dimensional process. In the model, the overall channel network is divided into a series of channel links with the channel

geometry and roughness parameters being constant within each link. Each such link is then composed of a number of nodes, where each node corresponds to an individual grid cell. For each link, the channel width, depth and Manning n are defined and the bed elevation of each node in the link is derived from the elevation of that cell. Figure 3.3 shows a schematic view of the channel configuration.

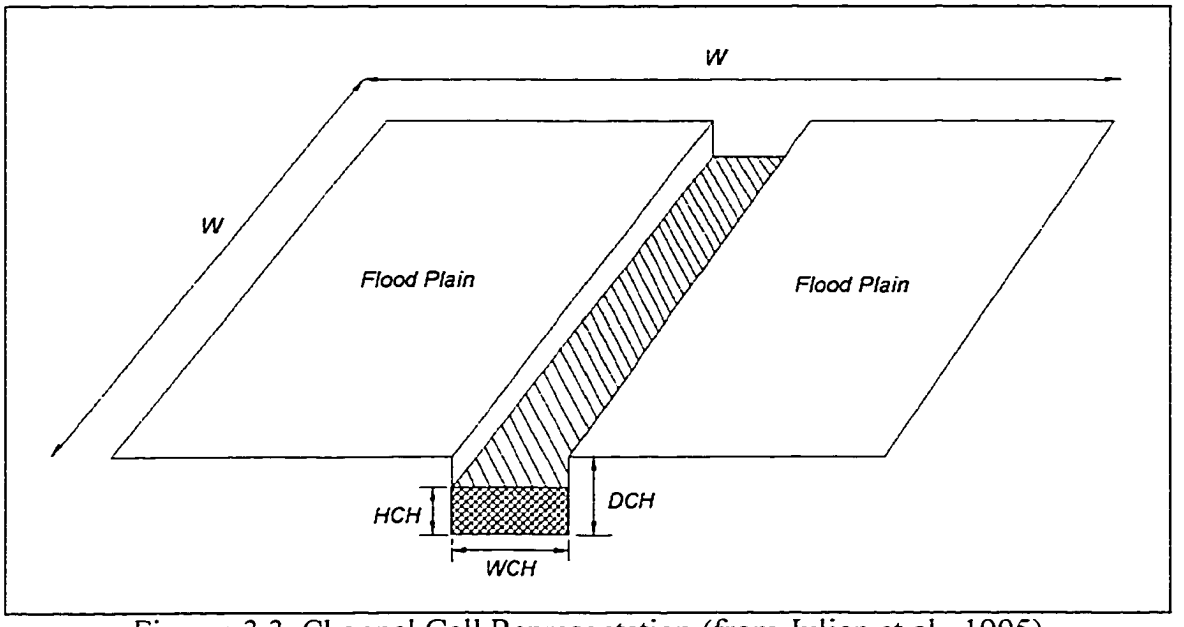

Figurre 3.3 Channel Cell Representation (from Julien et al., 1995)

The continuity equation for the channel flow in the model is:

$$\frac{\partial A}{\partial t} + \frac{\partial Q}{\partial x} = q_l \tag{3.14}$$

where,

A = cross-sectional area of channel flow

Q = total channel discharge

q_l = lateral inflow to the channel or outflow from the channel per unit length

The following form of the Manning resistance equation is applied based on the assumption of turbulent flow to compute the channel discharge rate:

$$Q = \frac{1}{n} A R^{2/3} S_f^{1/2} \tag{3.15}$$

where,

n = Manning roughness coefficient

A = cross-sectional area of channel flow

R = hydraulic radius

S_f = friction slope

The equations used for determining the friction slope on overland cells based on the diffusive wave approximation to the momentum equation, equations (3.9) and (3.10), are also used to compute the friction slope for the channel cells or nodes. The bed slope is evaluated based on the bed elevations and distance between adjacent channel cells or nodes. The channel routing in the model commences at the most upstream or first order links and proceeds downstream to the outflow point or outlet of the basin.

3.3.4 Precipitation

The infiltration, overland flow, and channel routing functions of CASC2D serve only to model or estimate the flow of water that results from a particular precipitation event. In the CASC2D model, precipitation input may be in the form of observed rain gauge data, a uniform rainfall intensity over the entire watershed, or radar rainfall data, each of which provide the model with a rainfall rate which is used to compute infiltration and runoff. If rain gauge or radar data are used, the precipitation must be spatially distributed over the watershed in some manner. For rain gauge data, the spatial

distribution of the precipitation over the grid cells in the model is done using either an inverse distance squared technique or by using the Thiessen polygon approach. For radar data, the appropriate method is the Thiessen polygon method for spatial distribution.

3.4 MODEL OUTPUT

Output from lumped parameter models is generally limited to discharge hydrographs for the various subbasins in the model. The CASC2D model, however, offers much more. In addition to discharge hydrographs, which can be defined for any number of locations in the channel network, the model computes and can generate time series maps of spatial output. These time series maps include surface water depth, cumulative infiltration depth, surface soil moisture, infiltration rate, and distributed rainfall intensity. For each of these, a map can be saved at specified time increments during a simulation. These maps can be animated similar to a video tape or film loop to allow the user to easily see the temporal and spatial variation of each of the above parameters for the simulation.

3.5 CASC2D SUMMARY

Hydrologic modeling has been performed using lumped parameter models, empirical relationships, and stochastic methods for many years. With current computer technology and the vast availability of watershed spatial data, physically based distributed watershed models such as CASC2D are becoming the modeling method of choice for many applications. Flow forecasting is one area where distributed modeling has not been widely studied or applied, but the potential is great for such an approach to provide solutions that have been heretofore difficult to attain.

Chapter 4

THE STUDY WATERSHEDS

4.1 INTRODUCTION

Two watersheds have been modeled for this study, the Cave Creek watershed and the Hassyampa River watershed located in central Arizona near Phoenix. This chapter details the process of setting up the CASC2D model for the Cave Creek and Hassyampa River watersheds and calibrating the models using rain gauge data for several observed events. The general outline of the modeling and calibration process includes data collection, data processing, model construction, model calibration and model verification. The data collected for the CASC2D model includes elevation data, land use data, soil data, rain gauge data, flow gauge data, channel cross-section data, and channel roughness data. The following sections provide a brief description of the various data and their sources, processing of the data for the model, construction of the Cave Creek and Hassyampa River models, and the model calibration and verification processes.

4.2 THE WATERSHEDS

Cave Creek is located just north of the City of Phoenix, and its drainage area above the gauging station is approximately 350 km^2. The outlet of the study area is located approximately 8 km upstream of the Cave Creek Dam that serves as a flood

control structure for the Phoenix metropolitan area. Below the Cave Creek Dam, flow continues another 20 km into the City of Phoenix where Cave Creek terminates into the Arizona Canal. The Hassyampa River basin covers approximately 1,111 km^2 and is located to the northwest of Phoenix with the outlet of the basin approximately 75 km northwest of Cave Creek near Wickenburg, Arizona. Downstream of the gauging station near Wickenburg, the river flows South and ultimately into the Gila River. Figure 4.1 provides a location map for the Cave Creek and Hassyampa River basins.

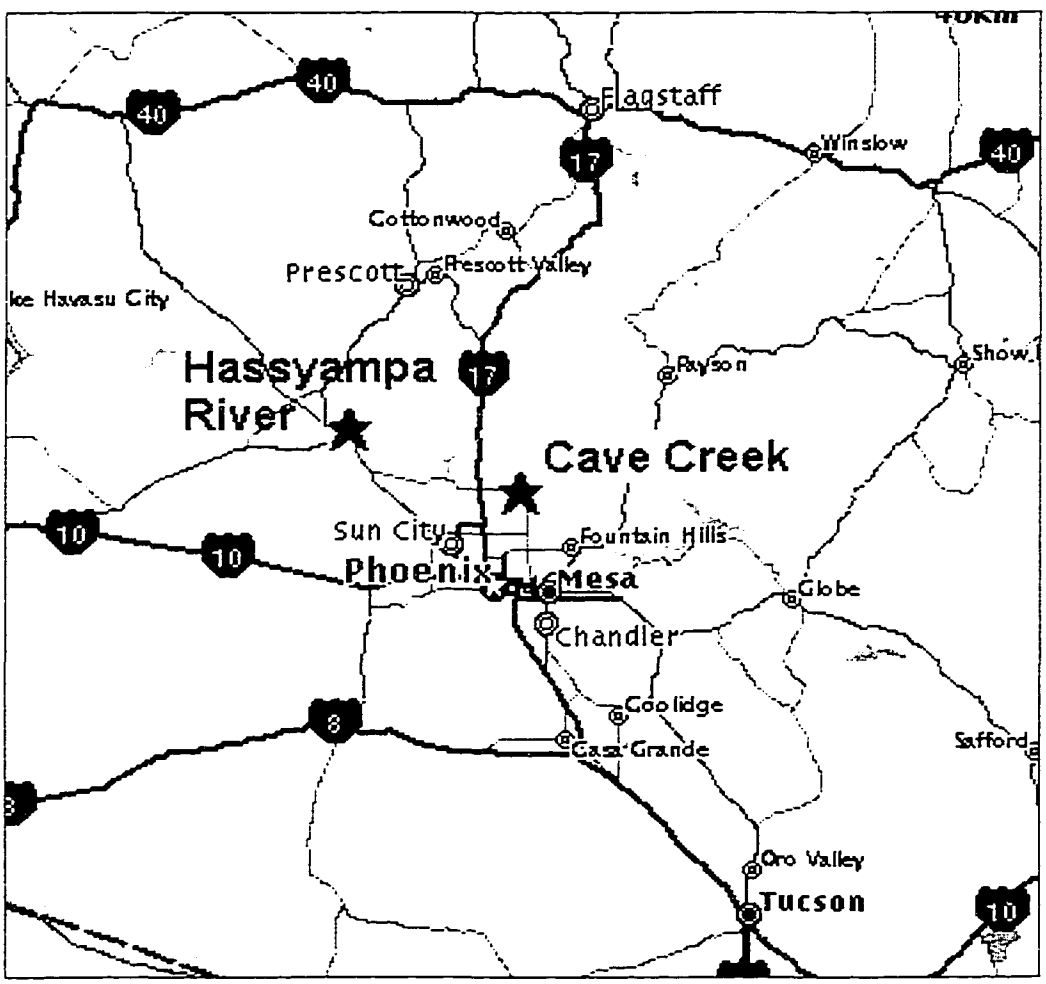

Figure 4.1 Cave Creek and Hassyampa River Vicinity Map

Cave Creek has its headwaters in the Tonto National Forest and the upper portions of the watershed are characterized by steep mountainous terrain and mountain brush vegetative cover. The lower portions of the basin are fairly flat with desert brush cover. Streams in the basin vary from steep well incised channels in the upper reaches of the basin to wide braided "washes" lower in the basin. Elevations range from a high of approximately 1,600 meters to a low elevation of 540 meters at the basin outlet. The Hassyampa River's headwaters are located in the Prescott National Forest, and the majority of the basin is in fairly mountainous terrain. The streams in the basin are generally steep and well incised with a very few washes in the lowest part of the basin. The elevations in the basin range from 2,400 meters to the low elevation of 750 meters at the basin outlet.

Both the Cave Creek and Hassymapa River basins have similar climates of the warm semi-arid Sonoran desert with average daily maximum temperatures of 60-70 degrees F in winter and over 100 degrees F in summer. The upper reaches of the Hassyampa River basin experience some cooler temperatures due to the higher elevations. Precipitation events in the area are typically of two distinct varieties. High intensity, short duration thunderstorms are common in the late summer months while rainfall from slower moving frontal systems generally occur in the winter and spring months (CH2M Hill, 1990).

4.3 DATA COLLECTION

The data that were collected for modeling the watersheds with CASC2D included digital elevation data, land use / land cover data, soil data, channel cross section and

roughness data, precipitation data, and stream flow data. The following sections provide a brief summary of the data sources and details on the types of data that were used.

4.3.1 Elevation Data

Elevation data for the models were obtained from the United States Geological Survey (USGS) in the form of 1:250000 scale Digital Elevation Model (DEM) data. The 1:250000 scale DEM data provides elevation data points in a raster format with 3 arcsecond spatial resolution. The 3 arcsecond resolution equates to approximately 90 meters, and the elevation data are provided in meters (USGS, 1987). Each of the 1:250000 scale DEM files from the USGS covers a 1 degree by 1 degree area, and the Cave Creek and Hassyampa River watersheds cover portions of four such DEM regions. The four DEM files were merged together, and the drainage basin area for each basin was determined using the TOPAZ (TOpographic PArameteriZation) model (Brigham Young University, 1999). The resultant elevation grids were resampled to a spatial resolution of 200 meters using the GRASS GIS system (U.S. Army Corps of Engineers, 1991), with the Cave Creek basin including 8,726 grid cells (drainage area 349 km^2) and the Hassyampa River basin including 27,774 cells (drainage area 1,111 km^2). Figures 4.2 and 4.3 show color contour maps of the Cave Creek and Hassyampa River watersheds with the red hues representing higher elevations and green and yellow representing the lower elevations in the basins.

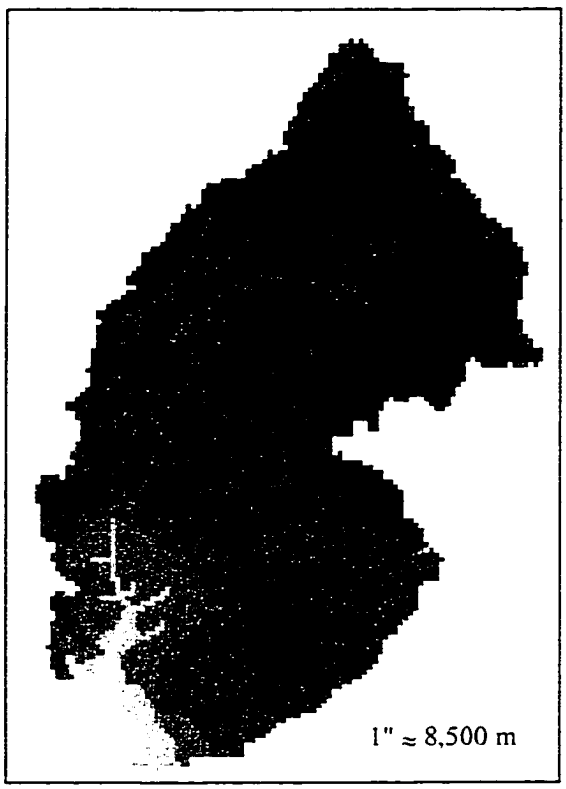

Figure 4.2 Cave Creek Elevation

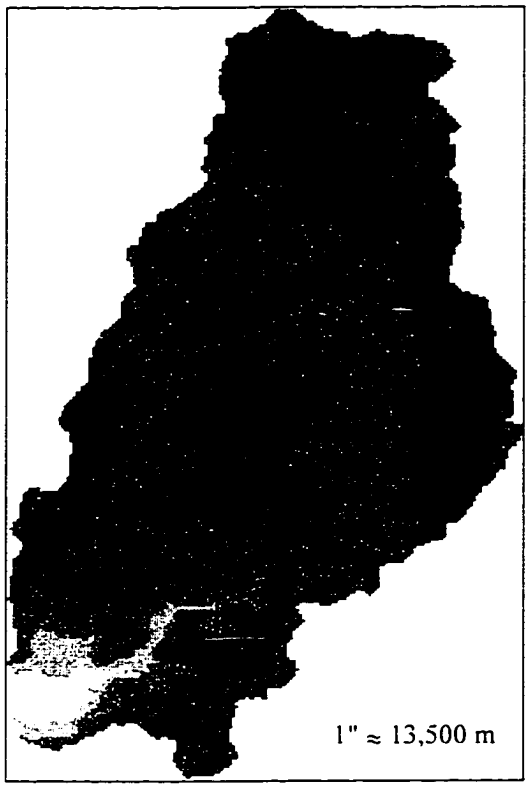

Figure 4.3 Hassyampa River Elevation

4.3.2 Surface Roughness

Overland routing in CASC2D requires a Manning n roughness parameter for each grid cell. Manning n values were assigned based on the land use and vegetative cover that exists on a given cell. Land use / land cover data at 1:250000 scale were obtained from the USGS which provide raster coverage at a spatial resolution of 200 meters (USGS, 1990). The data were imported into the GRASS GIS system and regions that coincided with each of the study watersheds were cropped out of the larger map. The resultant land use / land cover maps included 13 land use categories, and initial estimates of the Manning n roughness coefficient for each of the categories were established as shown in Table 4.1 based on data provided by Engman (1986).

Land Use Description	Manning n
Residential	.011
Commercial and Services	.011
Industrial	.011
Transportation, Communications and Utilities	.011
Other Urban or Built-up Land	.011
Cropland and Pasture	.125
Other Agricultural Land	.125
Herbaeous Rangeland	.125
Shrub and Brush Rangeland	.125
Mixed Rangeland	.125
Evergreen Forest	.06
Sandy Areas Other then Beaches	.03
Strip Mines, Quarries & Gravel Pits	.03

Table 4.1 Manning n Values for Land Use / Land Cover Categories

The 13 land use categories in Table 4.1 correlated to only four different roughness values. Thus, the land use maps for each basin were reclassified to reflect these four surface roughness values as shown in Table 4.2

Roughness Category	General Description	Manning n
1	Developed Areas	0.011
2	Crop and Range Lands	0.125
3	Forest	0.06
4	Mines and Quarries	0.03

Table 4.2 Four Surface Roughness Categories

Figures 4.4 and 4.5 show color maps of the surface roughness categories for the Cave Creek and Hassyampa River watersheds. The Cave Creek watershed primarily consists of roughness category 2 (crop and range land) with only small areas of the other categories, while the Hassyampa River basin is fairly evenly divided between category 2

(crop and range lands) and 3 (forest). Table 4.3 shows the percentages of each basin that are covered by the four surface roughness categories.

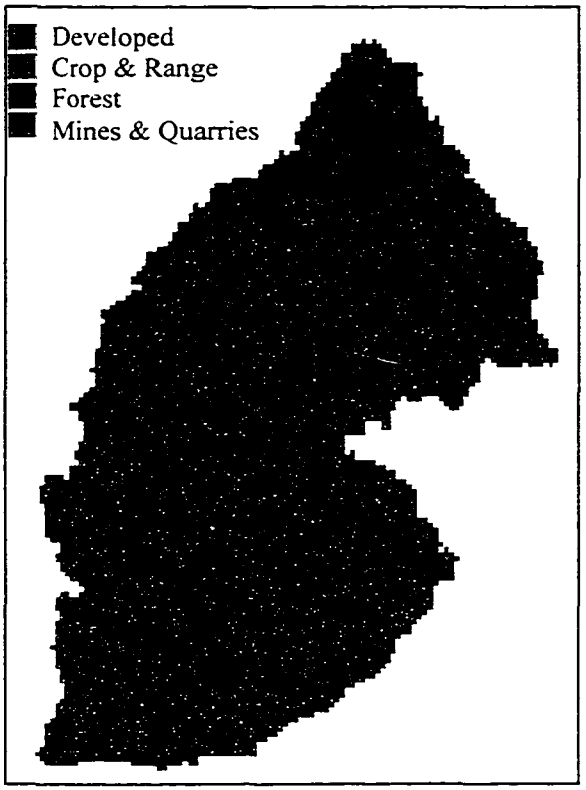

Figure 4.4 Cave Creek Land Use

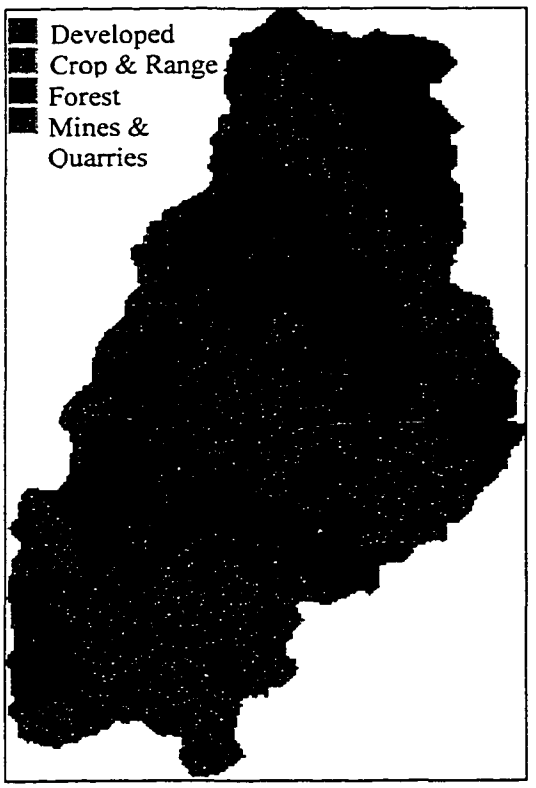

Figure 4.5 Hassyampa River Land Use

Roughness Category	Cave Creek	Hassyampa River
Developed Areas	2.1%	0.1%
Crop and Range Land	93.8%	58.4%
Forest	3.6%	41.3%
Mines and Quarries	0.5%	0.2%

Table 4.3 Roughness Categories for Study Watersheds

4.3.3 Soil Data

To compute infiltration, CASC2D uses the Green-Ampt approach that requires values of saturated hydraulic conductivity, effective porosity, capillary suction head, and soil moisture deficit for each cell. Typically, these parameters are estimated based on data from Rawls et al. (1983) who provide a listing of soil textures and the associated soil parameters, a copy of which is included in Table C.1 of Appendix C. Soil data for the Cave Creek and Hassyampa River basins were obtained from the Natural Resources Conservation Service (NRCS) State Soil Geographic (STATSGO) Data Base (USDA, 1994). These data are at 200-meter spatial resolution, and each raster cell has a soil "map unit" identification that consists of several components or soil series. The percentage of each soil series that make up a map unit is provided along with the percentage of coarse fragments, sand, silt, and clay for each soil series. Based on these data, the composite percentage of sand, silt and clay for each map unit was computed. The soil texture (sandy loam, silty clay, etc.) for each map unit was then determined using the standard U.S. Department of Agriculture Triangle Chart and the infiltration parameters assigned based on Table C.1 in Appendix C and after making the necessary adjustments where high levels of coarse fragments exist. Figures 4.6 and 4.7 provide maps of the soils in the Cave Creek and Hassyampa River basins, and Table 4.4 provides the associated soil textures. Note that those soils that had the same soil texture were not combined because each of them had a different percentage of coarse material that resulted in slightly different infiltration parameters.

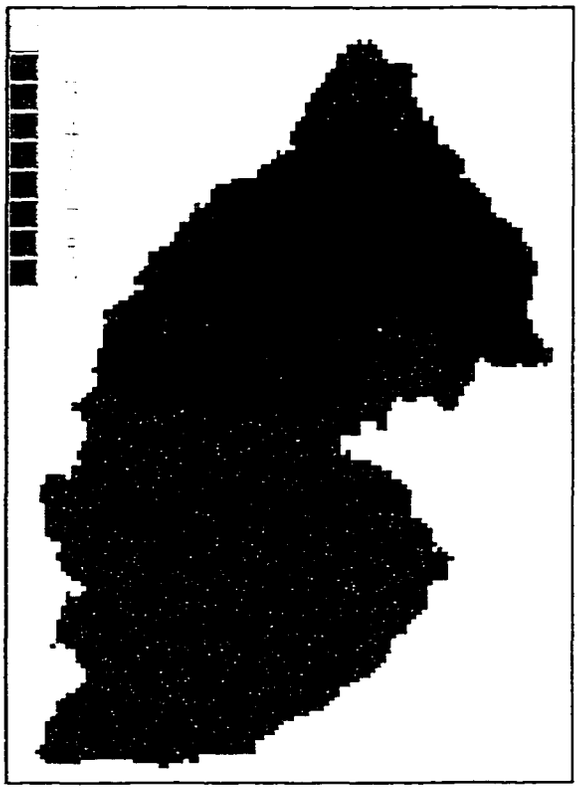

Figure 4.6 Cave Creek Soils

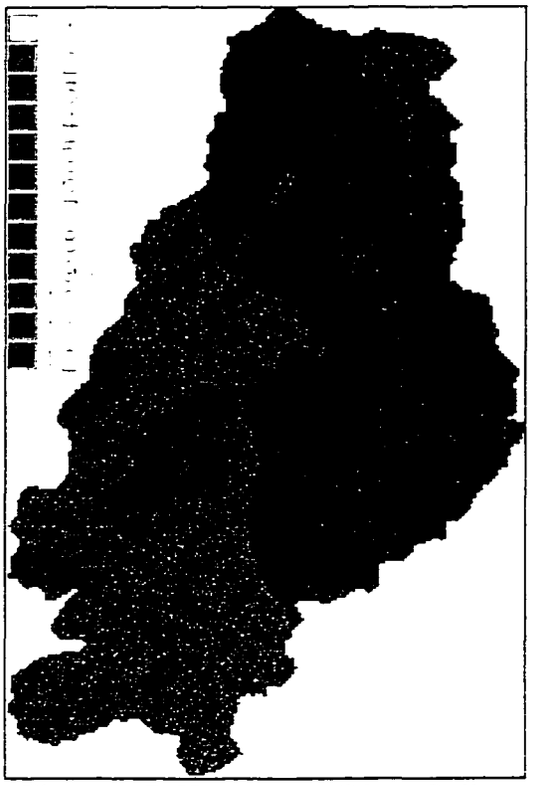

Figure 4.7 Hassyampa River Soils

Cave Creek		Hassyampa River	
Soil ID	Soil Texture	Soil ID	Soil Texture
1	clay	1	clay-loam
2	clay	2	sandy-clay
3	sandy-clay	3	sandy-clay-loam
4	clay-loam	4	clay-loam
5	clay-loam	5	clay-loam
6	loam	6	loam
7	sandy-clay	7	clay-loam
8	sandy-loam	8	clay-loam
9	loam	9	cay-loam
		10	sandy-loam
		11	loam
		12	clay-loam

Table 4.4 Soil Textures

4.3.4 Channel Data

Channel data for the Cave Creek basin were obtained from a floodplain delineation study that was performed during 1997 for the Flood Control District of Maricopa County, Arizona (George V. Sabol Consulting Engineers, 1997a and 1997b). The models of the watershed and channel from that study were reviewed and rectangular channel cross-section approximations and roughness values were taken for use in the CASC2D model. No detailed cross-section data were available for the Hassyampa River basin, so channel properties for that basin were assumed to be similar to those in the Cave Creek basin based on topography and contributing drainage area. Similarly, channel roughness values for the Hassyampa River basin were assigned based on those for similar channels in the Cave Creek basin. Table 4.5 provides a summary of the total number of channel grid cells, total channel length, and drainage density for each watershed model. Figures 4.8 and 4.9 provide images of the channel networks in the Cave Creek and Hassyampa River basins that were included in the respective CASC2D models. Provided in Appendix C are the channel input files that were used in each model showing the channel width, depth, and Manning n values.

	Cave Creek	**Hassyampa River**
Total Cells in Basin	8726	27774
Channel Cells	536	1278
% Channel Cells	6.1%	4.6%
Total Stream Length (km)	107.2	255.6
Drainage Density (km^{-1})	0.31	0.23

Table 4.5 Channel Summary

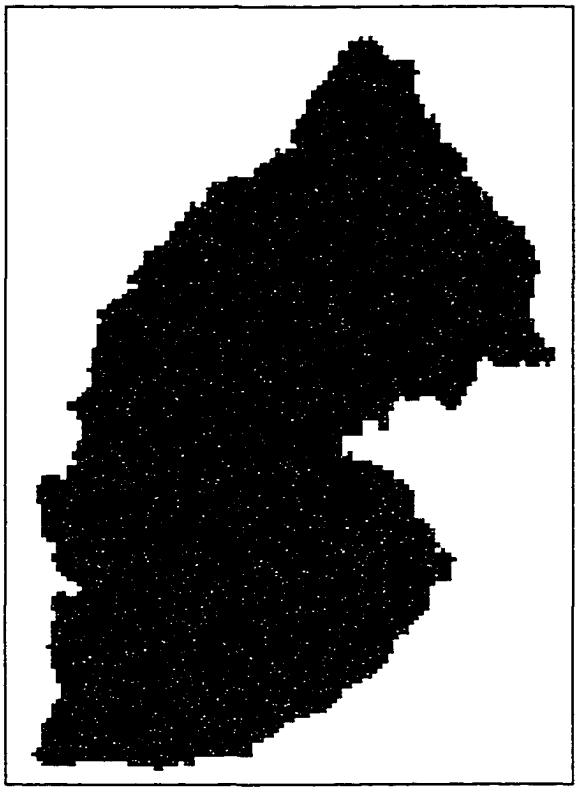

Figure 4.8 Cave Creek Channels

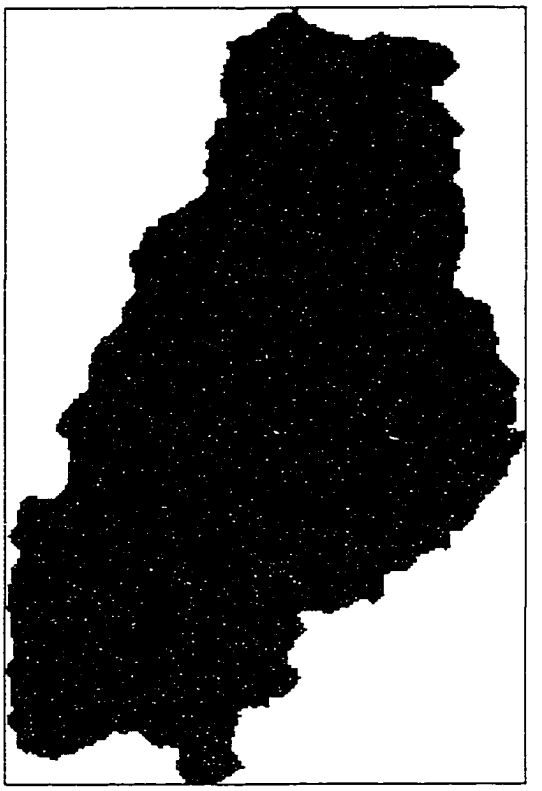

Figure 4.9 Hassyampa River Channels

4.3.5 Precipitation Data

Once all of the above data were incorporated into the models, observed precipitation data were used to run the models such that the resultant hydrographs could be compared with the observed runoff from the basins to begin the calibration process. Precipitation data for the basins were obtained from the Maricopa County Flood Control District, Maricopa County, Arizona for 5 gauges in and near the Cave Creek basin and 7 gauges in and near the Hassyampa River basin. Figures 4.10 and 4.11 show the location of those gauges with respect to the watersheds.

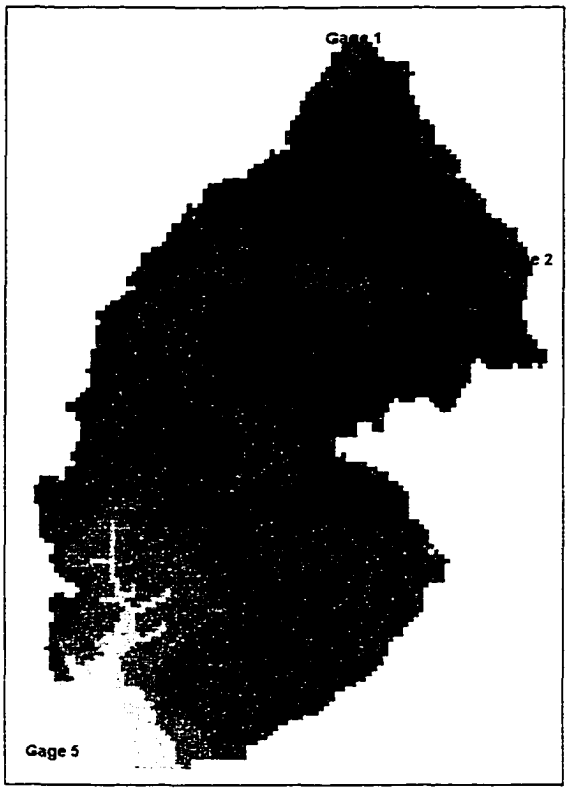

Figure 4.10 Cave Creek Rain Gauges

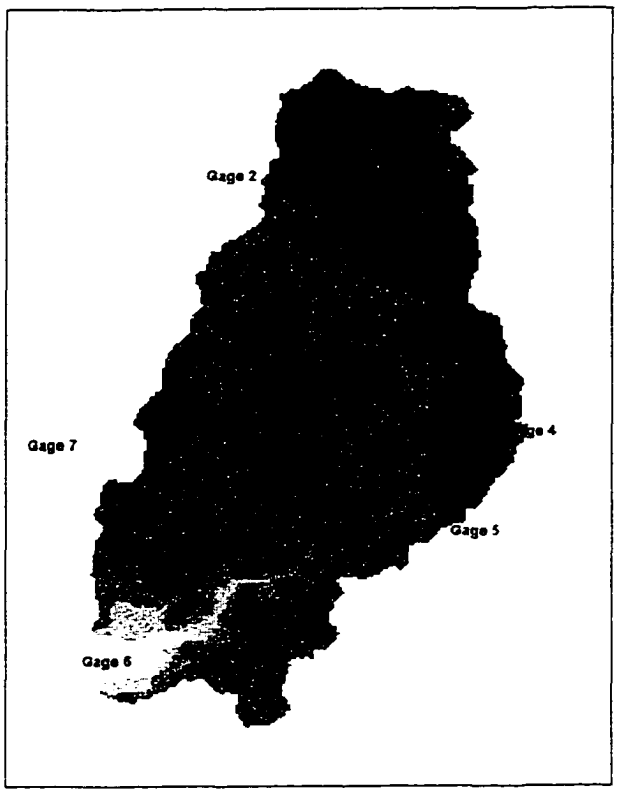

Figure 4.11 Hassyampa River Rain Gauges

4.3.6 Flow Data

Discharge data for the same events as the rainfall data were provided for a gauge at the outlet of each basin. These data provided flow in cubic feet per second at 15 minute time intervals, and again were provided by the Maricopa County Flood Control District, Maricopa County, Arizona. These discharge data were used as the basis against which the model results were compared during the calibration and verification processes that are outlined in the following sections.

4.4 MODEL CALIBRATION

The CASC2D models of Cave Creek and Hassyampa River for this study were each calibrated using observed precipitation and discharge data from a precipitation event

in February 1995. Precipitation gauge data for the event were used as the model input, and the hydrographs computed by the CASC2D model were compared to the observed hydrographs from the gauges at the outlets of the Cave Creek and Hassyampa River basins. The two principal criteria used in the calibration process were the peak discharge and the time to peak, with the objective of the calibration process to make necessary adjustments to the initial model parameter estimates such that the computed hydrographs matched the observed flows for this event. Initial calibration of the models using the February 1995 event is described in the remainder of this section, and the verification process with additional rainfall events is described in section 4.5.

4.4.1 Cave Creek Calibration

The Cave Creek model was calibrated using the February 1995 event that started early on February 12 and continued through the morning hours of February 15 lasting approximately 72 hours. Precipitation totals from the five gauges are summarized in Table 4.6. Figure 4.12 shows the cumulative average rainfall for the gauges on Cave Creek through that event. The highest intensity measured during any five minute interval for this event was 48.8 mm/hr (1.92 in/hr).

Gauge #	1	2	3	4	5
Precipitation (mm)	70.1	64.0	59.9	47.2	31.0
Precipitation (in)	2.76	2.52	2.36	1.89	1.22

Table 4.6 Cave Creek Precipitation Gauge Data - February Event

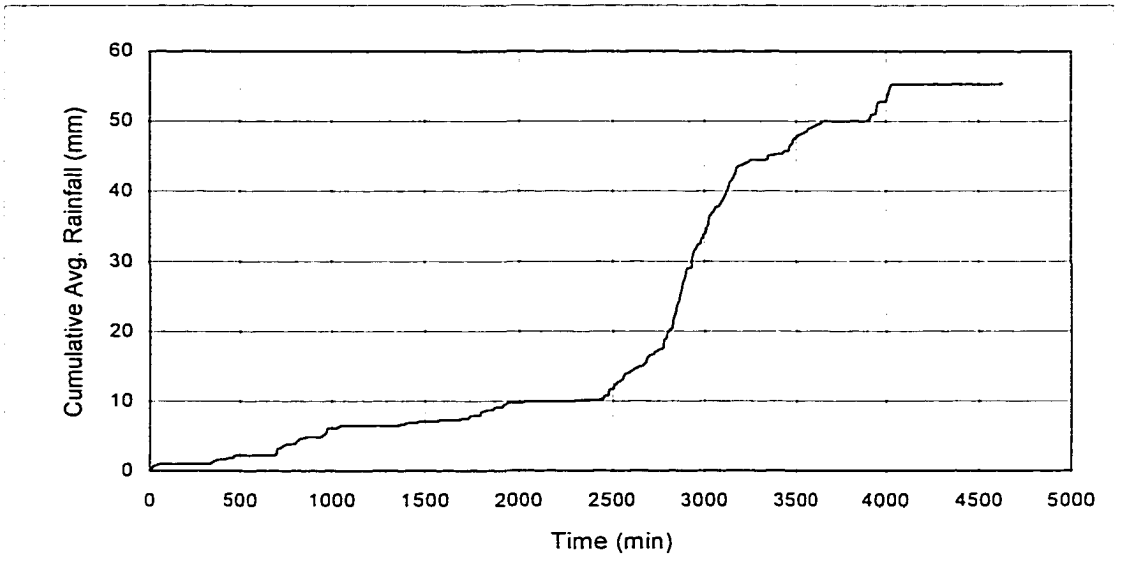

Figure 4.12 Cumulative Average Precipitation for Cave Creek – February Event

Results with the initial parameter estimates showed a runoff hydrograph with a peak that was too low and with a time to peak that was too late. To increase the peak, hydraulic conductivity values for each of the soils in the basin were gradually reduced through a series of trials until the peak flow was reasonably close to that of the observed hydrograph. Simultaneously, Manning n values of the overland cells were reduced to decrease the time to peak. Since well over 90% of the basin is crop and range land, changing the Manning n for that category was the only one that had any measurable impact on the hydrograph. Ultimately, the hydraulic conductivity values were reduced to 80% of the originally estimated values, the Manning n value for crop and range land was reduced to 0.065, and the initial soil moisture deficit was 30%. Figure 4.13 shows the computed and observed hydrographs for this event, and Table 4.7 provides a summary of the peak discharges and times to peak for the observed and computed hydrographs.

Hydrograph	Peak Flow	Time to Peak
Observed	2847 cfs	3240 min
CASC2D	2850 cfs	3111 min
% Difference	0.1 %	4.0 %

Table 4.7 Calibration Results for Cave Creek – February Event

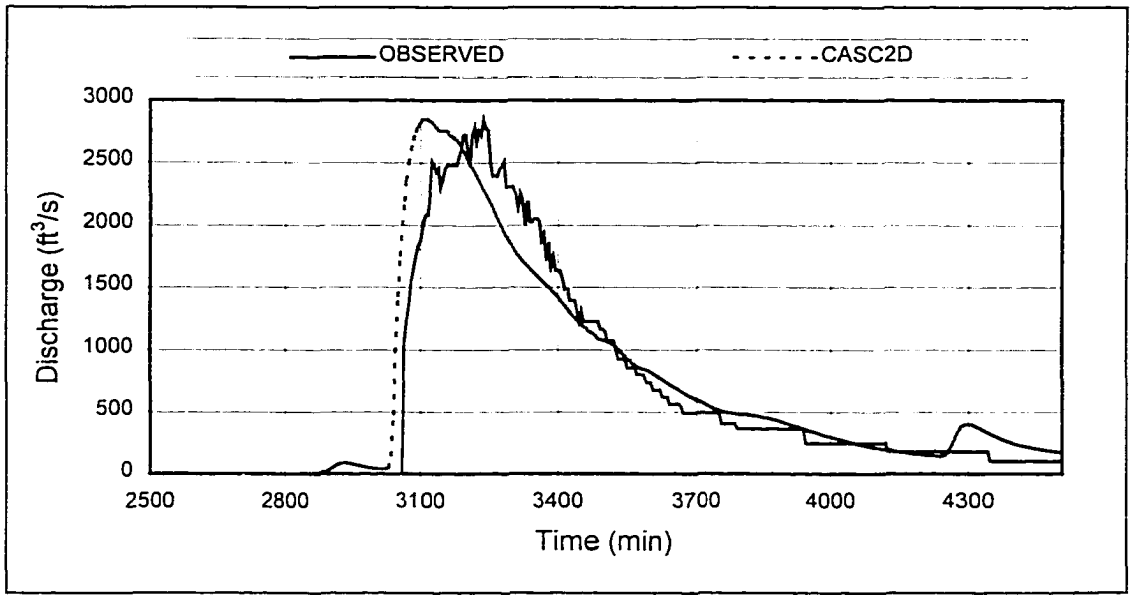

Figure 4.13 Cave Creek Computed vs. Observed Hydrographs - February Event

4.4.2 Hassyampa River Calibration

The Hassyampa River model was also calibrated using the precipitation event of February 1995. Precipitation totals from the seven gauges over the Hassyampa basin are summarized in Table 4.8 and Figure 4.14 shows the cumulative average rainfall for the gauges on the Hassyampa River. The highest intensity during any fifteen minute interval for this event over the Hassyampa basin was 39.6 mm/hr (1.56 in/hr).

Gauge #	1	2	3	4	5	6	7
Precipitation (mm)	176.8	57.9	59.9	64.0	102.6	81.0	112.8
Precipitation (in)	7.0	2.3	2.4	2.5	4.0	3.2	4.4

Table 4.8 Hassyampa River Precipitation Gauge Data - February Event

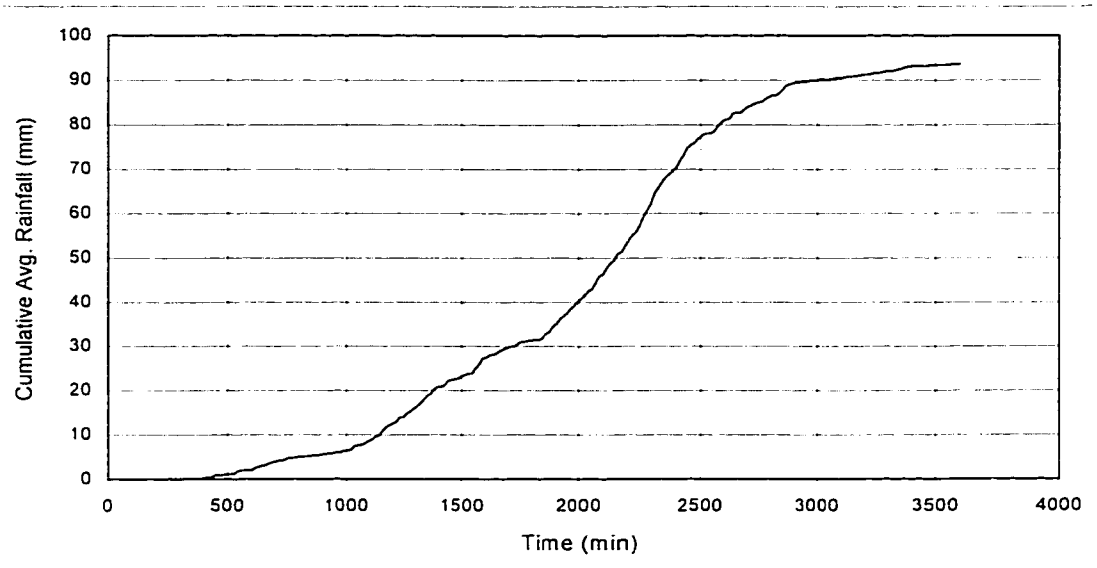

Figure 4.14 Cumulative Average Precipitation for Hassyampa River – February Event

Initially for the Hassyampa River model, soil moisture deficit and surface roughness parameters were set to the same values used in the Cave Creek calibration, and the infiltration parameters were left equal to the original estimates. Results produced a hydrograph with a peak slightly higher than the observed and time to peak earlier than the observed peak. Thus, the infiltration parameters were not changed, but the surface roughness value for the crop and rangeland was increased until a value of 0.09 was reached. This increased the time to peak and lowered the peak flow to achieve the results shown in Table 4.9 and Figure 4.15. Recall that all agricultural and range land were

merged into a single surface roughness category. In reality, each of these two basins has a different mix and different specific types of agricultural and range lands, thus slightly different Manning n values for this category of land use is reasonable. Table 4.9 provides a summary of the peak discharges and times to peak for the observed and computed hydrographs, and Figure 4.15 shows the computed and observed hydrographs.

Hydrograph	Peak Flow	Time to Peak
Observed	13061 cfs	2700 min
CASC2D	13796 cfs	2697 min
% Difference	5.6 %	0.1 %

Table 4.9 Calibration Results for Hassyampa River– February Event

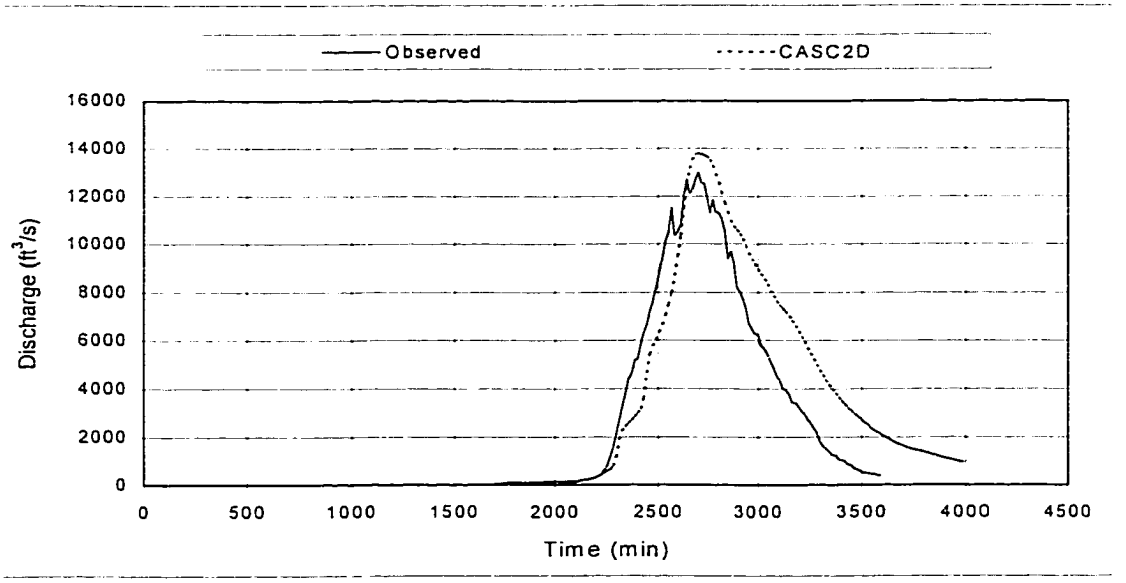

Figure 4.15 Hassyampa River Computed vs. Observed Hydrographs - February Event

Figures 4.16 through 4.30 provide color images from the CASC2D model for the February calibration event on the Hassyampa River watershed. These figures contain

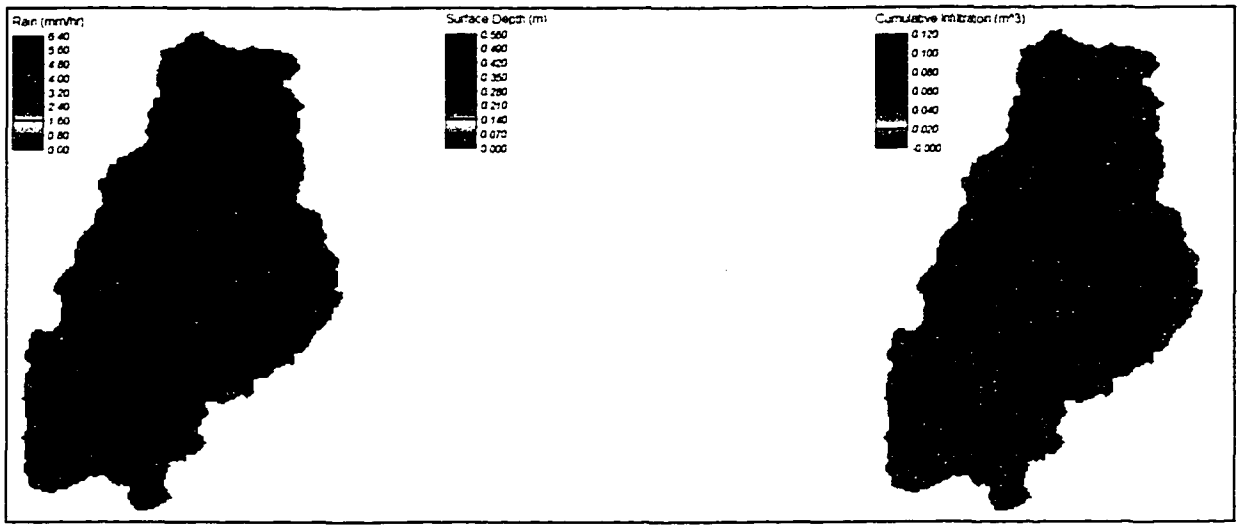

Figure 4.16 Rain, Surface Depth, and Cumulative Infiltration - Time = 480 min

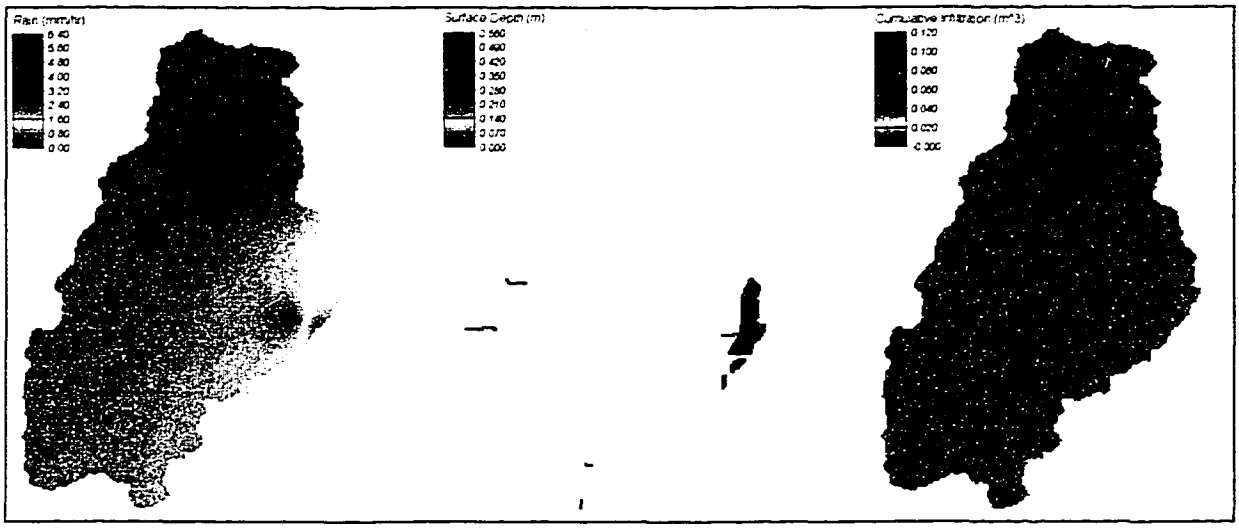

Figure 4.17 Rain, Surface Depth, and Cumulative Infiltration - Time = 720 min

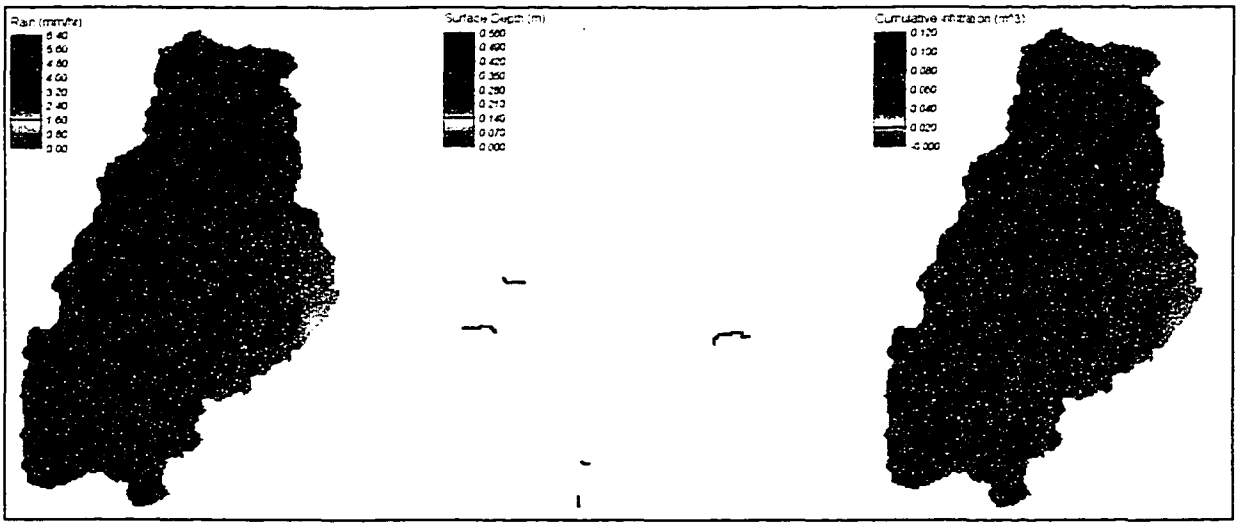

Figure 4.18 Rain, Surface Depth and Cumulative Infiltration - Time = 960 min.

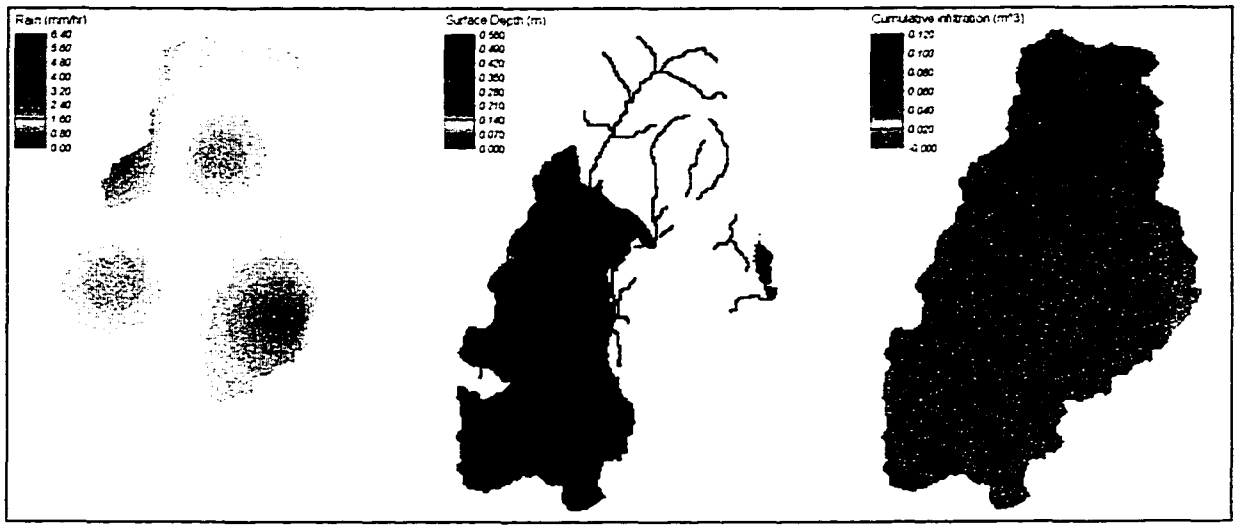

Figure 4.19 Rain, Surface Depth and Cumulative Infiltration - Time = 1200 min.

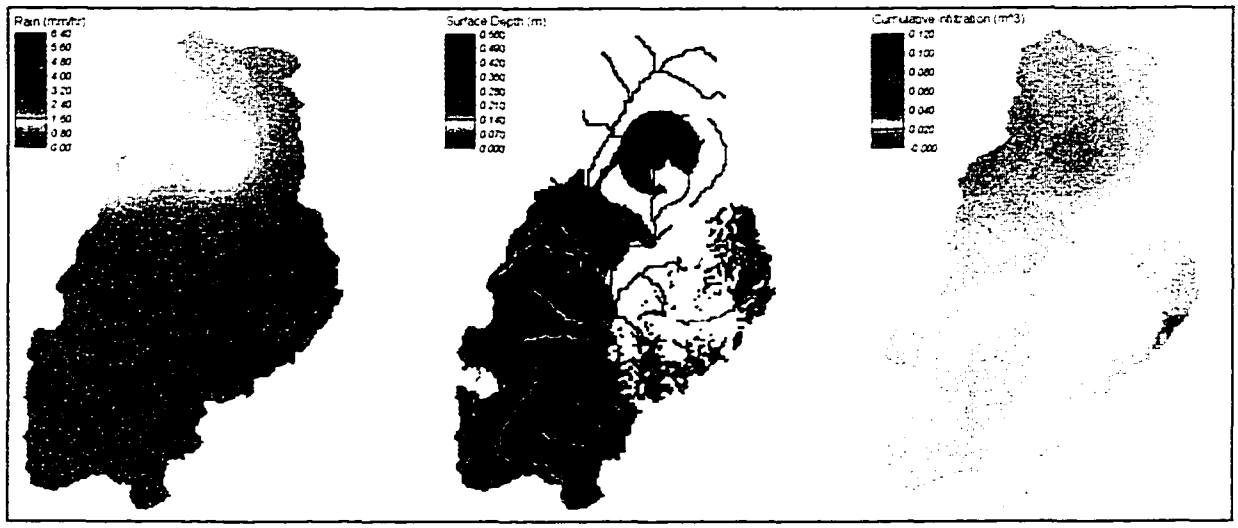

Figure 4.20 Rain, Surface Depth and Cumulative Infiltration - Time = 1440 min.

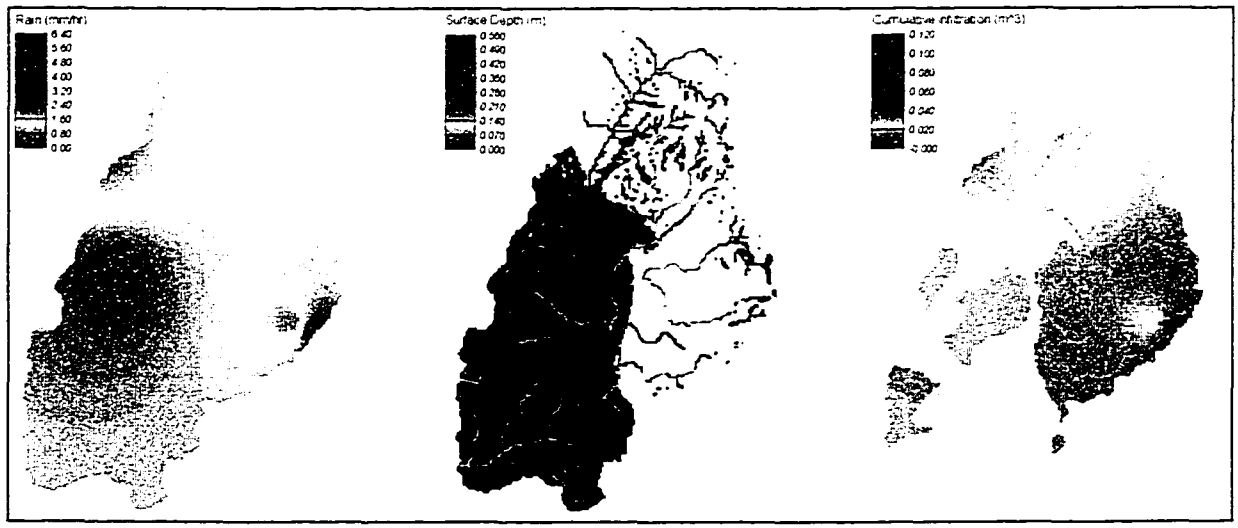

Figure 4.21 Rain, Surface Depth and Cumulative Infiltration - Time = 1680 min.

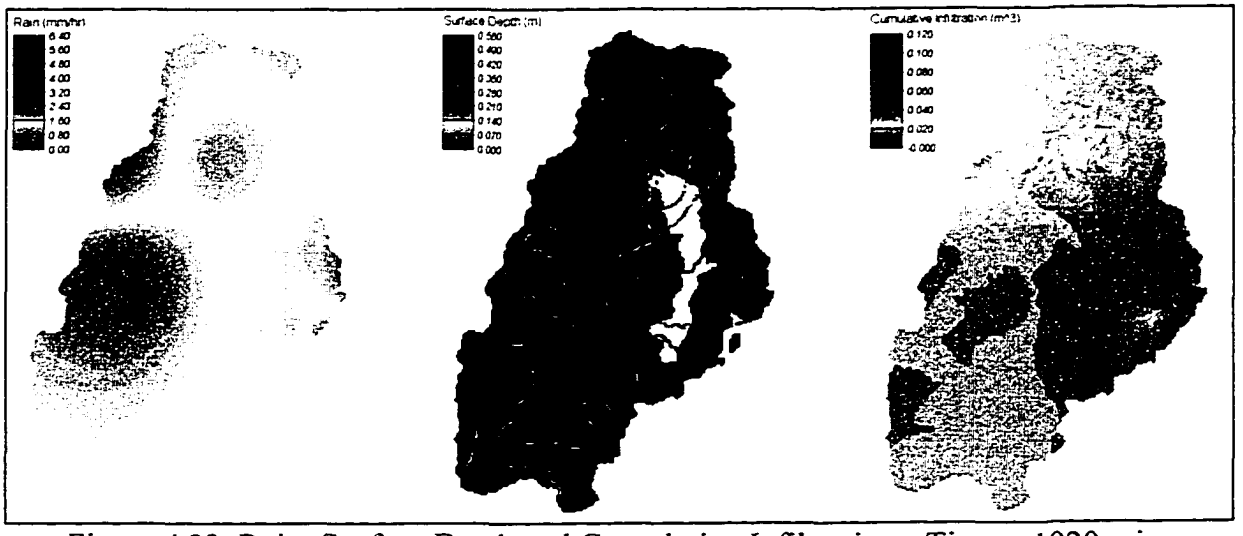

Figure 4.22 Rain, Surface Depth and Cumulative Infiltration - Time = 1920 min.

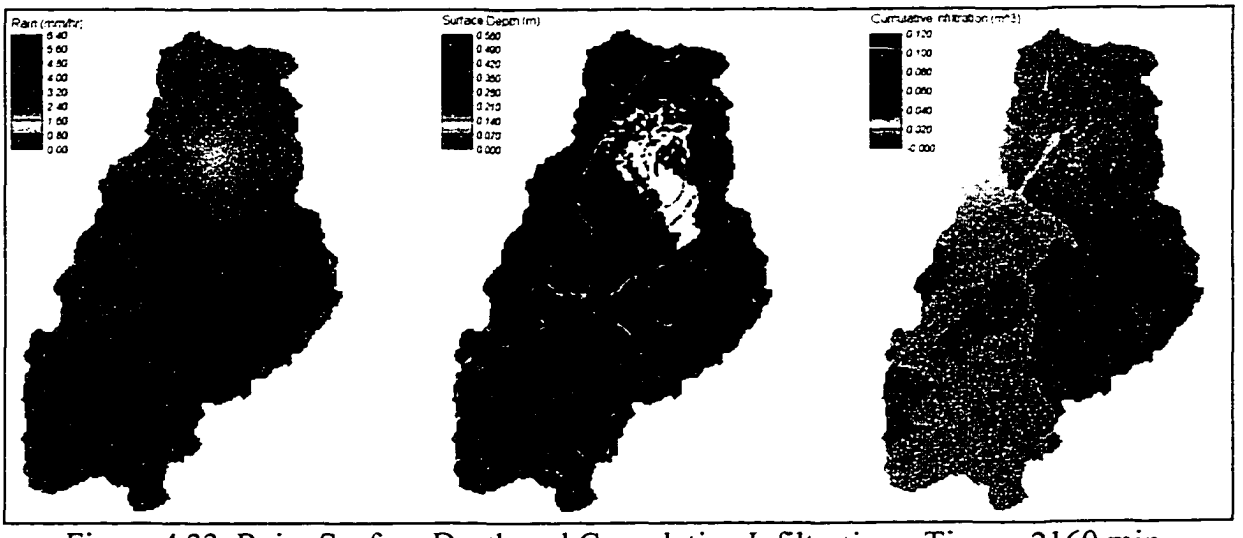

Figure 4.23 Rain, Surface Depth and Cumulative Infiltration - Time = 2160 min.

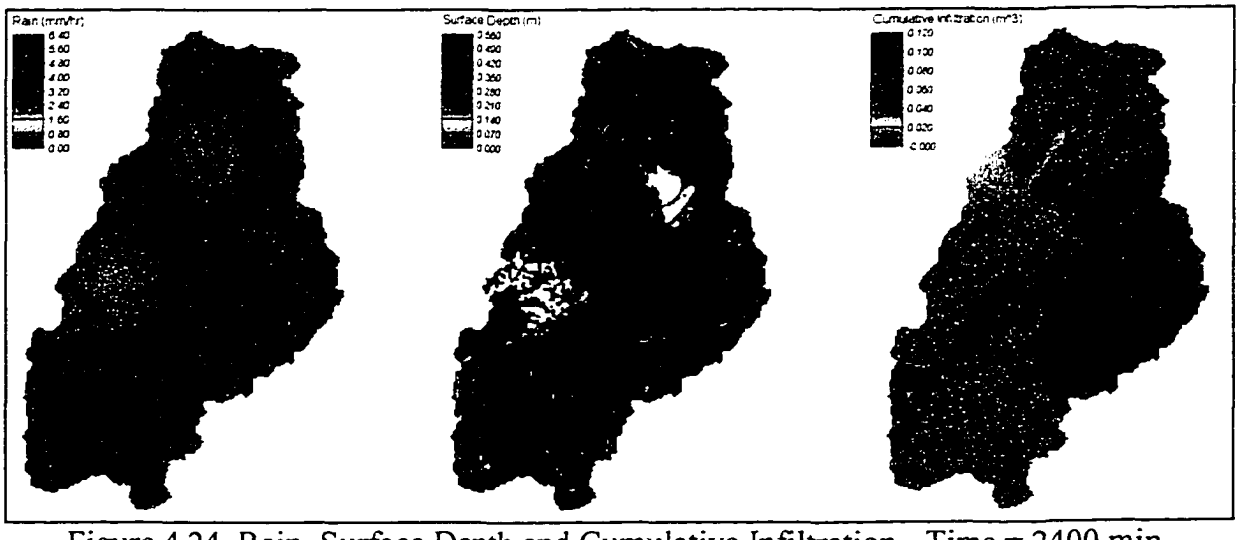

Figure 4.24 Rain, Surface Depth and Cumulative Infiltration - Time = 2400 min.

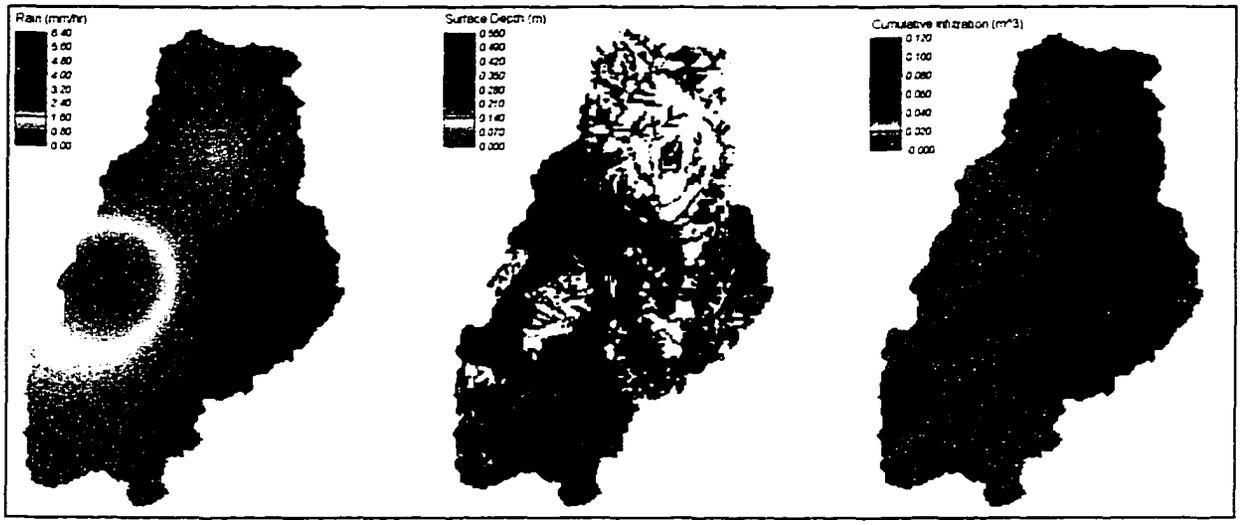

Figure 4.25 Rain, Surface Depth and Cumulative Infiltration - Time = 2640 min.

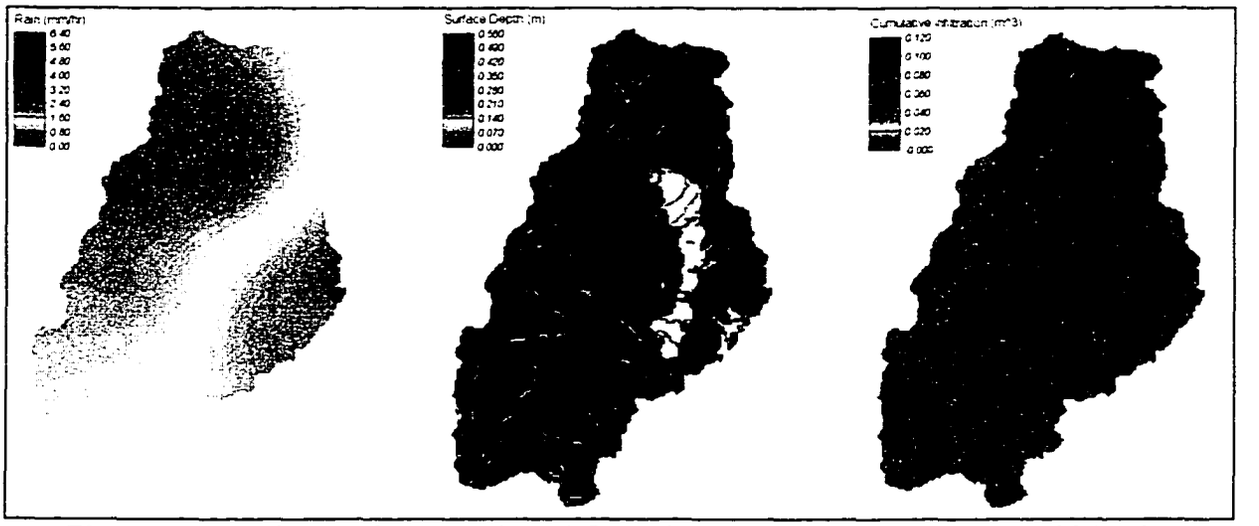

Figure 4.26 Rain, Surface Depth and Cumulative Infiltration - Time = 2880 min.

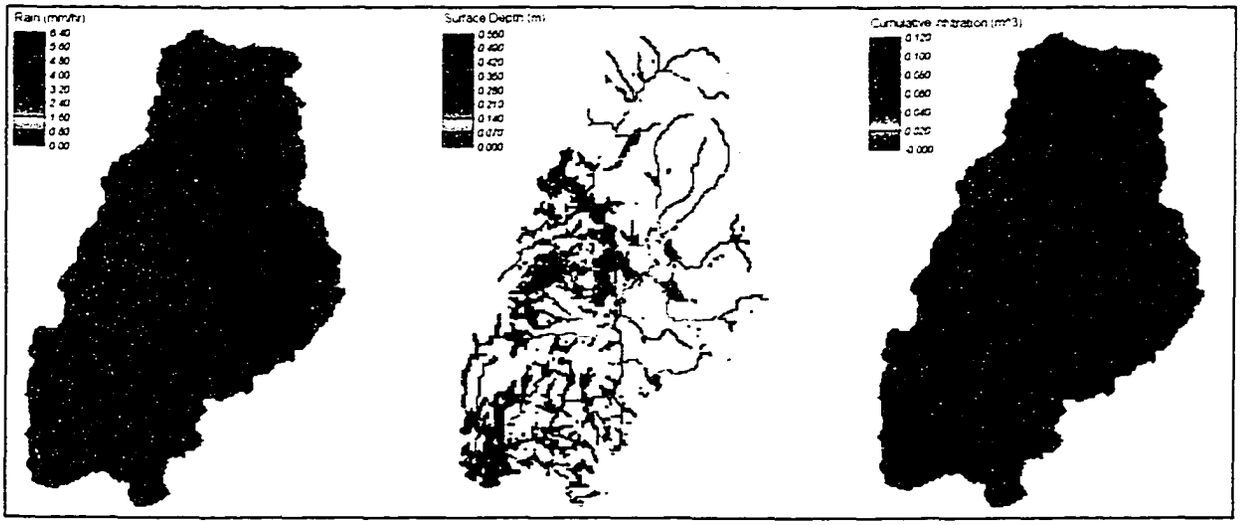

Figure 4.27 Rain, Surface Depth and Cumulative Infiltration - Time = 3120 min.

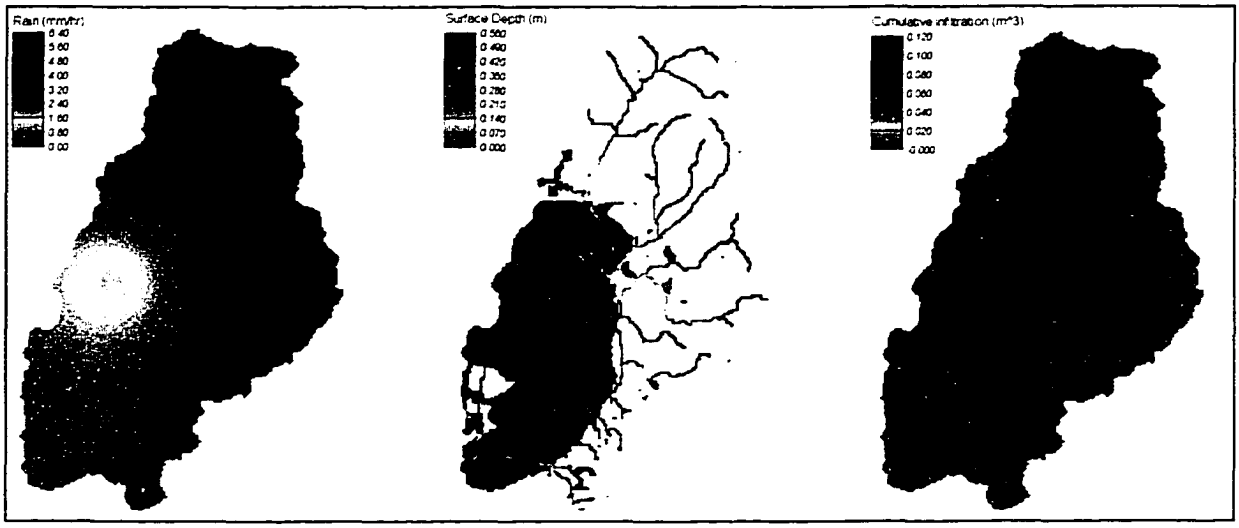

Figure 4.28 Rain, Surface Depth and Cumulative Infiltration - Time = 3360 min.

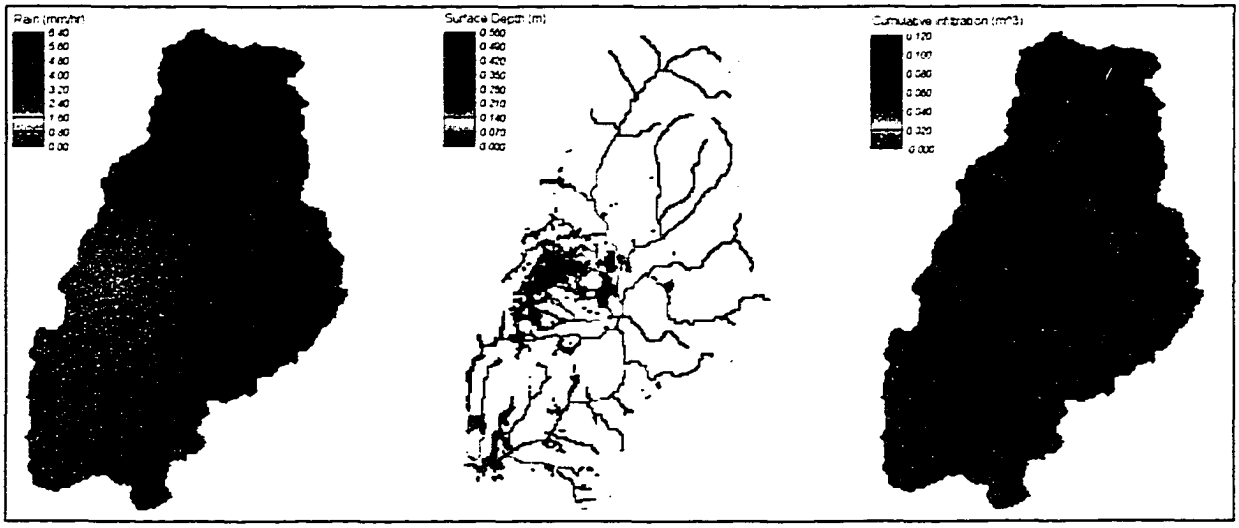

Figure 4.29 Rain, Surface Depth and Cumulative Infiltration - Time = 3600 min.

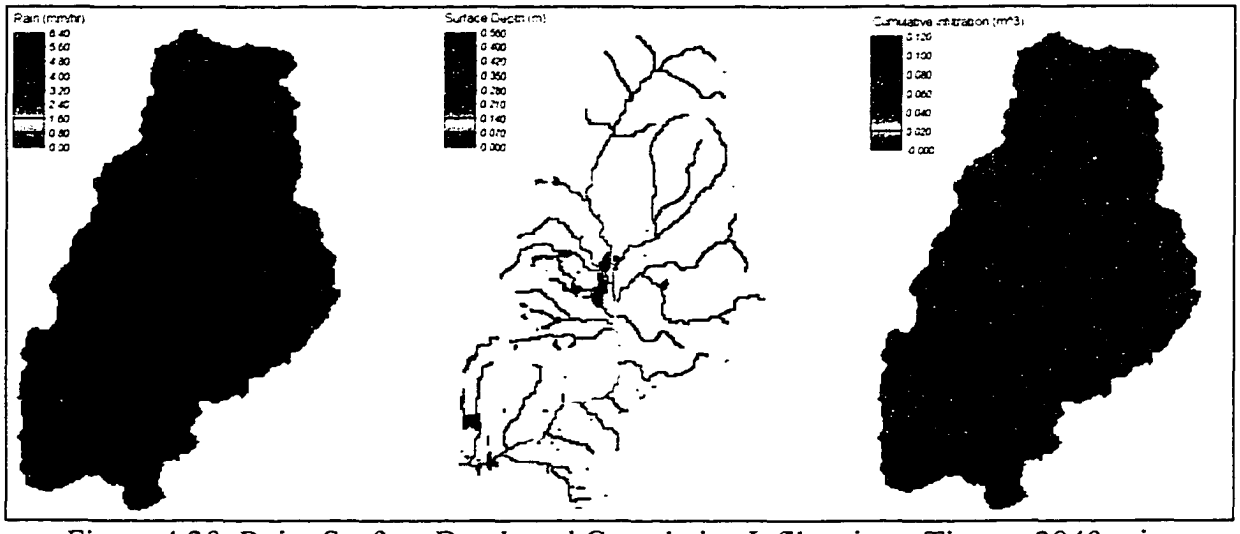

Figure 4.30 Rain, Surface Depth and Cumulative Infiltration - Time = 3840 min.

4.5 MODEL VERIFICATION

The final process in developing the CASC2D models for the Cave Creek and Hassyampa River basins was to verify the models. This was accomplished by running the models for additional precipitation events using the parameters determined during the calibration. The intent of this process was to verify that the models are reasonably valid for more than just the unique conditions of the precipitation event for which the model parameters were initially calibrated. The one parameter in the models that can change from one precipitation event to another is the soil moisture deficit, which reflects the initial moisture conditions in the soil at the start of a precipitation event. If no rain has fallen for some period of time prior to an event, then the soil moisture deficit may be large. However, if precipitation has fallen over a basin within a short period of time prior to an event, then there would be a smaller deficit of soil moisture. If the models can successfully reproduce hydrographs for other precipitation events by only changing the initial moisture conditions, then this indicates that they are capable of adequately simulating the watershed response to a given precipitation input.

4.5.1 Cave Creek Verification

The Cave Creek model was verified using two additional precipitation events that occurred in January and March 1995. The first event occurred during January 1995 when precipitation began falling on the evening of January 2 and continued for approximately 48 hours ending in the evening of January 4, 1995. Table 4.10 shows precipitation totals for the five rain gauges, and Figure 4.31 shows the cumulative average rainfall amounts for the gauges over Cave Creek.

Gauge #	1	2	3	4	5
Precipitation (mm)	62.0	37.1	49.0	62.0	39.9
Precipitation (in)	2.44	1.46	1.93	2.44	1.57

Table 4.10 Cave Creek Precipitation Gauge Data - January Event

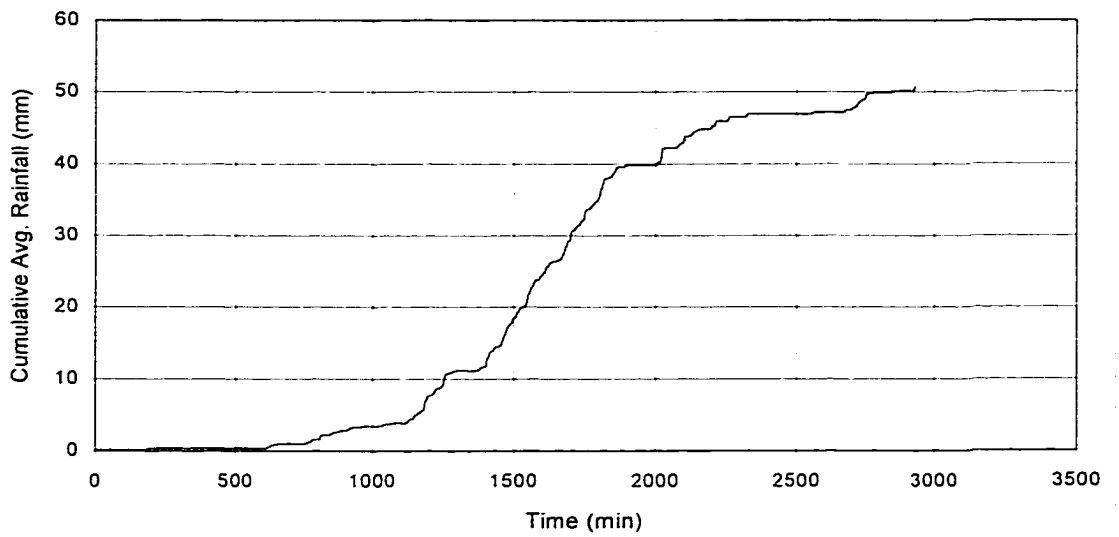

Figure 4.31 Cumulative Average Precipitation for Cave Creek – January Event

Initial results using the calibration parameters resulted in a hydrograph with a peak flow that was too high, indicating that soil moisture conditions in the basin were wetter than those for the February 1995 calibration event. The initial soil moisture deficit was lowered, and when the soil moisture deficit reached 5%, the peak flow and time to peak were reasonably close to the observed hydrograph. Figure 4.32 shows the observed vs. the computed hydrographs for this verification event and Table 4.11 summarizes the peak flows and times to peak for the observed and computed hydrographs. The only parameter changed from the calibration event was the soil moisture deficit that was lowered from 30% to 5% to obtain the results shown in Figure 4.32 and Table 4.11.

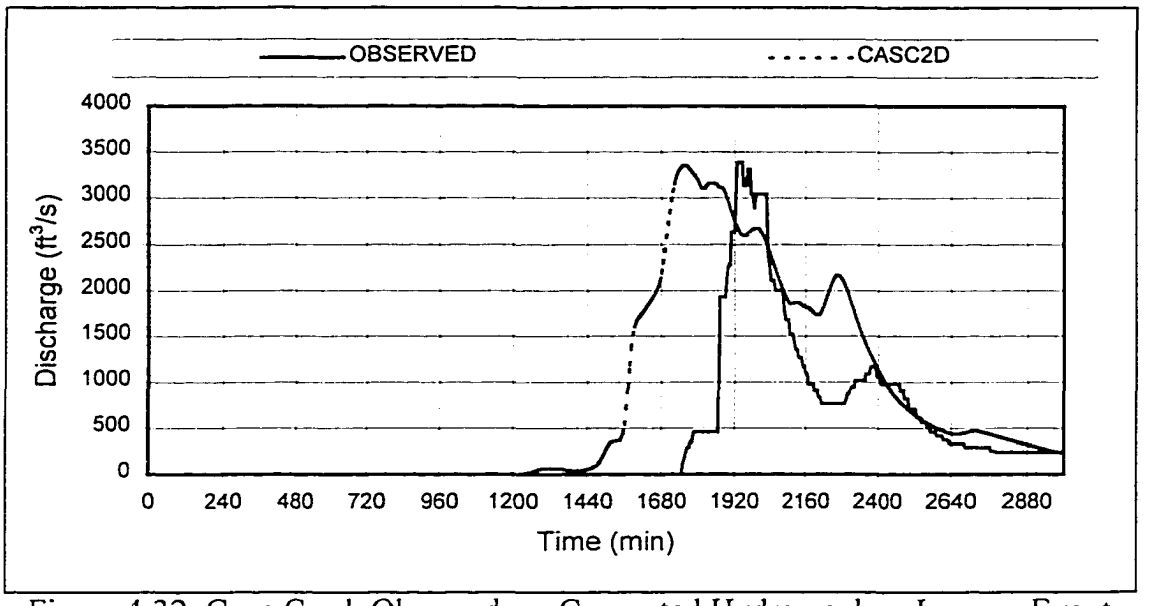

Figure 4.32 Cave Creek Observed vs. Computed Hydrographs - January Event

Hydrograph	Peak Flow	Time to Peak
Observed	3383 cfs	1930 min
CASC2D	3352 cfs	1755 min
% Difference	-0.9 %	-9.1 %

Table 4.11 Verification Results for Cave Creek– January Event

The second verification event for Cave Creek occurred in March 1995 when rain fell starting in the afternoon of March 4, 1995 and continued through the very early afternoon of March 5, 1995 lasting a total of less than 24 hours. Precipitation measurements from the five precipitation gauges are summarized in Table 4.12 and Figure 4.33 shows the cumulative average rainfall for the gauges.

Gauge #	1	2	3	4	5
Precipitation (mm)	34.0	30.0	33.0	22.1	34.0
Precipitation (in)	1.34	1.18	1.30	0.87	1.34

Table 4.12 Cave Creek Precipitation Gauge Data - March Event

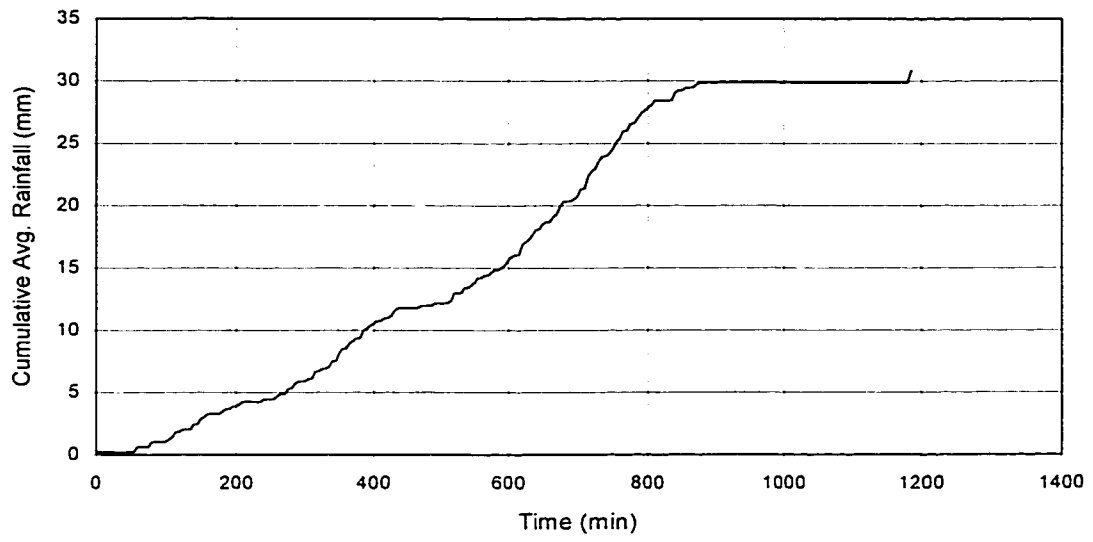

Figure 4.33 Cumulative Average Precipitation for Cave Creek – March Event

The initial run of the model with the calibration parameters for this event resulted in a hydrograph with a peak flow that was too high indicating that the soil moisture conditions in the basin prior to this March 1995 event were wetter than those for the February 1995 calibration event. The soil moisture deficit for the calibration event had been 30%, and when the soil moisture deficit was lowered to 10% the model results for the March 1995 event very closely matched the observed flow data. Figure 4.34 shows the observed vs. the computed hydrographs for this March 1995 verification event and Table 4.13 summarizes the peak flows and times to peak for the observed and computed hydrographs. Again, the only change in the model parameters from the calibration event was that the soil moisture deficit was lowered from 30% to 10% to obtain the results shown in Figure 4.34 and Table 4.13.

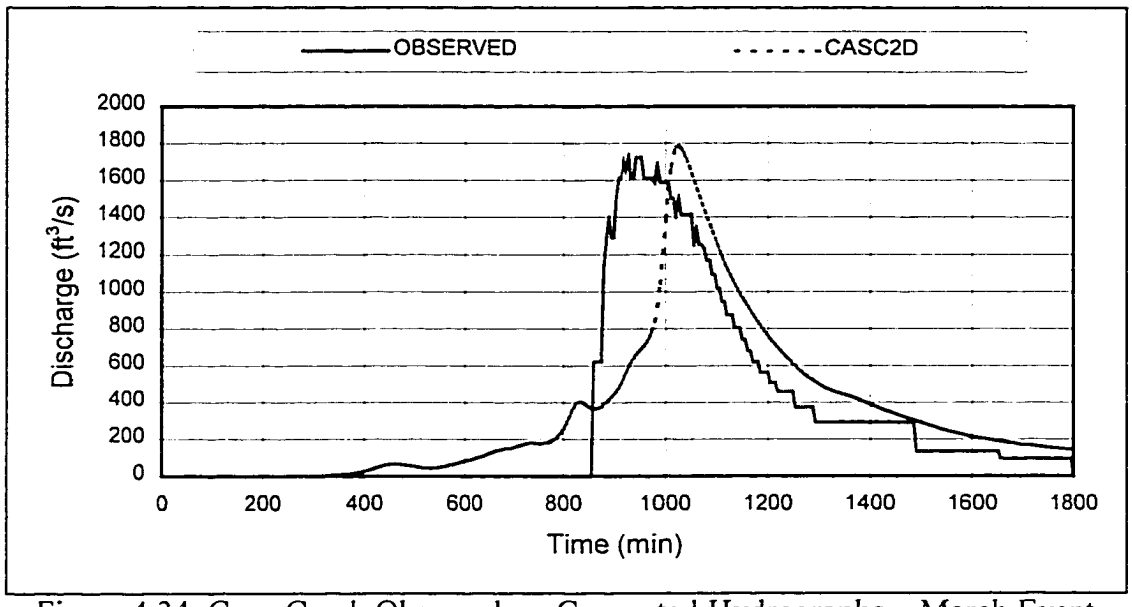

Figure 4.34 Cave Creek Observed vs. Computed Hydrographs – March Event

Hydrograph	Peak Flow	Time to Peak
Observed	1721 cfs	955 min
CASC2D	1784 cfs	1024 min
% Difference	+3.7 %	+7.2 %

Table 4.13 Verification Results for Cave Creek–March Event

4.5.2 Hassyampa River Verification

Data were available for only one additional runoff event for the Hassyampa River basin, and that was the event of March 1995. The event of January 1995 which produced runoff at Cave Creek and was used in the Cave Creek verification did not produce measurable runoff in the Hassyampa River. Thus, the March 1995 event was used as the sole verification event for the Hassyampa River model. Table 4.14 provides the precipitation totals for the seven Hassyampa River gauges, and Figure 4.35 shows the cumulative average precipitation for the event.

Gauge #	1	2	3	4	5	6	7
Precipitation (mm)	117.8	26.4	20.3	48.8	38.6	28.4	73.1
Precipitation (in)	4.4	1.0	0.8	1.9	1.5	1.1	2.9

Table 4.14 Hassyampa River Precipitation Gauge Data - March Event

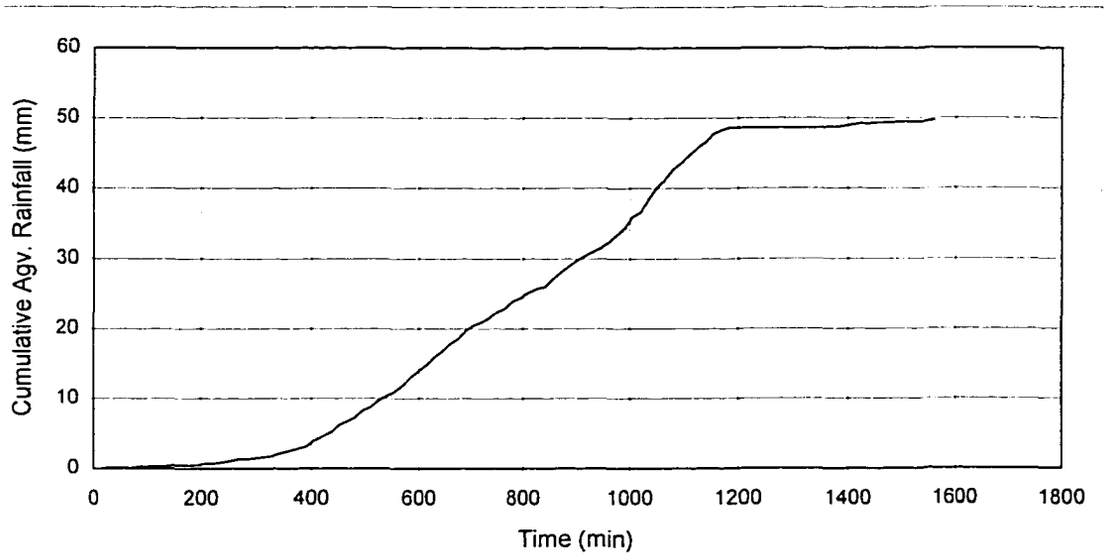

Figure 4.35 Cumulative Average Precipitation for Hassyampa River– March Event

For verification of the Hassyampa River model, the calibration parameters were used, with the exception of the initial soil moisture conditions. The initial soil moisture for the March event on Cave Creek had been adjusted to a 10% initial soil moisture deficit in the verification process. Since the Hassyampa River is located relatively near the Cave Creek basin, it was assumed that the initial soil moisture conditions in the Hassyampa River basin were the same as those in the Cave Creek basin for this March 1995 event. With this assumption, the model was run and the resultant hydrograph is shown in Figure 4.36 with a summary of the peak and time to peak data from the model and observed data provided in Table 4.15.

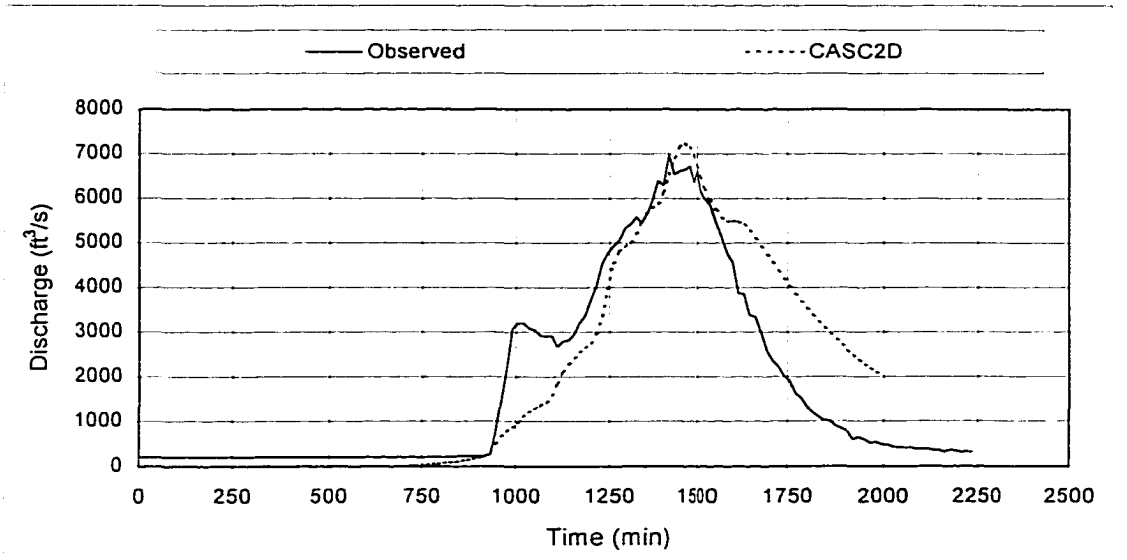

Figure 4.36 Hassyampa River Observed vs. Computed Hydrographs – March Event

Hydrograph	Peak Flow	Time to Peak
Observed	6974 cfs	1410 min
CASC2D	7236 cfs	1454 min
% Difference	+3.8 %	+3.1 %

Table 4.15 Verification Results for Hassyampa River – March Event

4.6 SUMMARY

The CASC2D model was used to model the Cave Creek and Hassyampa River watersheds located near Phoenix, Arizona. Digital elevation data were used to delineate the watersheds and stream networks, and model resolution of 200 meters was used. Land use / land cover data were obtained and analyzed from which four land use categories were established. Soil data were similarly processed to produce soil maps of the watersheds. Initial estimates of the Manning n parameter were determined from land use data and estimates of the Green-Ampt infiltration parameters from the soil data. Observed precipitation data from five precipitation gauges for Cave Creek and seven

from the Hassyampa River were obtained along with observed flow data for the gauges at the basin outlets.

Calibration of the Cave Creek model was performed using a February 1995 precipitation event. Adjustments were made to the initial parameter estimates such that the computed hydrograph closely reproduced the peak flow and time to peak of the observed hydrograph. The hydraulic conductivity parameters were reduced from the initial estimates, as were the surface roughness parameters, and the final calibration results produced a peak flow 0.1% greater than the observed peak with the time to peak 4.0% less than the observed time to peak. Calibration of the Hassyampa River model was also conducted using the February 1995 event with results being a peak flow 5.6% greater than the observed peak with the time to peak 0.1% less than the observed time to peak.

Model verification was then performed with two additional precipitation events for the Cave Creek basin and one additional event for the Hassyampa River. In the verification process, only the initial soil moisture parameter was changed and all other parameters were left unchanged from the model calibrations. The models were able to produce good results using this approach. For all verification events, the models were able to reproduce the observed peak discharge to within 5% of the observed peak and the time to peak to within 10% of the observed.

The results of this calibration and verification indicate the these CASC2D models of the Cave Creek and Hassyampa River basins do produce peak flows with times to peak that are within reasonable proximity of the observed conditions. The fact that the verification results were obtained without changing any model parameters other than the initial soil moisture deficit indicates that the remaining model parameters are valid.

These calibrated models now served as the models with which the parametric analysis of moving storms was performed and as the models with which radar data was used in a practical application of flow forecasting. These portions of the study are presented in the following chapters.

Chapter 5

RAINFALL DATA ANALYSIS

5.1 INTRODUCTION

The radar data that were available for this research were from the National Weather Service WSR-88D radar system in Phoenix, Arizona. The specific data format used was the Stage I Digital Precipitation Array (DPA). The Stage I DPA data are produced directly from the reflectivity measurements of the radar system using an assumed rainfall-reflectivity relationship. These data are produced at the radar site in real time, and undergo no quality control or calibration based on ground observations. Stage II and III precipitation data do undergo quality control and calibration based on ground and other observations, but those data were not available at the time of this research. Thus, the original radar data available had undergone no calibration or verification process. Many researchers have shown that the accuracy of radar rainfall estimates is greatly improved when ground observations are incorporated (Anagnostou and Krajewski, 1999a,b). The use of rain gauge data can be through the calibration process of the reflectivity-rainfall (Z-R) relationship or by performing real-time adjustments to the radar estimates, but in either case the use of rain gauge data is essential in providing realistic validation of radar rainfall estimates (Ciach and Krajewski, 1999).

For this research, validation of the radar rainfall estimates was performed through calibration of the Z-R relationship. This calibration process was performed by comparing the probability distributions of rainfall intensity measurements from the radar and from rain gauges for four precipitation events and adjusting the Z-R relationship for the radar data to match that from the rain gauges. The rain gauge data used was from 19 gauges located in and near the Cave Creek and Hassyampa River watersheds and data were provided at 15 minute time intervals. The following sections provide a summary of this process and an analysis of general storm characteristics derived from the radar data.

5.2 RADAR RAINFALL CHARACTERISTICS AND RADAR CALIBRATION

Rainfall characteristics are relevant to many aspects of watershed processes. Excess rainfall and the resultant overland surface runoff are not only responsible for streamflow, but are related to other processes such as transport of chemicals and sediment. There are a number of characteristics that describe precipitation, including intensity, duration, and areal extent, and radar observations of precipitation can be analyzed for each of these characteristics. First, the rainfall intensity characteristics of the radar rainfall data for the four events used in this research will be analyzed, and those characteristics will then be compared to rain gauge observations for the same rainfall events. Since the original radar data used in this research underwent no calibration to ground observations, the results of the following comparison between that original radar data and the rain gauge observations will provide a basis on which necessary calibration of the radar can be performed. Storm size, velocity, and duration will be examined later in this chapter.

5.2.1 Radar Rainfall Intensity

Rainfall intensity i has been shown to fit an exponential distribution where the probability distribution function, p(i), is

$$p(i) = \lambda_1 e^{-\lambda_1 i} \tag{5.1}$$

where the rainfall intensity parameter λ_1 is the inverse of the average rainfall intensity as

$$\lambda_1 = 1/\bar{i} \tag{5.2}$$

such that the exponent in (5.1) becomes

$$-\lambda_1 i = -i/\bar{i} \tag{5.3}$$

Good agreement has been shown between this exponential probability density function for rainfall intensity data by many researchers (Eagleson, 1978; Nguyen and Rouselle, 1981; Julien, 1982, Julien and Frenette, 1985). A method of transforms is presented by Julien (1996) whereby the properties of the probability distribution can be evaluated. This method was used in this research to evaluate whether the probability distribution of the radar rainfall data followed an exponential distribution. A brief summary of that approach is presented, followed by application of the method to the radar and rain gauge data for this research.

The properties of an exponential probability density function of a variable x allow that a reduced variable ϕ be defined by dividing the variable x by the mean value of x as

$$\phi = x/\bar{x} \tag{5.4}$$

The properties of the density function p(ϕ) and exceedance probability P(ϕ) are such that

$$P(\phi) = p(\phi) = e^{-\phi} \tag{5.5}$$

The objective of using such a transform is to determine if the probability density function is an exponential of variable ϕ after the transform

$$\phi = ax^c \tag{5.6}$$

where a and c are the transform coefficient and exponent, respectively, and are referred to as the transform parameters. Combining the natural logarithm of (5.5) with (5.6) yields

$$-\ln P(\phi) = \phi = ax^c \tag{5.7}$$

Taking the natural logarithm of (5.7) provides a means of evaluating the transform parameters graphically from

$$\Pi = \ln(-\ln P) = \ln a + c \ln x \tag{5.8}$$

where Π designates the double logarithm of the exceedance probability P. To evaluate the transform parameters a and c graphically, a straight line is fitted on a graph of Π as a function of $\ln x$. If the points plot as a straight line then the slope of that line gives the transform exponent c. If the probability density function for the data is exponential then the transform exponent c will be close to unity.

The probability density function for the radar data was analyzed using the above method by treating the rainfall intensity value for each radar data grid cell as an separate data point. The values from every radar grid cell from all four events were combined into one data set. Figure 5.1 shows a plot of Π as a function of *ln i*, where i is the precipitation intensity data from the radar for the four events.

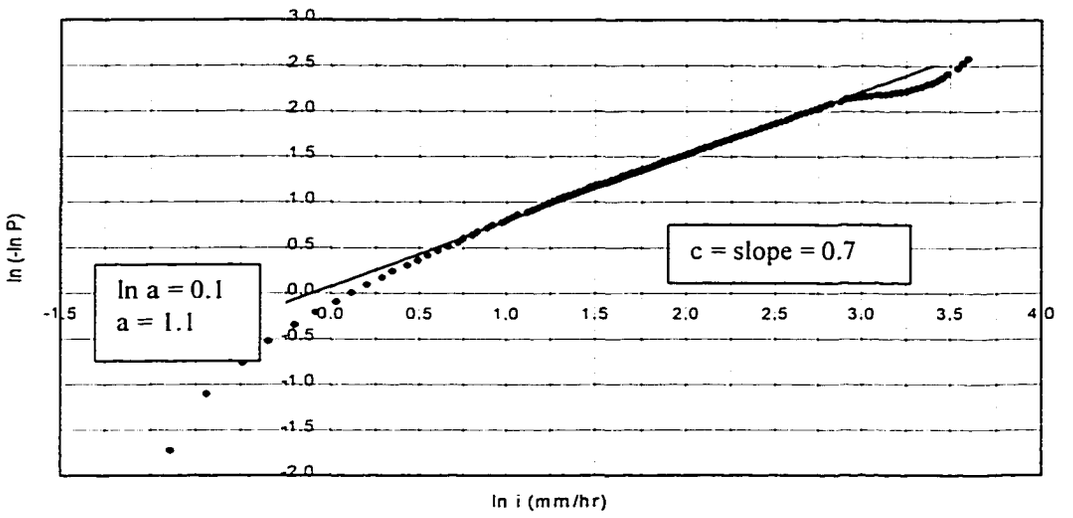

Figure 5.1 Transform Diagram for Radar Rainfall Intensity

In Figure 5.1, the points shown are from rainfall intensity data, and the solid line is fitted through the straight portion of the points. From that line, the transform parameter c is estimated as $c = 0.7$. Since these data represent precipitation intensity, it may be expected that the probability density function is exponentially distributed with the parameter c near 1.0. Previous researchers who have shown an exponential distribution of rainfall intensity have done so for data from independent events, such as monthly precipitation. However, the data plotted above do not necessarily represent a set of independent intensity values. These data represent many observations from four events and those observations are not necessarily independent from each other. Thus, the exponential distribution may or may not be expected for these data. Since the parameter c for these data is only approximately 0.7, the distribution is not exactly exponential. For comparison, this same procedure is presented for the precipitation measurements from the rain gauges located in and near the Cave Creek and Hassyampa River watersheds. Ideally

the probability density functions for the radar and rain gauge measurements from these events will be similar. If they are not, then it will be assumed that the rain gauge data are correct and that the radar data must be calibrated in some form to correlate more closely with the rain gauge measurements.

5.2.2 Rain Gauge Rainfall Intensity

Radar rainfall data were hourly accumulations in units of millimeters, so the values from the radar represent intensity in mm/hr. The rain gauge data were 15-minute totals in units of inches. The rain gauge data were processed to derive hourly accumulations with the units converted to mm, such that both sets of precipitation data had common units of mm/hr. Data from 19 gauges were available for this study, and the data were from the same four rainfall events as was the radar data. The same procedure that was used for the radar data was used for the rain gauge data, and the results are presented in Figure 5.2 which shows the transform diagram for the rain gauge data.

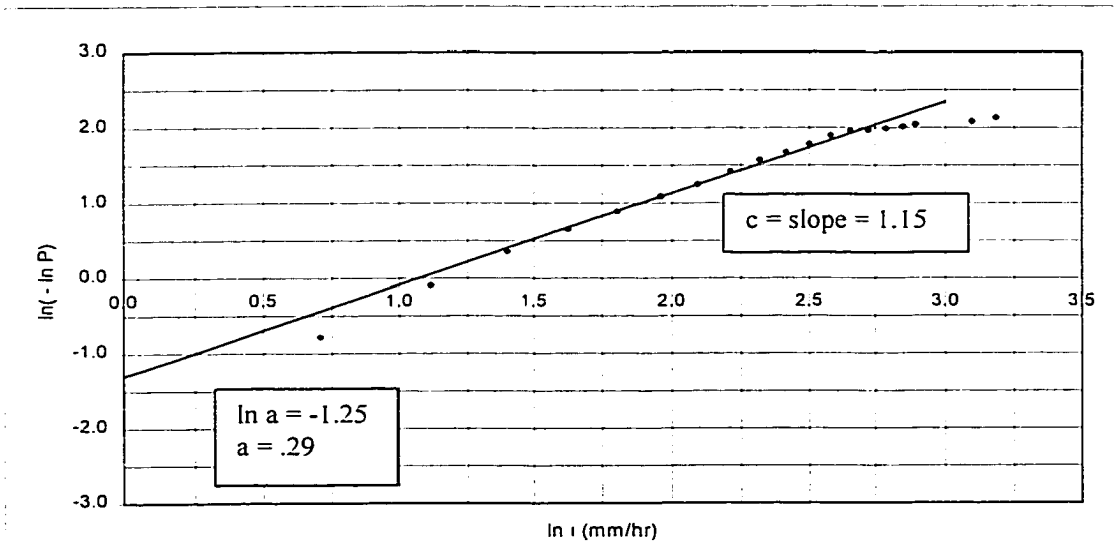

Figure 5.2 Transform Diagram for Rain Gauge Rainfall Intensity

From Figure 5.2, the transform parameter c for the gauge data is $c = 1.15$. This is nearer 1.0 than for the radar data and thus the probability function more closely fits an exponential distribution. Figure 5.3 shows the transform diagrams for the radar and rain gauge data, and Figure 5.4 shows a traditional plot of the probability density functions.

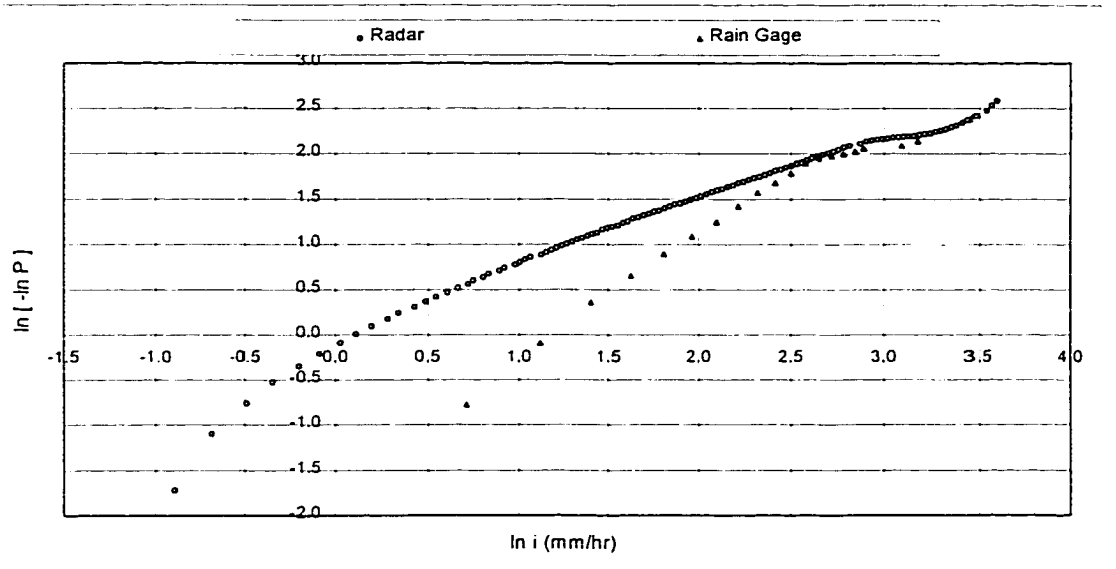

Figure 5.3 Transform Diagrams for Radar and Rain Gauge Data

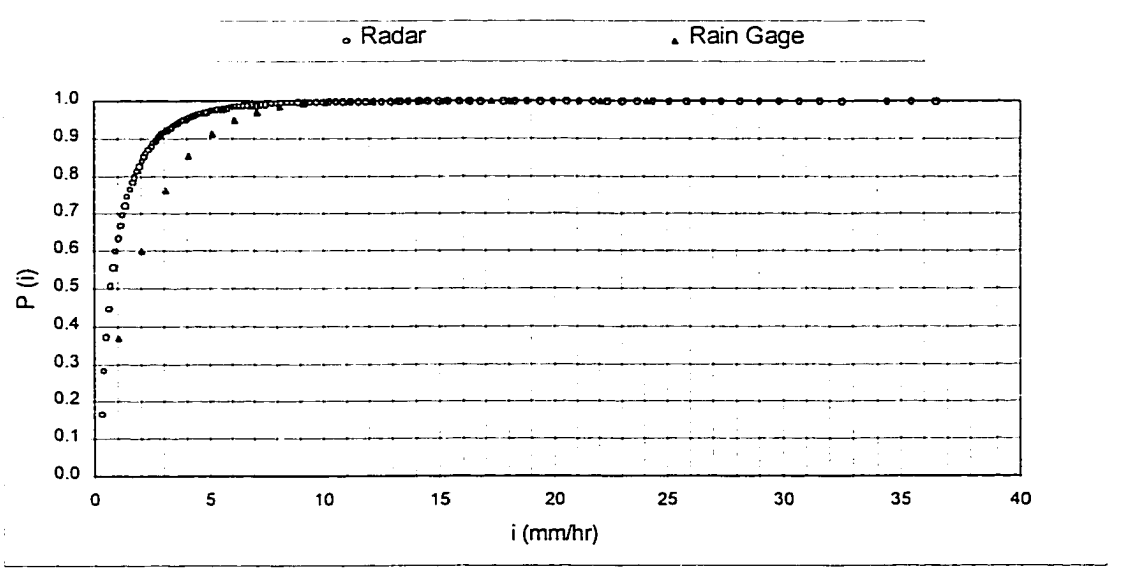

Figure 5.4 Cumulative Distribution Function for Radar and Rain Gauge Data

It is apparent from Figures 5.3 and 5.4 that the probability distributions for the radar and rain gauge data are not close to being the same, and some calibration of the radar data to the ground observations is required. Based on the measurements made by the radar, the minimum rainfall intensity measured is 0.307 mm/hr and the maximum measured during the four rainfall events represented here was 36.5 mm/hr. The distribution of these measurements is very heavily weighted towards the lower rainfall intensities, with approximately 90 % of the measurements being less than 2.54 mm/hr (0.1 inches per hour). Intensities exceeding 12.7 mm/hr (0.5 inches per hour) represent only 0.1 % of the measured observations, and intensities exceeding 25.4 mm/hr (1.0 in/hr) occurred at a rate of 0.008%. The minimum hourly intensity computed from the rain gauge data was 1.02 mm/hr, and the maximum for these storms was 24.1 mm/hr. As with the radar data, the gauge data were fairly heavily distributed towards the lighter intensities with approximately 66% of the measurements being less than 2.54 mm/hr (0.1 in/hr). Intensities greater than 12.7 mm/hr (0.5 in/hr) account for approximately 0.37% of the observations, while intensities greater then 25.4 mm/hr (1.0 in/hr) represent 0.0 % of the measurements.

5.2.3 Calibration of Radar to Rain Gauge Data

Since rain gauges provide direct measurement of precipitation that falls to the ground and radar estimates are based on a less direct and more uncertain approach, the rain gauge data were considered to be the ground truth. Thus, since the radar and rain gauge data from these events are not distributed equally, an adjustment or calibration of the radar data to correlate more closely with the rain gauge data was needed. A calibration approach based on the radar reflectivity – rainfall relationship was pursued.

This reflectivity – rainfall relationship is the Z-R relationship and is of the form:

$$Z = \alpha R^{\beta} \tag{5.9}$$

where, R is the rainfall rate, Z is the reflectivity, and α and β are fit parameters. For the original uncalibrated radar data from the Phoenix, Arizona radar site, the parameters α and β had values of 300 and 1.4, respectively, such that the Z-R relationship for these radar data was:

$$Z = 300R^{1.4} \tag{5.10}$$

This Z-R relationship is not necessarily the relationship that is most applicable for the rainfall occurring in Arizona. There are a number of Z-R relationships that have been derived that are applicable for particular regions or types of rainfall events. For instance, one Z-R relationship might be considered applicable for rainstorms over the central plains of the United States while that same Z-R relationship would be inadequate to describe storms in desert regions. Also, Z-R relationships for frontal systems might be different than those for convective rainfall systems. Thus, the Z-R relationship used for these radar data was one which was most likely developed for some region other than the desert environment of Arizona, and as such a different Z-R relationship might provide a better relationship between the rain gauge measurements and the radar measurements.

A number of Z-R relationships were tested to determine one that would result in a distribution function for the radar data that more closely matched the distribution of the rain gauge data. Ultimately, a relationship with the parameters $\alpha = 50$ and $\beta = 1.96$ produced good results. This established a new Z-R relationship for these radar data as:

$$Z = 50R^{1.96} \tag{5.11}$$

This relationship was applied to the original radar data to derive "calibrated" radar rainfall estimates and the probability distribution of the resultant intensity values was determined. Figure 5.5 shows transform diagrams for the original radar data, the calibrated radar data and the rain gauge data, and Figure 5.6 shows the more traditional cumulative distribution functions. It is apparent that the calibrated radar rainfall intensity data are distributed in a manner that is much more closely correlated with the rain gauge data. On the transform diagram, the parameter for the calibrated radar data was estimated as c = 1.01, which is essentially equal to the value of 1.0 for an exponential distribution.

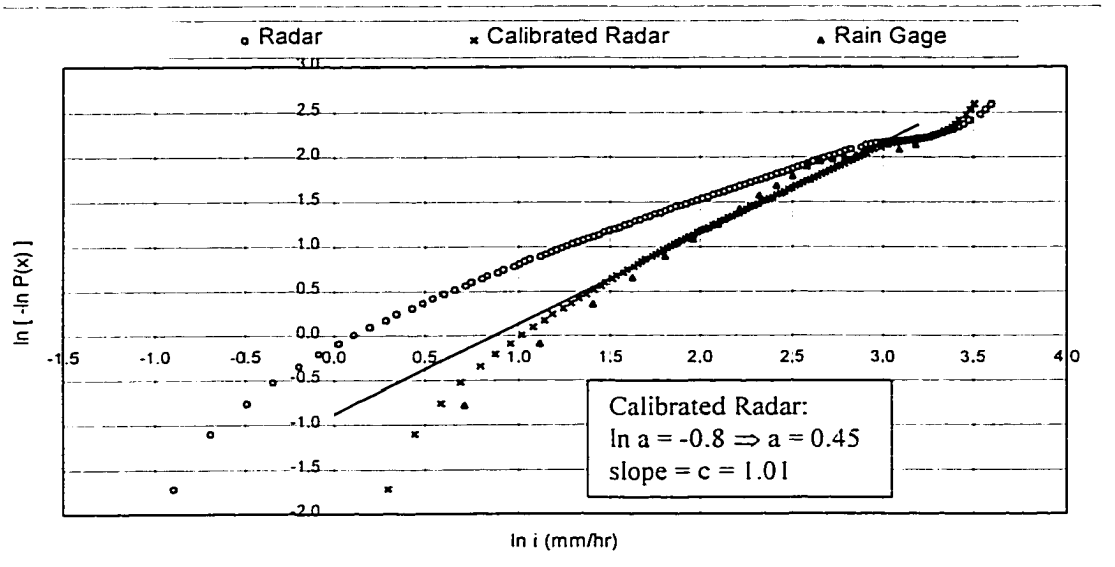

Figure 5.5. Transform Diagrams for Radar, Calibrated Radar and Rain Gauge Data

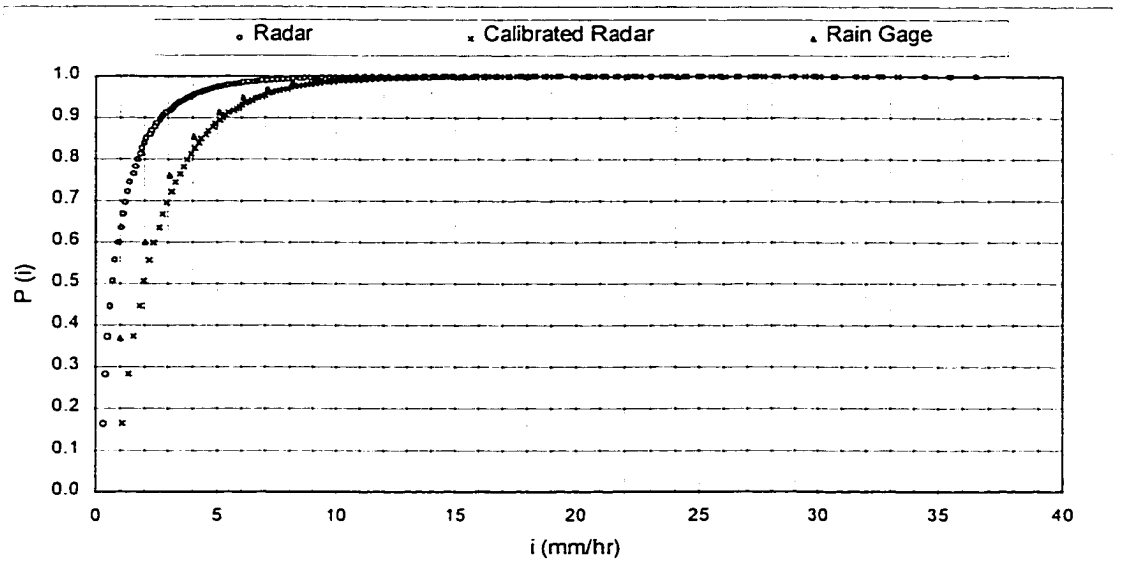

Figure 5.6 Cumul. Dist. Functions for Radar, Calibrated Radar and Rain Gauge Data

5.2.4 Comparison of Data at Rain Gauge Locations

The preceding analysis was performed using data from the entire radar scan and a total of 19 rain gauges in the region. The final use of the radar data, as detailed in Chapter 7, will be to apply the radar data to the watershed model for the Hassyampa River watershed. Thus, it is informative to compare the calibrated radar measurements directly with rain gauge measurements specifically at the rain gauge locations for the precipitation events to be modeled. For this analysis, rainfall measurements at 6 rain gauges located in the Hassyampa River watershed were compared to the calibrated radar rainfall measured by the radar at those same 6 locations. Since the radar data are provided for 4 x 4 km cells, the cells from the radar data which contained the locations of the gauges were chosen for this comparison.

Rainfall data from rain gauges were available for two rainfall events that produced runoff over the Hassyampa River watershed that occurred during February and March

1995. As an initial comparison between rain gauge and radar measurements for those events, the total precipitation measured at each gauge for these two events is presented in Table 5.1. Shown are the event precipitation totals for each of the 6 gauge locations as measured by the gauges, the original radar data and the calibrated radar data. At the bottom of the table is the total precipitation summed over all 6 gauges.

Gauge #	Rain Gauge (mm)	Original Radar (mm)	Calibrated Radar (mm)
1	109.4	30.9	121.1
2	141.2	73.8	265.6
3	112.8	17.9	94.6
4	80.2	18.9	93.7
5	84.3	2.4	17.7
6	177.8	21.3	107.7
Total	705.7	165.2	700.4

Table 5.1 Rain Gauge and Radar Precipitation Totals for February and March Events

It is evident from the data in Table 5.1 that even with the calibrated radar, the rain gauge and radar data do not provide the same rainfall measurements at each gauge location. However, when taken across the entire basin from the total of all 6 gauge locations, these variations average out to produce total values from the rain gauges and radar that are within 1% of each other. When the data from each of the two precipitation events are plotted over time, the adjustment made to the radar data using the new Z-R relationship does produce rainfall estimates that are much more in line with the rain gauge data than the original radar data. Figures 5.7 and 5.8 show these data plotted for the February and March events. The cumulative precipitation in these figures was

derived by summing the precipitation data from all gauge locations to generate a "basin wide" precipitation value.

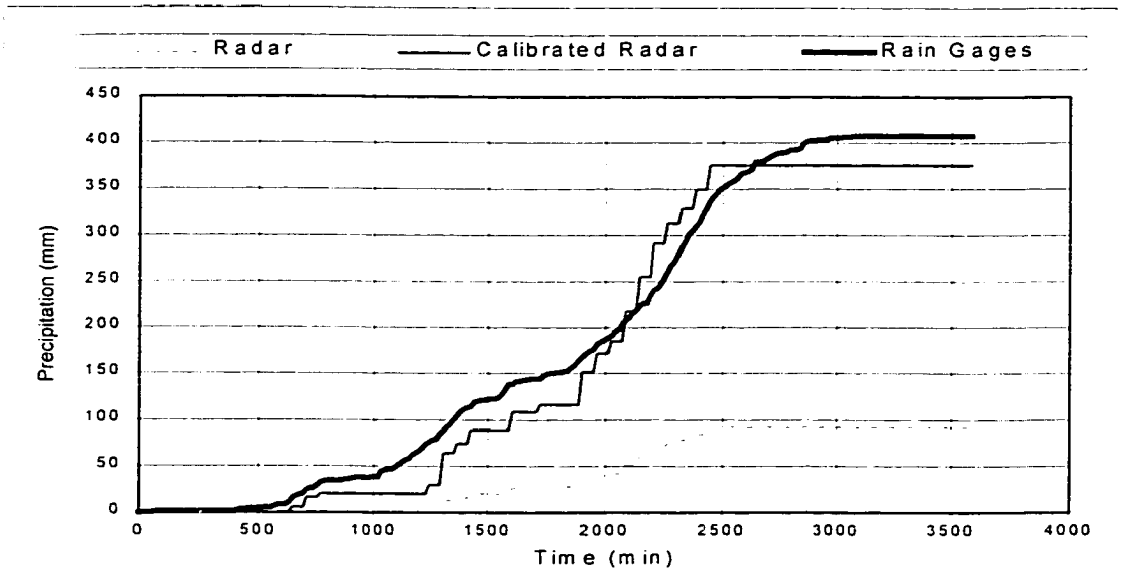

Figure 5.7 Rain Gauge and Radar Cumulative Precipitation – February Event

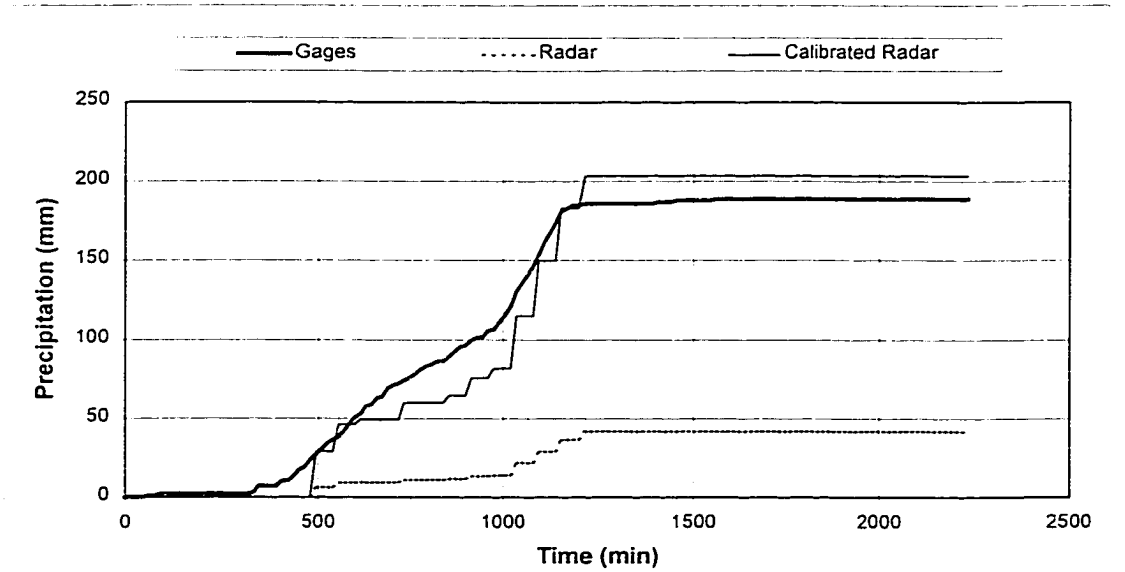

Figure 5.8 Rain Gauge and Radar Cumulative Precipitation – March Event

5.3 MODEL RESULTS WITH RADAR DATA

As a final test of the calibrated radar data, they were used as precipitation input to the calibrated CASC2D model of the Hassyampa River watershed for the February and March events. The rainfall intensities in the original radar data were so low that no runoff resulted from the model using those data. The calibrated radar data, however, should more closely reproduce the observed flow since they have been shown to provide rainfall measurements for the watershed that are very close to those from the rain gauges. Figures 5.9 and 5.10 show the runoff hydrographs on the Hassyampa River watershed for the February and March events, respectively. In these model runs, no parameters were changed from the calibration and verification process. Table 5.2 provides a summary of these results, and Figures 5.11 through 5.22 provide color images from the CASC2D model for the March event on the Hassyampa River using the radar rainfall data as precipitation input. The "checkerboard" patterns in those images reflect the 4 x 4 km grid cells of the radar data.

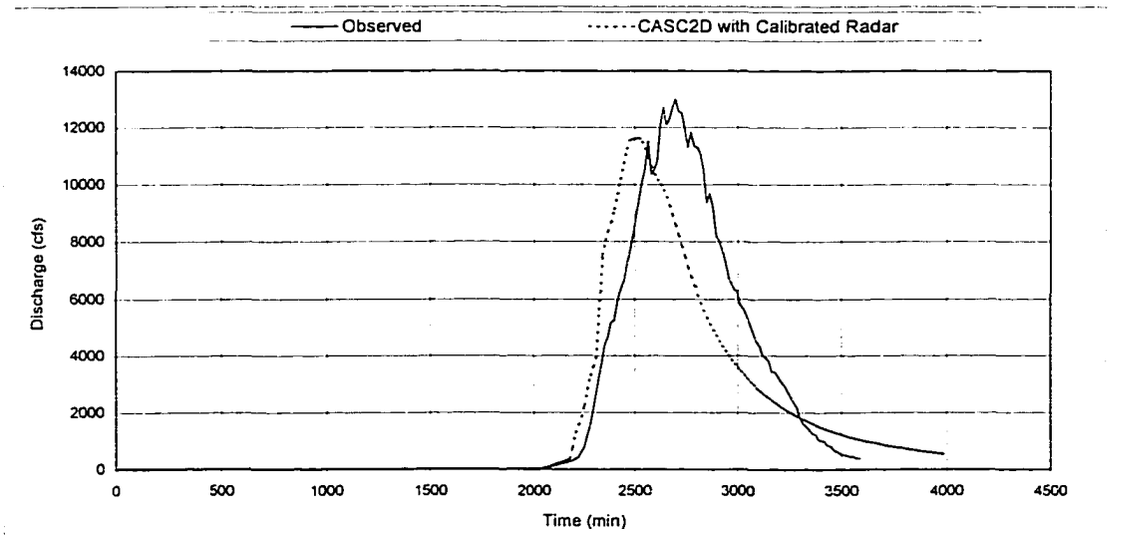

Figure 5.9 Model Results with Calibrated Radar Data - February Event

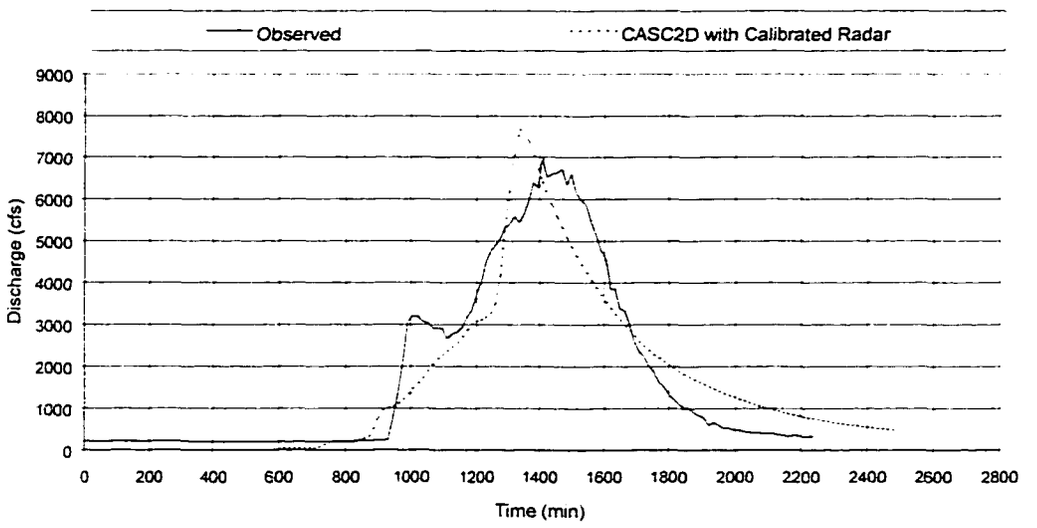

Figure 5.10 Model Results with Calibrated Radar Data - March Event

	February Event		March Event	
Hydrograph	**Peak Flow**	**Time to Peak**	**Peak Flow**	**Time to Peak**
Observed	13061 cfs	2700 min	6974 cfs	1410 min
CASC2D	11631 cfs	2517 min	7714 cfs	1335 min
% Difference	-10.9 %	-6.8%	+10.6%	-5.3%

Table 5.2 Model Results with Calibrated Radar Data - Hassyampa River

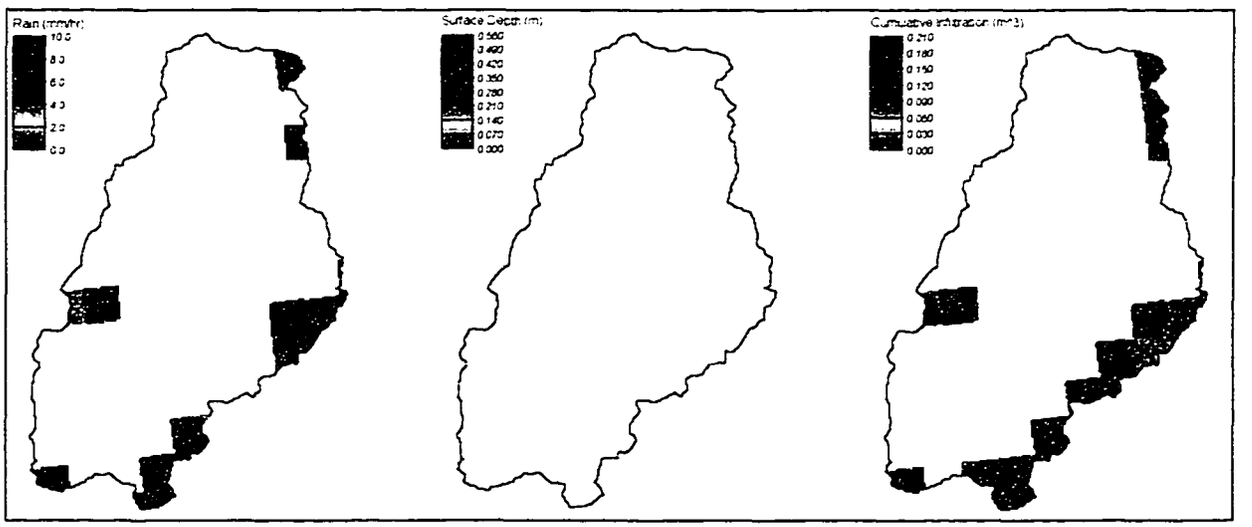

Figure 5.11 Rain, Surface Depth and Cumulative Infiltration - Time = 200 min.

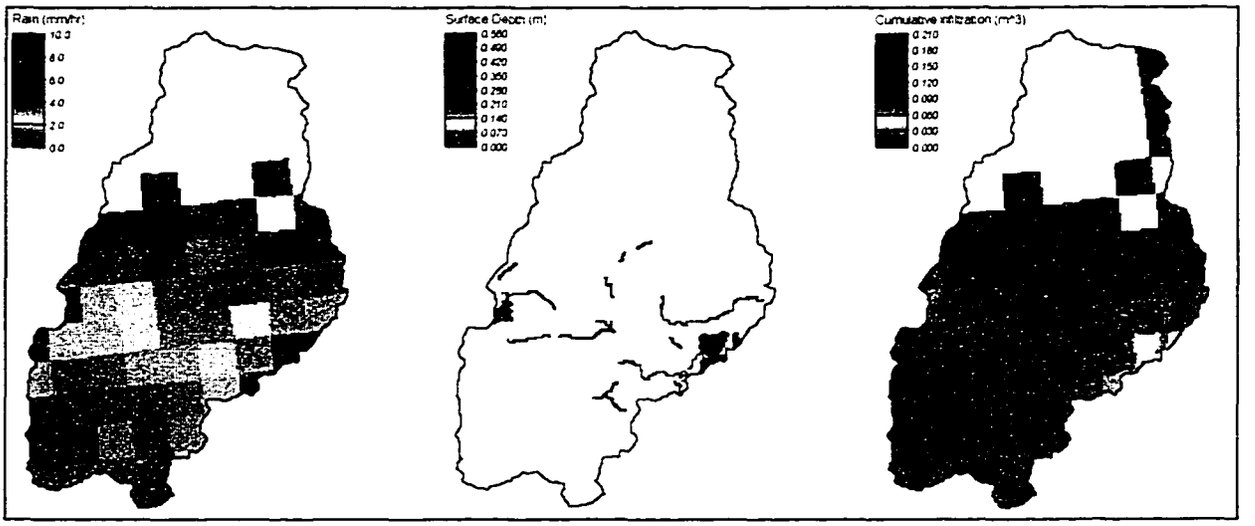

Figure 5.12 Rain, Surface Depth and Cumulative Infiltration - Time = 400 min.

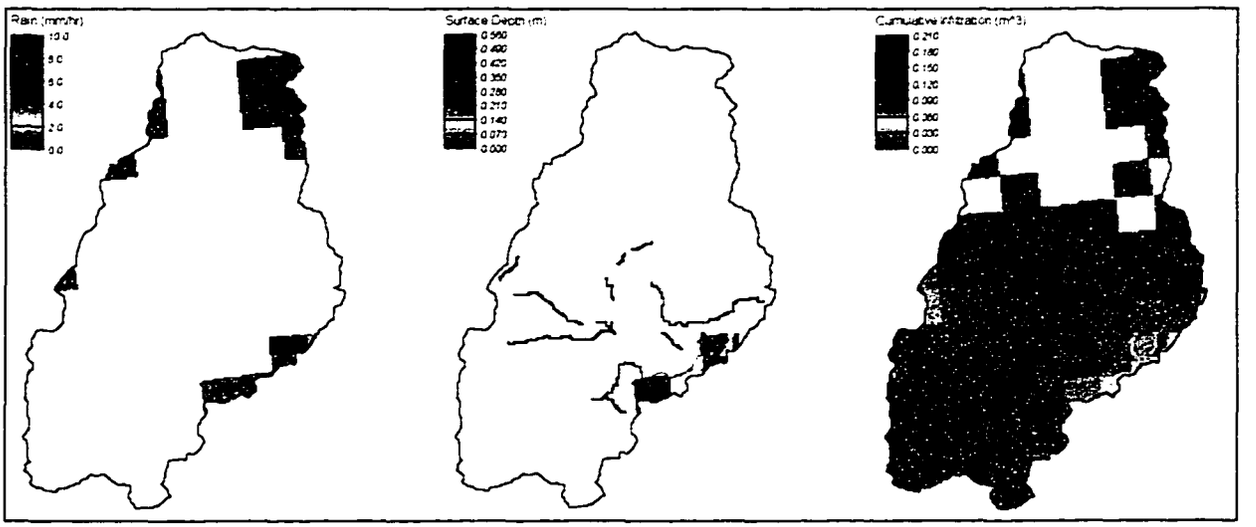

Figure 5.13 Rain, Surface Depth and Cumulative Infiltration - Time = 600 min.

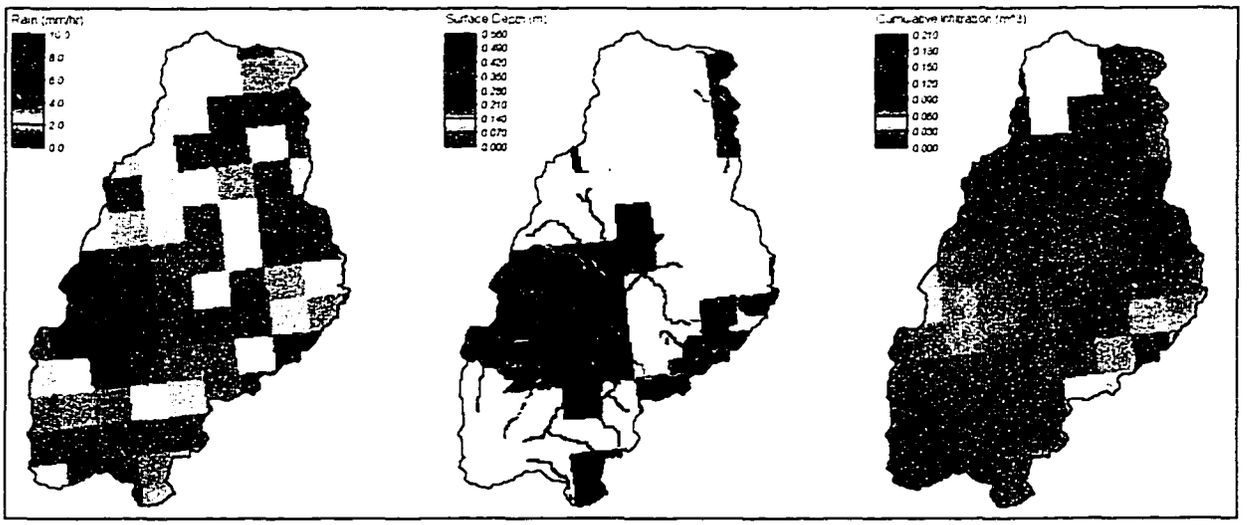

Figure 5.14 Rain, Surface Depth and Cumulative Infiltration - Time = 800 min.

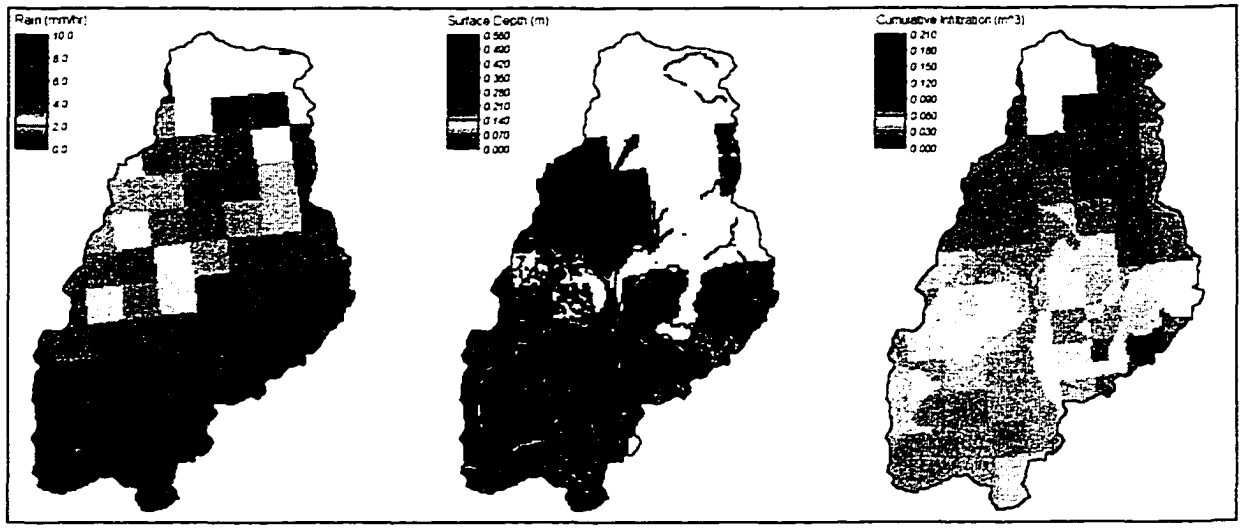

Figure 5.15 Rain, Surface Depth and Cumulative Infiltration - Time = 1000 min.

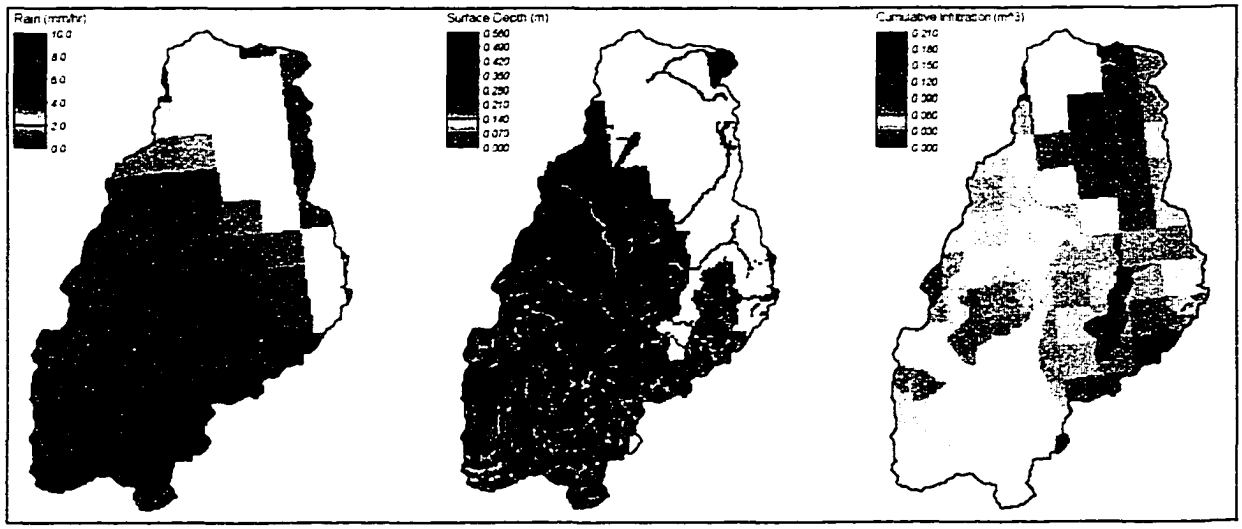

Figure 5.16 Rain, Surface Depth and Cumulative Infiltration - Time = 1200 min.

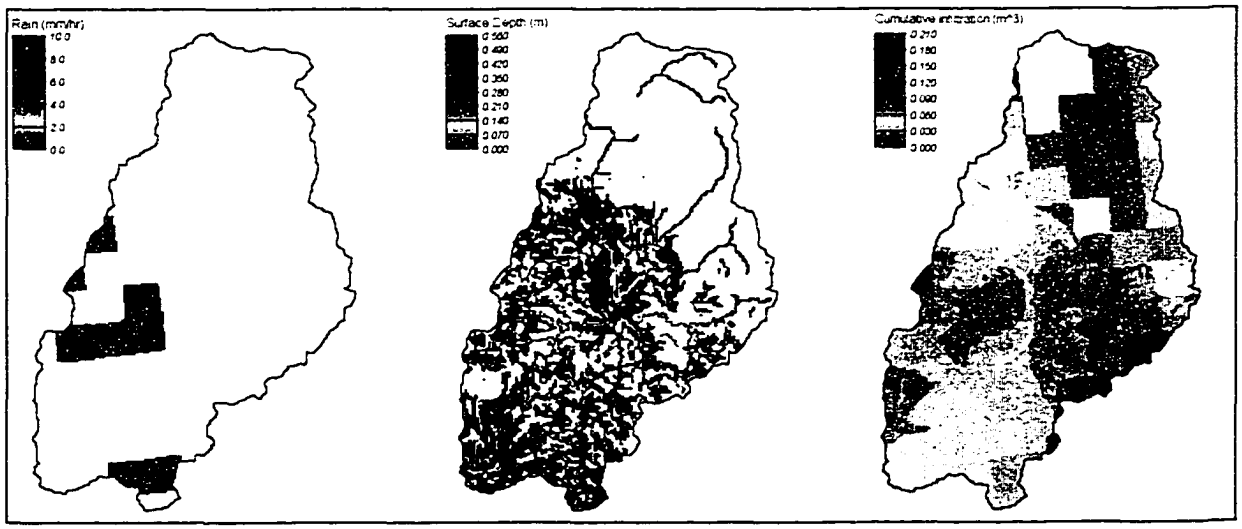

Figure 5.17 Rain, Surface Depth and Cumulative Infiltration - Time = 1400 min.

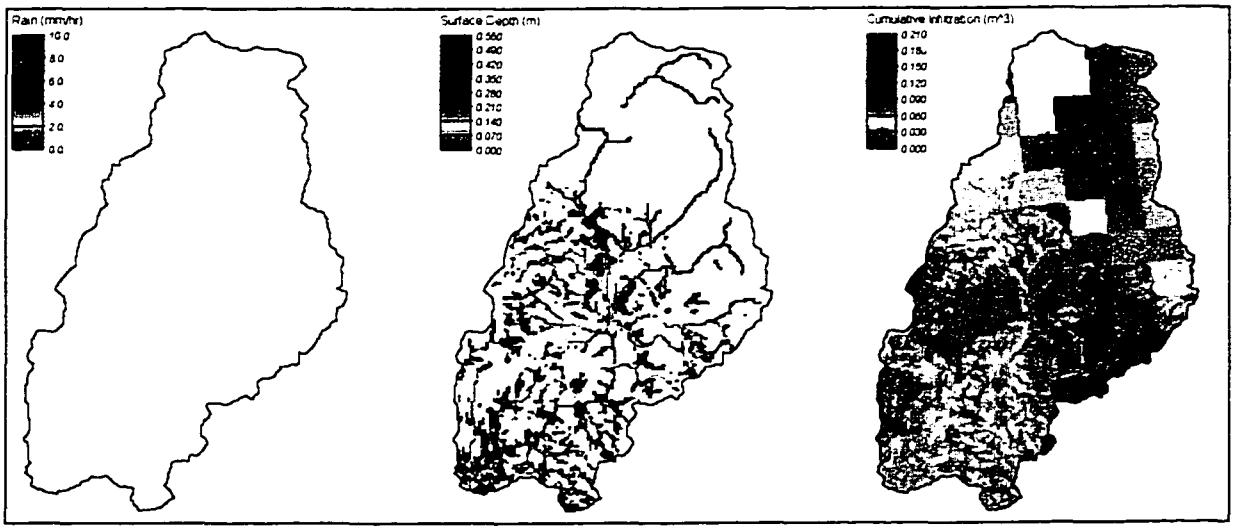

Figure 5.18 Rain, Surface Depth and Cumulative Infiltration - Time = 1600 min.

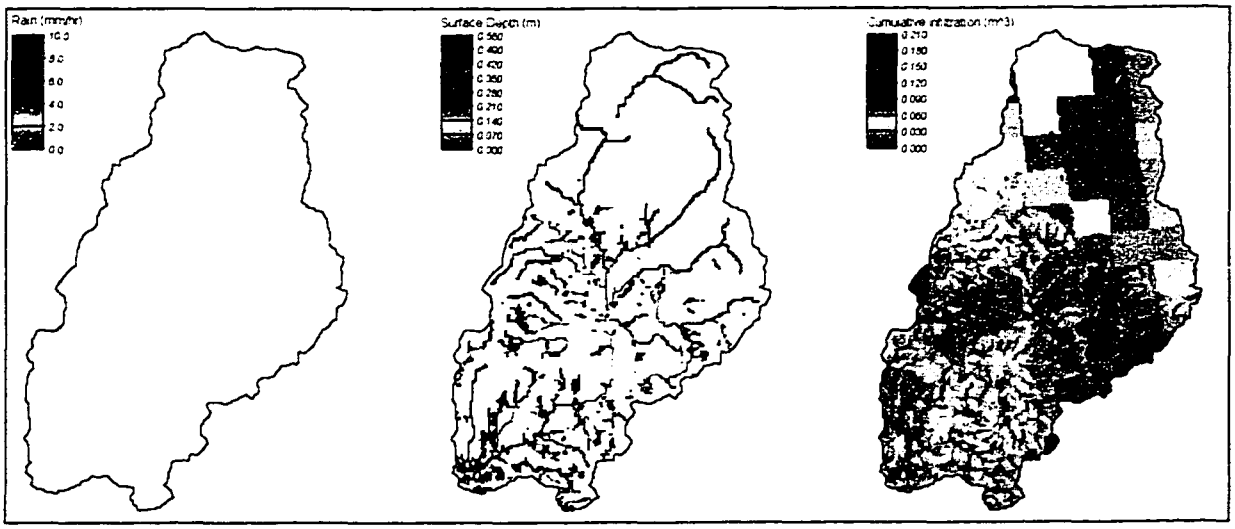

Figure 5.19 Rain, Surface Depth and Cumulative Infiltration - Time = 1800 min.

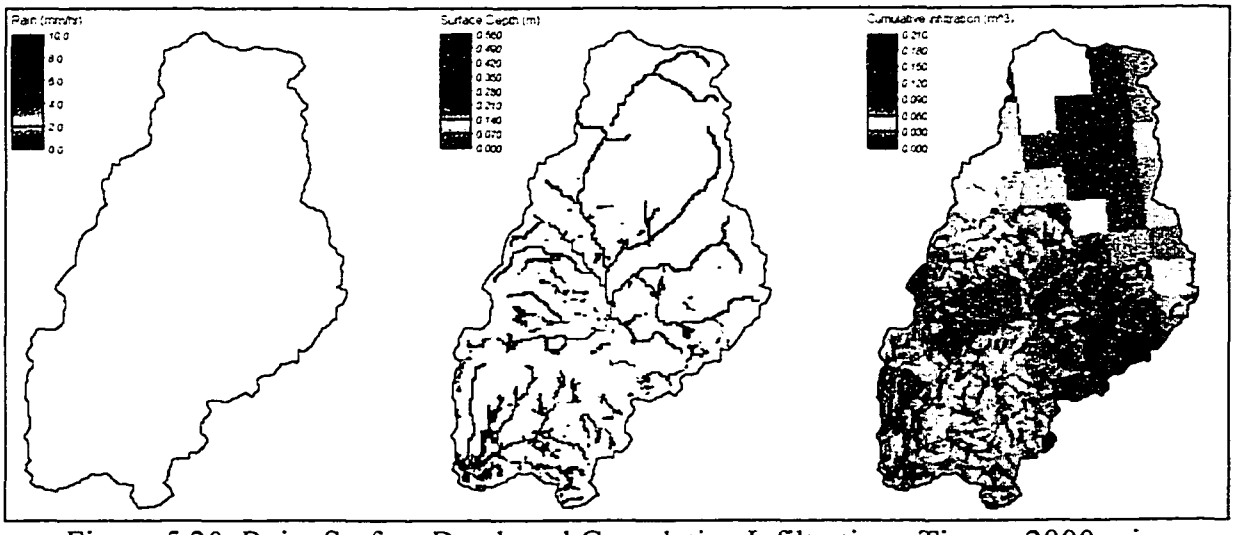

Figure 5.20 Rain, Surface Depth and Cumulative Infiltration - Time = 2000 min.

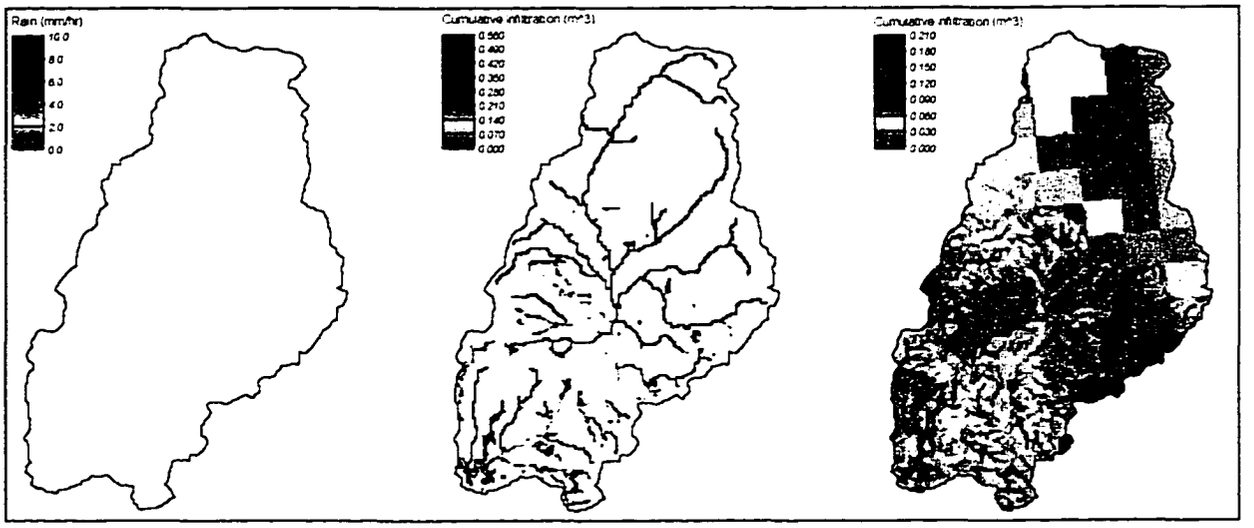

Figure 5.21 Rain, Surface Depth and Cumulative Infiltration - Time = 2200 min.

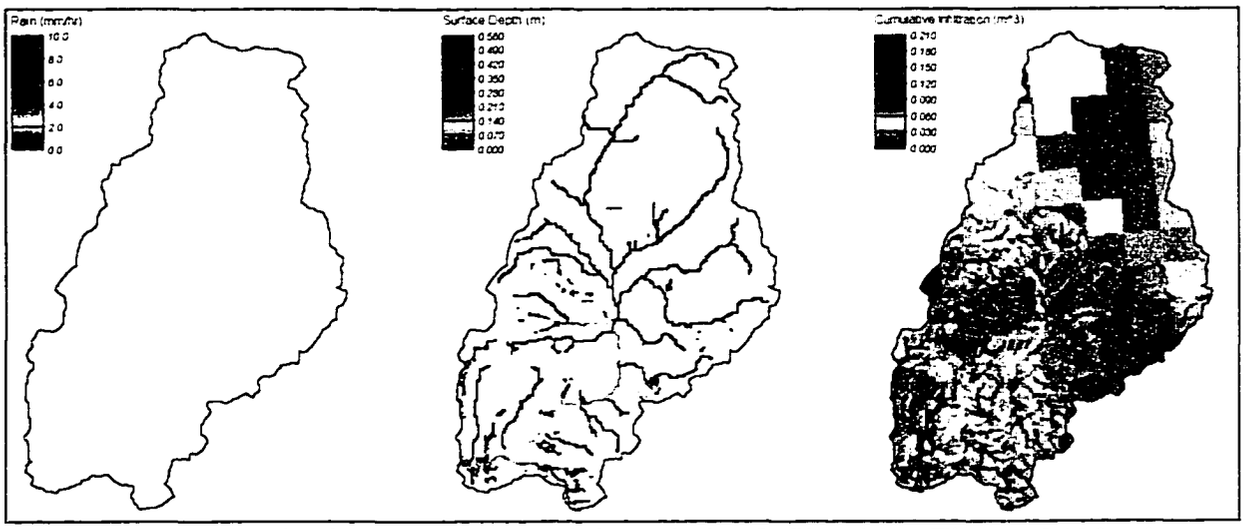

Figure 5.22 Rain, Surface Depth and Cumulative Infiltration - Time = 2400 min.

The intent of this effort was not to pursue the most rigorous possible treatment of the adjustment of radar data based on observed rain gauge data. Rather, the intent was to derive an adequate adjustment to the radar data for these events such that they may be considered representative of the actual rainfall over the watershed for modeling purposes. The revised Z-R relationship approach that was used herein to adjust the radar data may not be the best overall approach for dealing with radar data from the Phoenix, AZ radar

site, but the data presented above do indicate that this approach does produce rainfall estimates from the radar that are very well in line with the rain gauge measurements.

5.4 CHARACTERISTICS OF MOVING RAIN CELLS

The preceding analysis of radar data focused on the intensity of the rainfall data and the end result was a calibration process with which the radar data were adjusted to produce values that correspond more closely with measurements made by rain gauges. Another aspect of this dissertation is to perform a parametric analysis of moving rain storms to study the effects of storm size, intensity, and velocity on the peak flow for a watershed. This parametric analysis is presented in Chapter 6 and consists of applying a test matrix of moving storms across the Cave Creek and Hassyampa River watersheds, summarizing the peak flow that results from each of the moving storms, and ultimately analyzing the relationship between the storm parameters and peak runoff.

In order for such a parametric analysis to be meaningful, the range of values for the parameters of the storms chosen for the test matrix must be realistic. That is, it would not be particularly meaningful to use a series of storms moving across a watershed at a velocity of 500 km/hr with rainfall intensities of 500 mm/hr since those values are not within the realm of reality. Hence, some basis for the range of values for the storm parameters is needed. To that end, an analysis of the radar data from the four events for which data were available was performed to determine some estimates of typical storm sizes, velocities, and intensities. Of course these four storms cannot be considered to be representative of all storms in this region, but the procedure that was followed to analyze the storm parameters could be extended as more data are available.

Using the radar data from the four events, 100 rain cells were isolated and were tracked from their origins to the point at which they decayed and died out. Of these 100 cells, 25 were chosen from each of the four events. In this context, the term "rain cell" refers to any area over which the radar scan contains a contiguous series of grids with measurable precipitation that can be tracked as it moves over time. This may consist of anywhere from just a few radar grids up to thousands of radar grids. The process followed for each of the 100 rain cells was to isolate a particular cell from the radar scan and determine the centroid, size and average intensity for that cell. Then that same cell was isolated from the following radar scan and the same physical parameters determined. This was repeated at each update of the radar data until the cell decayed and died out entirely. Ultimately for each cell, the average size and average intensity were determined over the life span of the cell, and using the centroid and time increment information, the average velocity of each cell was also computed. The life span or duration of each cell was computed as the time interval from when the cell first appeared on the radar scan until the cell was gone.

An example of this process is illustrated in Figures 5.23 through 5.26. These images show a rain cell over four time intervals. Although these images represent only four time intervals from the life span of this rain cell, they illustrate the process used to derive the storm parameters for the 100 rain cells. Assume that the images in Figures 5.23 through 5.26 represent the entire life span of that rain cell. If this were the case, then the parameters for the rain cell at those time intervals might be as shown in Table 5.3

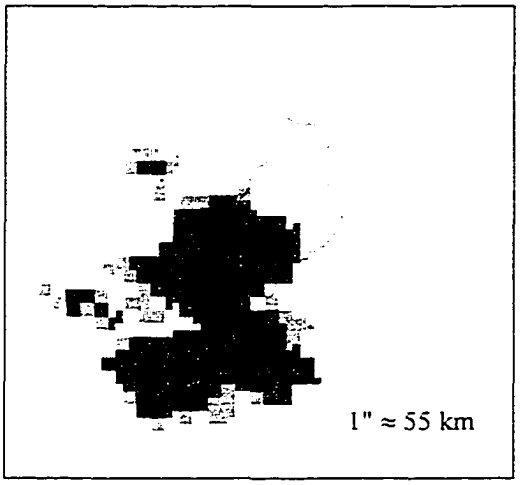

Figure 5.23 Radar Scan, Time = 01:00

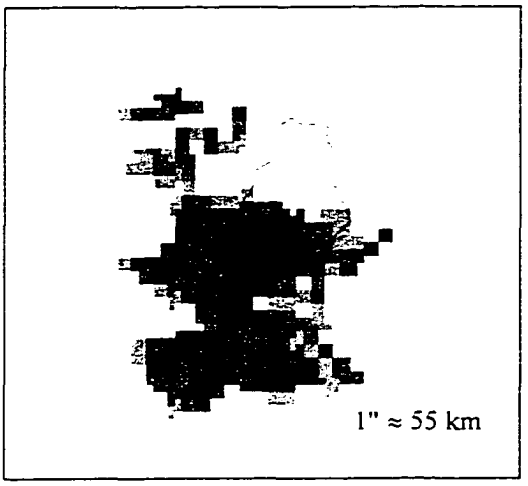

Figure 5.24 Radar Scan, Time = 01:12

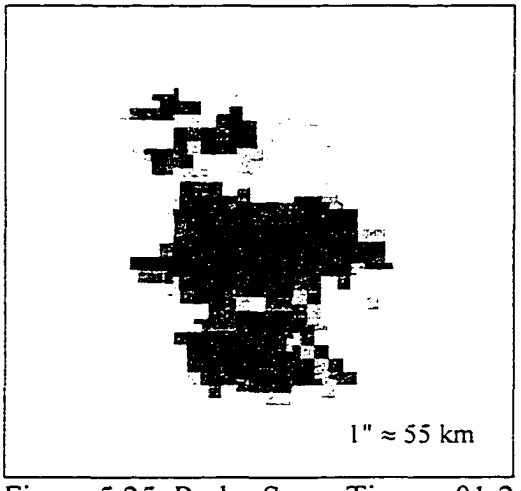

Figure 5.25 Radar Scan, Time = 01:24

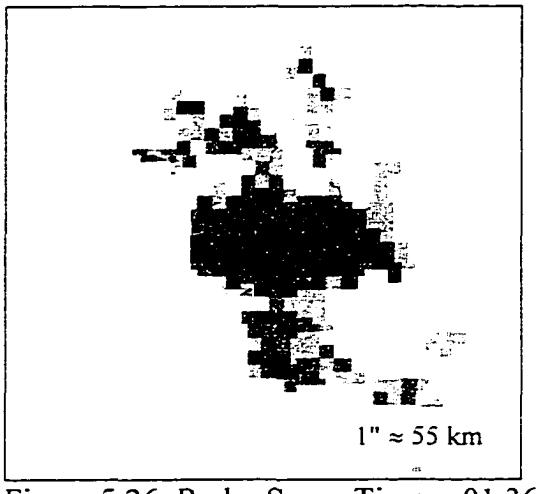

Figure 5.26 Radar Scan, Time = 01:36

Time (hr:min)	Centroid		Average Intensity (mm/hr)	Size (km^2)
	Easting (m)	Northing (m)		
01:00	274700	3733800	.77	2900
01:12	278100	3738900	.78	3120
01:24	282500	3744200	.75	3200
01:36	285200	3751000	.71	3800

Table 5.3 Sample Rain Cell Data

From the sample data in Table 5.3, the velocity of the rain cell is computed as the distance traveled by the centroid of the cell divided by the time interval. The storm parameters for this sample rain cell would be summarized as shown below in Table 5.4.

Time (hr:min)	Velocity (km/hr)	Intensity (mm/hr)	Size (km^2)	Life Span (hr)
01:00		0.77	2900	
01:12	30.6	0.78	3120	
01:24	34.4	0.75	3200	
01:36	36.6	0.71	3800	
Average	33.6	0.75	3255	0.6

Table 5.4 Summary of Sample Rain Cell Parameters

As a summary of the analysis of the radar data for all 100 rain cells, Table 5.5 provides a listing of the average size, velocity, intensity, and duration of the 25 storm cells from each of the four rainfall events. Values for the average of all 100 cells over the four events are shown in the last row of this table. Table 5.6 provides a more complete statistical picture of the parameters of these 100 rain cells.

Event	Avg. Velocity (km/hr)	Avg. Intensity (mm/hr)	Avg. Size (km2)	Avg. Life Span (hr)
05 Jan 95	26.7	5.0	2095	2.2
26 Jan95	24.0	5.1	1079	2.1
14 Feb 95	24.3	5.1	850	2.7
06 Mar 95	19.7	4.6	930	2.2
All Events	23.7	5.0	1239	2.3

Table 5.5 Summary of Rain Cell Parameters for 100 Cells

	Intensity (mm/hr)	Size (km^2)	Velocity (km/hr)	Life Span (hr)
Mean	2.0	1239	23.7	2.3
Std Dev	0.6	2270	14.3	1.6
Maximum	4.3	15178	63.3	9.8
Minimum	1.2	43	1.5	0.4

Table 5.6 Statistical Measures for 100 Moving Rain Cells

The cumulative distribution functions for each of these parameters are also plotted to provide a more graphical depiction of the data. Figures 5.27 through 5.30 show the cumulative distribution functions for the average intensity, average size, average velocity, and life span parameters of the 100 storm cells. The distributions shown in Figure 5.27 for the average intensity show the cumulative distribution functions based on both the original and calibrated radar data to show how that distribution was effected by the application of the calibration process to the radar data in the 100 rain cells.

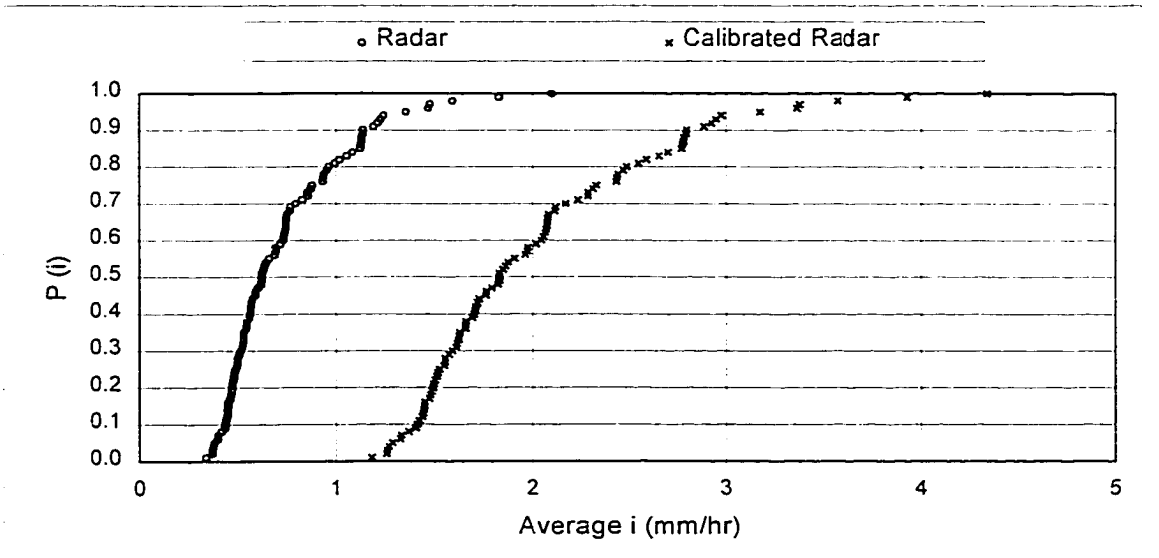

Figure 5.27 Cumulative Distribution Function for Average Intensity of 100 Rain Cells

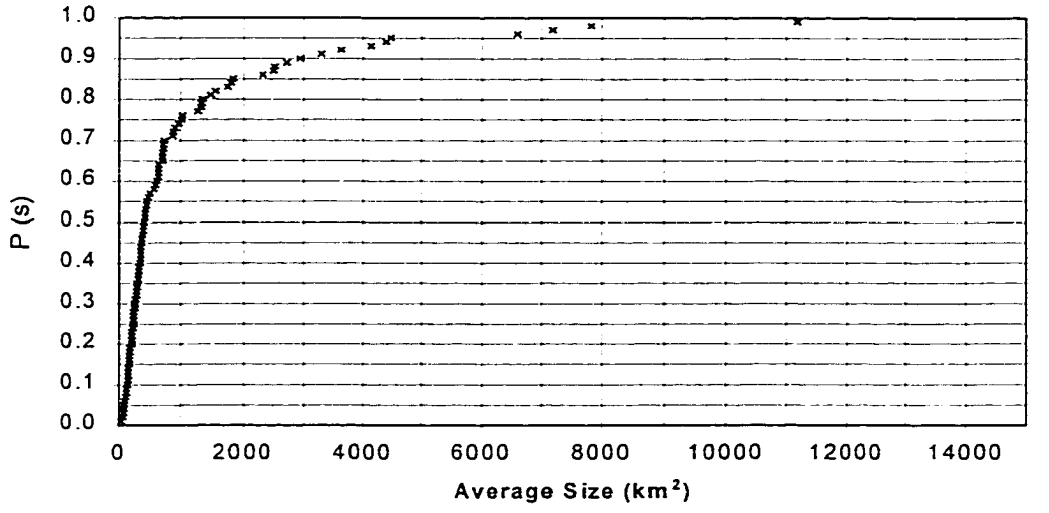

Figure 5.28 Cumulative Distribution Function for Average Size of 100 Rain Cells

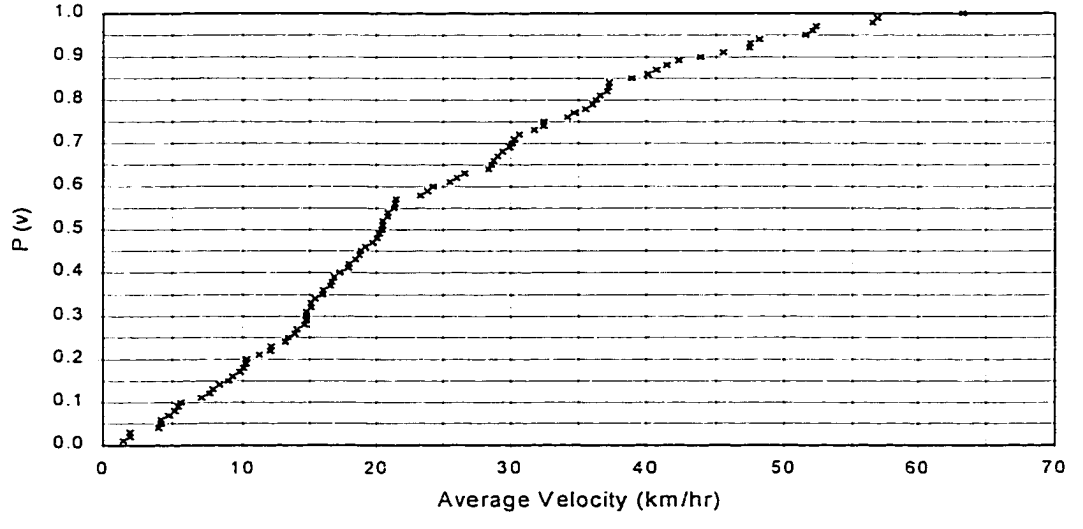

Figure 5.29 Cumulative Distribution Function for Average Velocity of 100 Rain Cells

Figure 5.30 Cumulative Distribution Function for Life Span of 100 Rain Cells

5.5 SUMMARY

Through comparison with ground observations from rain gauges for four rainfall events, the original radar rainfall intensity data available for this research was shown to provide precipitation intensities much lower than the rain gauge data. Rainfall intensity data have been shown by earlier researchers to have an exponential probability density function, but these original radar rainfall intensity data were shown to have a probability density function that is not distributed exponentially. The rain gauge data for these same rainfall events did have a probability density function that was more closely distributed exponentially. To calibrate the radar data to more closely correspond to the rain gauge data, a new Z-R relationship was applied. This resulted in a "calibrated" radar data set that was shown to have an exponential distribution that matched the distribution of the rain gauge data quite well. Further comparison of the rain gauge and radar measurements over the gauge locations revealed that the calibrated radar data produced a cumulative

precipitation total over the Hassyampa River watershed for two rainfall events that was within less than 1% of the cumulative precipitation total based on the six rain gauges in the watershed. The calibrated radar data were then used as the input to the calibrated CASC2D model for the Hassyampa River for two rainfall events, and for each event the model using these radar data input produced results that matched the observed flow quite well. Based on these findings, the calibrated radar data were considered accurate for the purposes of applying to the Hassyampa River watershed model as presented in Chapter 7.

Analysis of the radar rainfall data was also performed on 100 moving rain cells to quantify the typical range of values for precipitation intensity, storm velocity, storm size, and storm life span that occur in the region. These data revealed average intensity values ranging from 1.2 to 4.3 mm/hr, average rain cell sizes ranging from 43 to 15178 km^2, average velocities from 1.5 to 63.3 km/hr, and life spans from 0.4 to 9.8 hours. In Chapter 6, an analysis of storm parameters is presented wherein the effects of storm intensity, velocity and size on the peak runoff from a watershed are studied. Although the results of this rain cell analysis are representative of only data from four precipitation events, these results will serve as one basis on which the range of values for the storm intensity, velocity, and size are selected for that parametric analysis.

Chapter 6

EFFECTS OF STORM PARAMETERS ON PEAK RUNOFF

6.1 INTRODUCTION

Three of the parameters of a storm that can be estimated from radar measurements with greater detail than has generally been possible from rain gauges are the areal extent or size of the storm, the intensity of the precipitation, and the movement or velocity of the storm. It can certainly be argued that rainfall intensity is better determined from rain gauges, but the few point measurements provided by the typically sparse network of gauges do not provide a very complete picture of the spatial distribution of intensity that exists in a storm. The intent of the parametric analysis presented in this chapter was to analyze the response of a watershed to moving rainstorms of various size, intensity, and velocity to determine if a relationship exists between those storm parameters and the resultant maximum peak flow from the basin. If a correlation between these storm parameters and peak flow can be established, then the measurements of these parameters obtained from radar may be used to estimate peak runoff for an event before a storm actually reaches a basin or while an event is in progress. This information could provide a relatively simple tool for emergency managers or military planners to predict when potential flooding conditions might exist based on observations of storm parameters. For a given combination of storm

size, average intensity, and storm velocity, such managers could estimate if a storm has the potential to produce peak runoff above a specified threshold and could then take appropriate action.

6.2 BACKGROUND

Although this analysis will be conducted using a two-dimensional runoff model on actual watersheds with spatially varying parameters, a theoretical basis which defines the relationship between peak runoff and storm size, velocity and intensity will be explored starting with flow on a simple rectangular inclined plane. The first step in this process is to specify whether a partial equilibrium hydrograph or a complete equilibrium hydrograph represents the runoff. Partial equilibrium and complete equilibrium describe the two basic runoff conditions that may exist for a simple plane or a complex watershed. To answer this question, the concept of time to equilibrium t_e and its relationship to the duration or time of rain t_r will be briefly introduced.

The time to equilibrium t_e is defined as the time at which surface runoff reaches an equilibrium state, or the time at which the outflow is in equilibrium with the net inflow. On a rectangular plane, this time to equilibrium is reached when the flow depth h is sufficiently large to convey the equilibrium discharge q. The flow depth h at time t_e is a function of the rainfall intensity i as

$$h = it_e \tag{6.1}$$

The equilibrium discharge q is related to the flow depth through the resistance relationship which is a power function of the flow depth for surface runoff as

$$q = \alpha h^{\beta} \tag{6.2}$$

where α is generally defined for turbulent flow in terms of such parameters as resistance coefficient, friction slope and gravitational acceleration depending on whether the Darcy-Weisbach, Chezy or Manning relationship is used. The parameter β is taken as 1.5 for the Darcy-Weisbach and Chezy relationship and 1.67 for the Manning approach. When equilibrium conditions are reached, the equilibrium discharge is related to the excess rainfall intensity and runoff length L as

$$q = iL \tag{6.3}$$

From equations (6.1) through (6.3), the general solution for t_e is a function of the flow resistance relationship, excess rainfall intensity and runoff length as

$$t_e = \left(\frac{L}{\alpha i^{\beta-1}}\right)^{1/\beta} \tag{6.4}$$

In the CASC2D model, the Manning resistance relationship is used wherein the resistance coefficient is n, the parameter α is $S^{1/2}/n$, and $\beta = 1.67$. Combining these with equation (6.4) gives the following solution for t_e using the Manning resistance relationship

$$t_e = \left(\frac{nL}{S^{1/2} i^{2/3}}\right)^{.6} \tag{6.5}$$

where n is the Manning resistance coefficient, L is the runoff length, S is the friction slope, and i is the excess rainfall intensity.

For complete equilibrium conditions to occur, the duration of rainfall must equal or exceed the time to equilibrium. This typically will occur on small watersheds where the runoff length L is small and therefore the time to equilibrium is small. On larger watersheds, the runoff length is usually large enough such that the time to equilibrium is

larger than the duration of rainfall and partial equilibrium conditions exist. For example, taking into account all 100 of the moving rain cells that were analyzed in Chapter 5, the time to equilibrium for all 100 of those storm cells would be greater than the duration of the rainfall over either the Cave Creek or Hassyampa River watersheds. Taking the average values from those 100 rain cells for size and velocity, the average duration of rainfall for them could be computed by using the square root of the storm area as representative of the length of the storm and estimating the duration of rainfall as the length of the storm divided by the velocity of the storm as

$$\bar{t}_r = \frac{\sqrt{\bar{A}_s}}{\bar{V}_s} = \frac{\sqrt{1238.5 km^2}}{23.7\, km/hr} \approx 1.5 hr \tag{6.6}$$

where A_S is the average area of the 100 rain cells and V_S is the average velocity of the 100 rain cells as shown in Table 5.5 of Chapter 5. Then, using the average rainfall intensity for those 100 rain cells as i = 2.0 mm/hr = .00000056 m/s, and the parameters for the Cave Creek watershed with average Manning n = 0.063, average slope S = 0.125, and runoff length estimated as the square root of the watershed area A_W = 349000000 m^2, the time to equilibrium from equation (6.5) would be computed as

$$\bar{t}_e = \left(\frac{nA_w^{1/2}}{S^{1/2} i^{2/3}} \right)^{.6} = \left(\frac{.063 * 349000000^{1/2}}{.125^{1/2} * .00000056^{2/3}} \right)^{.6} = 42325 \text{sec} = 11.7 hr \tag{6.7}$$

Given that the Hassyampa River watershed has similar slope and roughness parameters as the Cave Creek watershed and the area of the Hassyampa River basin is more than three times larger than the area of Cave Creek, the time to equilibrium for the Hassyampa River watershed would be longer than that computed above for Cave Creek.

Therefore, it is reasonable to conclude that complete equilibrium conditions are rarely, if ever, reached on the watersheds used for this study, and the remainder of this analysis will proceed based on an assumption of partial equilibrium conditions.

Returning to flow on a simple plane, for partial equilibrium conditions the unit discharge q is a function of Manning n, friction slope Sf, excess rainfall intensity i_e, and time t as:

$$q = \frac{S_f^{1/2}}{n}(i_e t)^{5/3} \tag{6.8}$$

For a partial equilibrium hydrograph, the time of rain is less than the time to equilibrium, and the peak discharge will occur at the time when the rain has been falling for the longest duration, or when $t = t_r$. Thus, for equation (6.8) to apply to the peak discharge, then the duration of rain t_r may be used as the time t as follows:

$$q_p = \frac{S_f^{1/2}}{n}(i_e t_r)^{5/3} \tag{6.9}$$

For a moving storm with length L_S and velocity V_S, the time of rain over any given location may be expressed as a function of the size and velocity of the storm as:

$$t_r = \frac{L_s}{V_s} \tag{6.10}$$

Substitution of (6.10) into (6.9) then leads to the following expression for peak discharge under partial equilibrium conditions:

$$q_p = \frac{S_f^{1/2}}{n}\left(i_e \frac{L_s}{V_s}\right)^{5/3} \tag{6.11}$$

If kinematic conditions are assumed to apply such that the friction slope equals the slope of the runoff surface as $S_f = S_0$, and that the values for S_0 and n on a given runoff surface are constant, then for that runoff surface the relationship $S_f^{1/2} / n$ will be defined as a constant κ as:

$$\frac{S_f^{1/2}}{n} = \frac{S_0^{1/2}}{n} = \kappa \tag{6.12}$$

Now, combining (6.11) and (6.12) yields

$$q_p = \kappa \left(i_e \frac{L_s}{V_s} \right)^{5/3} \tag{6.13}$$

In this manner, it is evident for a given runoff surface with constant slope and roughness under partial equilibrium kinematic flow conditions that the peak discharge can be expressed as a function of the storm intensity, size and velocity. Therefore, for a constant peak discharge q_p, the value of $(i_e L_S / V_S)$ must be constant. This constant value, which holds for a given constant value of q_p, will be called K_p and the values of L_S and V_S/i_e are then shown to be linearly related as:

$$\frac{i_e L_s}{V_s} = K_p \tag{6.14}$$

or,

$$L_s = K_p \frac{V_s}{i_e} \tag{6.15}$$

This requirement for a constant value of $i_e L_S/V_S$ makes sense physically in that this combination of parameters defines the depth of rainfall. If the depth of rainfall is constant, then the peak discharge resulting from that rainfall will be constant. A change

in any one of the three parameters must be offset by a corresponding change in one or both of the other parameters such that the depth of rainfall remains constant for a constant peak discharge. This linear relationship may be shown graphically in a non-dimensional form by dividing the storm length L_S by the constant value of the length of the runoff plane L_p, and plotting L_S/L_p vs. V_S/i_e. On this plot, storms that produce equivalent peak discharge q_p should plot on a straight line as shown in Figure 6.1. Different lines will exist for different values of q_p, and the lines will have a steeper slope for smaller values of q_p and a flatter slope for larger values of q_p. The lines will not continue to the origin because at the origin the storm velocity must be zero. If the velocity is zero, then the duration of rainfall is infinite and equilibrium conditions will occur, and this plot is valid only for partial equilibrium conditions. There is a point when either the velocity approaches zero or the intensity becomes very large that the duration of rainfall will exceed the time to equilibrium and the partial equilibrium condition will no longer be valid. Similarly, the lines will not continue at the constant slope indefinitely as the storm size increases. At some very large storm size, that storm will remain over the basin for a long enough duration that the duration of rainfall will again exceed the time to equilibrium. Thus, the plot shown in Figure 6.1 is valid only for that range and combination of parameters that will result in a partial equilibrium condition.

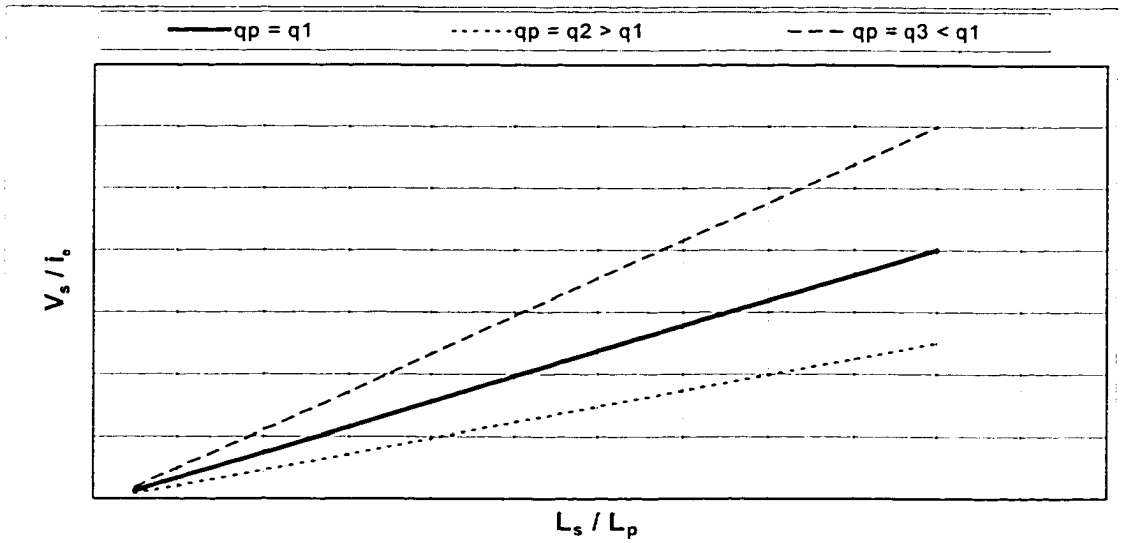

Figure 6.1 Theoretical Plot of L_s/L_p vs V_s/i_e for Storms with $q_p = q_1, q_2, q_3$

6.3 EQUIVALENT STORMS

This combination of storm parameters can be thought of in terms of equivalent storms that produce equivalent rainfall depths and thus equivalent peak discharge. Yen and Chow (1969) defined equivalent storms as storms moving at different speeds with the same duration of rainfall at each point on a watershed and identical total rainfall volume on the catchment. They maintained constant rainfall volume between equivalent storms moving at different speeds by holding the precipitation intensity constant and varying the storm size, which then required that the length be directly proportional to the speed of equivalent storms. Ogden et al. (1995) proposed an alternate definition of equivalent storms that specified that the volume of rainfall on the catchment be equal and that the physical size of equivalent storms be equal. This definition required that the intensity be directly proportional to the velocity for equivalent storms of equal size. An alternative definition of equivalent storms is introduced here in which equivalent storms are defined

as storms that have the same value of $i_e L_S/V_S$. This definition does not required that any of these three parameters be constant, but merely that for any two storms to be considered equivalent storms, the value of $i_e L_S/V_S$ for each storm must be equal. That is, if a given storm has parameters i_1, L_1, V_1 and another storm has parameters i_2, L_2, V_2, then the following must be true for those two storms to be considered equivalent storms

$$\frac{i_1 L_1}{V_1} = \frac{i_2 L_2}{V_2} \tag{6.16}$$

If (6.16) holds true for those two storms, then the peak discharge that results from those two storms on a given runoff surface will be equal.

The above derivation of the linear relationship between L_S and V_S/i_e and the concept of equivalent storms that possess equivalent values of $i_e L_S/V_S$ were based on flow from a simple plane. However, if these concepts can be shown to be applicable to runoff conditions on a watershed, then this would provide a very useful means of estimating peak runoff. For example, if the size, velocity and intensity of a storm can be estimated from radar images, then a plot such as in Figure 6.1 might be used to estimate the potential peak runoff for that storm. Alternatively, such a plot might be used to estimate whether or not a particular storm has the potential to create a peak runoff that exceeds a specified threshold level. The remainder of this chapter details an analysis of storm parameters that was conducted to extend these concepts to the watershed scale.

6.4 EXPERIMENTAL APPROACH

Using the calibrated CASC2D watershed models of the Cave Creek and Hassyampa River watersheds as presented in Chapter 4, a parametric analysis of storm velocity, intensity and size parameters was conducted. This parametric analysis consisted

of applying to each watershed a series of moving storms of various velocities, intensities, and sizes. The peak discharge from the watershed for each of the storms was determined, and the results summarized in a plot similar to that in Figure 6.1. The intent of this analysis was to determine if there exists a linear or near linear relationship between the storm parameters L_S and V_S/i_e for constant values of peak runoff from a watershed as was shown to exist for a simple inclined plane.

A test matrix of moving storms for this analysis was developed which included a range of storm velocities, intensities, and sizes. The ranges of these parameters were selected so as to include the range of values that each of the parameters might reasonably have in nature. Thus, minimum and maximum values for the storm velocity, intensity, and size were determined, and a range of values between those maximum and minimum values was chosen to complete the test matrix. A brief discussion of each storm parameter is provided in the following sections.

6.4.1 Storm Velocity

The storm velocity for the purposes of this analysis was considered to be the average velocity at which a storm traverses the watershed. No existing research was located which quantified typical storm velocities in the region of Arizona where Cave Creek and the Hassyampa River are located. However, personal correspondence (Dempsey and Skindlov, 1998) with meteorologists in Phoenix, AZ indicates that storm velocities moving through the region would typically have velocities in the range from 15 to 65 km/hr. Researchers conducting work with moving rainstorms in other regions (Bras, 1990; Singh, 1997) have used storms with velocities in the range from 10 to 50 km/hr. Analysis of the 100 moving rain cells in Chapter 5 indicated velocities in the

range from 1.5 to 63.3 km/hr with a mean value of 23.7 km/hr. For the test matrix of storms in this research, the range of storm velocities chosen was from 10 to 70 km/hr.

6.4.2 Storm Size

In nature, storms can assume a variety of shapes from circular to oval to more elongated or irregular shapes. For this work, storms with a block or square shape were chosen with sizes that correspond to the resolution of data from the WSR-88D radar system. The smallest storm was selected to be the size of a single radar grid cell which is 4 x 4 km or 16 km^2 in area. The largest size selected was the size that would completely encompass the watershed. For Cave Creek, the watershed is approximately 36 km in length along its longest axis, so a block storm of 36 x 36 km or 1,296 km^2 was chosen as the largest storm for the Cave Creek basin. The Hassyampa River watershed is approximately 64 km in length along its longest axis, so a block storm of 64 x 64 km or 4,096 km^2 was used as the largest storm for the Hassyampa River basin. For each of the two watersheds, the largest storm selected had an area approximately 3.7 times that of the watershed area.

6.4.3 Storm Intensity

The radar and rain gauge data for the few rainfall events used in this research provide a data set that is much too small to be considered representative of storms in the region. Thus, rainfall intensity values chosen for the test storm matrix were based on historical intensity-duration data for precipitation in central Arizona. The smallest intensity would be for a 1-year return period event with the longest duration and the largest intensity from a 100-year return period event with the shortest duration. The storm in the test matrix with the shortest duration (4 x 4 km storm traveling at 70 km/hr)

would take approximately 30 minutes to traverse each of the watersheds, and the storm with the longest duration would take approximately 4 hours to traverse each of the watersheds. The maximum rainfall for the test matrix was selected as the 100-year return period 30-minute duration event, which has an intensity of approximately 101.6 mm/hr (4 inches per hour). The minimum rainfall for the test matrix was selected as the 1-year return period 4-hour event, which has an intensity of approximately 6.4 mm/hr (0.25 inches per hour) (U.S. Department of Commerce, 1961).

6.4.4 Complete Test Storm Matrix

The maximum and minimum values for the storm velocity, size and intensity were selected as detailed in the previous sections. To fill in the test matrix of storms, additional values of each parameter were chosen to provide a complete range between the maximum and minimum values. For the storm size, each storm consisted of a square block of 4 x 4 km cells, such that the smallest was 4 x 4 km, the next largest 8 x 8 km, and on up to the largest of 64 x 64 km. Table 6.1 shows the parameter values that were chosen for the 400 storms in the test matrix. Note that the minimum precipitation intensity from the intensity-duration analysis in section 6.2.3 was 0.25 inches per hour (6.4 mm/hr), however, initial models runs with this precipitation intensity resulted in little or no runoff from the watersheds due to infiltration. Thus, the minimum intensity used was 12.7 mm/hr which does result in enough excess precipitation to generate runoff.

Velocity (km/hr)	Size (km^2)	Intensity (mm/hr)
10	16	12.7
25	64	25.4
40	144	50.8
55	256	76.2
70	400	101.6
	576	
	784	
	1024	
	1296	
	1600	
	1936	
	2304	
	2704	
	3136	
	3600	
	4096	

Table 6.1 Storm Parameters for Test Matrix

6.4.5 Storm Direction and Path

Two final variables considered were the direction in which a storm travels, and the path that a storm follows as it crosses a watershed. Each of these will influence the peak runoff. For example, storms traveling in the general downstream direction over a watershed have been shown to generate higher runoff than those traveling in an upstream direction. Additionally, a storm which crosses a watershed along a path where the watershed is narrow will certainly result in lower runoff than that same storm crossing a wider portion of the basin.

For this parametric analysis, the effects of storm direction were removed by only moving storms across the watersheds in one direction. Analysis of radar data and personal conversations with meteorologists in the region (Dempsey and Skindlov, 1998) indicate that the majority of storms crossing this area move in an easterly direction.

Thus, each of the storms in the test matrix were moved across the basin starting from the west of the basin and moved directly east across the watershed.

There are theoretically an infinite number of paths that a storm might follow. Since the focus of this research is on peak flows, and in particular peak flows which are large and might cause flooding or damage, an approach was taken to select the path for each storm that will result in the highest peak. The path of maximum peak was determined for each storm size in the test matrix by running storms of each size across the basin starting at the lowest end of the basin, then moving that same storm along a path 4 km to the North of the first path, and repeating this in increments of 4 km until the upper end of the storm coincided with the upper end of the basin. For example, the 8 x 8 km storm was run across the Cave Creek basin along seven paths as shown in Figure 6.2 The line labeled as Path 1 is the centerline of the first path and is located 4 km above the Southernmost portion of the basin. Thus, the 8 x 8 km storm moving along that path had its Southernmost edge coincident with the Southernmost edge of the basin and extended up to cover the 8 km to the North. Similarly, the line labeled Path 2 is the centerline of the second path and is 4 km above Path 1, and so on for the remaining paths.

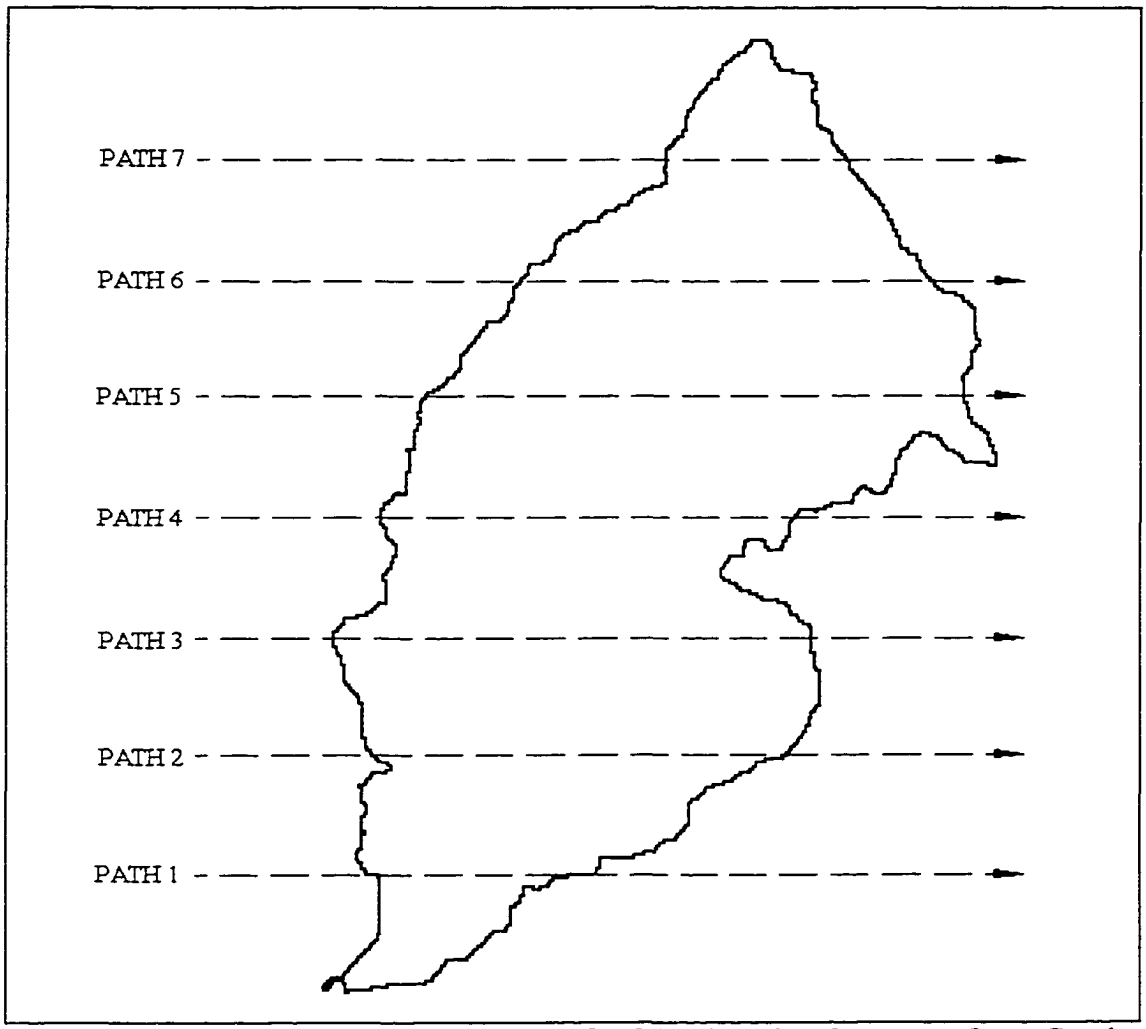

Figure 6.2 Centerlines of 7 Storm Paths for 8 km by 8 km Storm on Cave Creek

For each of the paths shown in Figure 6.2, a storm with the same intensity and velocity was moved across the basin to determine which path resulted in the highest peak flow. For the 8 x 8 km storm over Cave Creek, the hydrographs that resulted from the seven storm paths are shown in Figure 6.3.

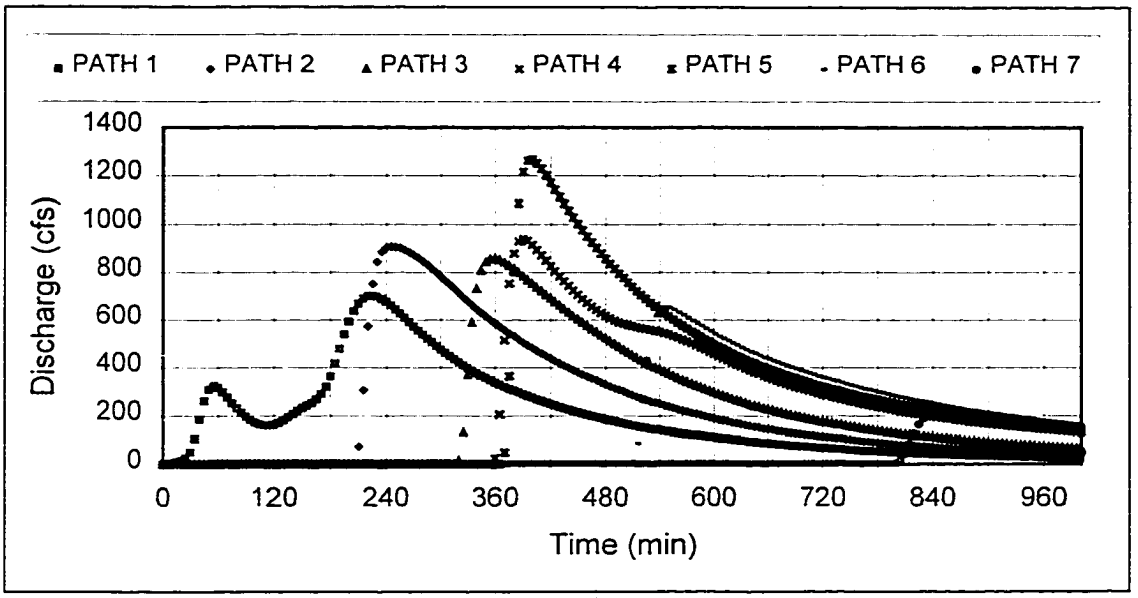

Figure 6.3 Hydrographs for 8 x 8 km Storm along 7 Storm Paths

The storm moving with its centerline along Path 5 resulted in the highest peak flow for the 8 x 8 km storm. From Figure 6.2 it is apparent that Path 5 crosses the basin at its widest location and thus a storm moving along that path will drop the largest volume of precipitation over the basin as compared to identical storms moving along any of the other six paths. This process was repeated for all of the storm sizes on both the Cave Creek and Hassyampa River watersheds to determine the path for each storm size that produced the highest peak flow. That path was then used as the path along which the storms of that size were moved for all subsequent model runs in the parametric analysis.

6.5 RESULTS

When considering potential flooding conditions, the two primary characteristics of a runoff hydrograph of importance are the peak flow and the time at which that peak flow occurs. Of these, the peak flow is arguably the more important in that it is the peak that determines whether or not flooding or damage will occur. If the peak is great enough

to reach the top of a levee or other retaining structure or if the peak is great enough to hinder movement of military vehicles, then actions will need to be taken to mitigate damage or implement contingency plans. If the peak is less than that threshold, then the peak may pass generally without incident. The time at which that peak will occur, or the time to peak, is the other hydrograph characteristic of importance, although it is not a primary focus of this research. The effects of storm parameters as they relate to peak runoff are detailed in the following sections.

6.5.1 Storm Parameter Effects on Peak Runoff for Cave Creek

Simulation results from the model runs using the storms in the test matrix, a total of 225 model runs for Cave Creek and 400 model runs for the Hassyampa River, were compiled by summarizing the peak flow for each simulation. From the storms in the test matrix, a plot of the test storm parameters was generated by plotting L_S/L_p vs. V_S/i_e for each of the storms. Shown in Figure 6.4 is a plot for the storms in the Cave Creek test matrix in which the representative storm length L_S is the square root of the storm size, the representative watershed length L_p is the square root of the watershed area, V_S is the storm velocity in km/hr, and i is the storm intensity in mm/hr.

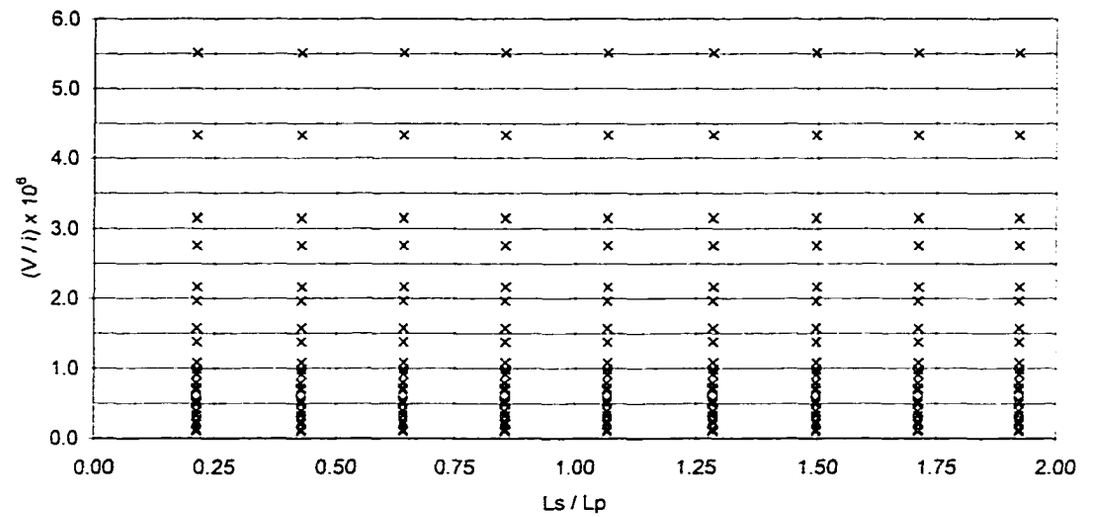

Figure 6.4 Plot of L_s/L_p vs V_s/i for Cave Creek Test Storm Matrix

The data plotted in Figure 6.4 simply reflect the range of storm parameters that were used in the test matrix and provide no indication of the peak flow resulting from each storm. All storms in the test matrix are represented on this plot, regardless of the peak flow associated with the storm. To make use of the data plotted in Figure 6.4, a particular peak flow value of interest must first be selected. For example, assume that for Cave Creek a peak flow of 20,000 cubic feet per second (cfs) results in a water level in the stream that causes flood damage to a substantial number of structures. For a peak flow of 20,000 cfs, some storms in the test matrix had peak flows that exceeded that level and the remainder had peak flows less than 20,000 cfs. The data in Figure 6.4 are plotted again, but in this new plot the storms with peak flow above 20,000 cfs are represented by red symbols while the storms with peak flow less than 20,000 cfs are shown with green symbols.

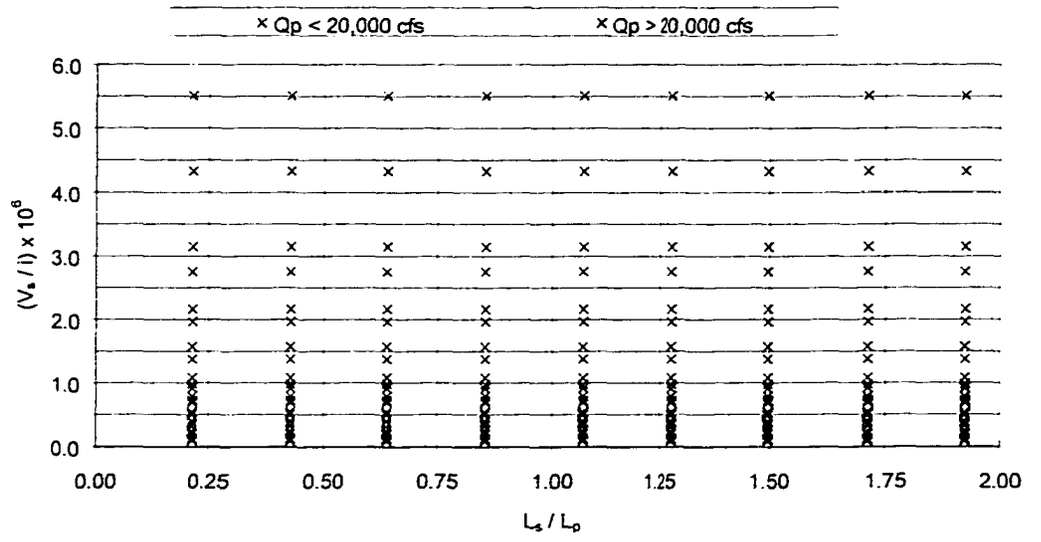

Figure 6.5 Storm Parameter Plot for 20,000 cfs Peak Flow on Cave Creek

The data in Figure 6.5 were plotted using the actual precipitation intensity, but the excess intensity is more appropriate. Expanding the vertical scale of Figure 6.5 and replotting the data using the excess precipitation intensity results in Figure 6.6 which shows a clear delineation between storms less than and greater than 20,000 cfs.

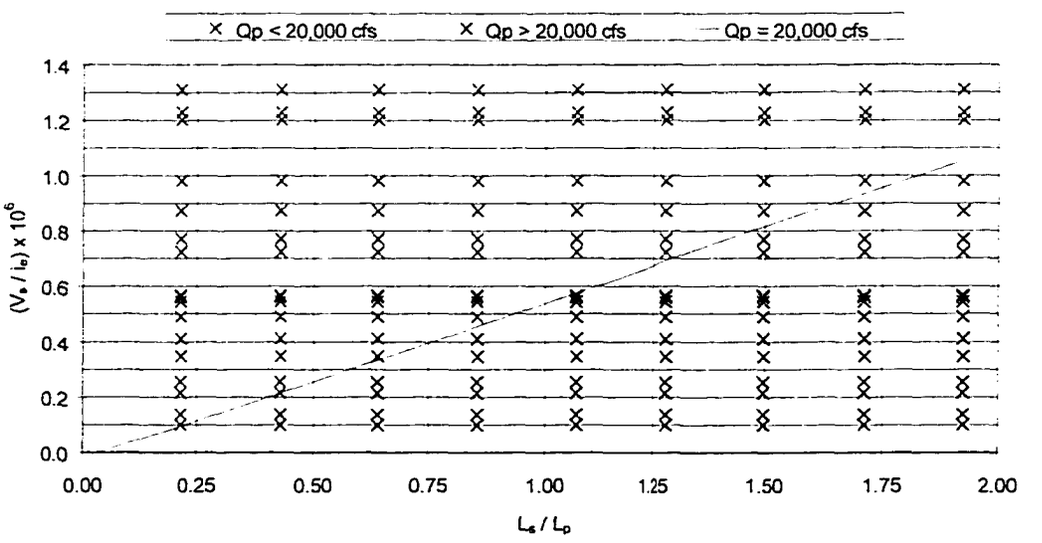

Figure 6.6 Expanded Storm Parameter Plot for 20,000 cfs Peak Flow on Cave Creek

The blue line in Figure 6.6 is drawn along the nearly linear delineation between storms above and below 20,000 cfs and represents a line of constant peak discharge. Storms that plot above the line would generally have peaks less then 20,000 cfs and those that plot below the line would generally have peaks greater than 20,000 cfs. Note that this supports the concept of the linear relationship between L_S and V_S/i for constant peak discharge presented in section 6.2 of this chapter. This same procedure can be used with the storm parameter plot for any peak flow of interest. Recall that all storms in the test matrix are represented on the storm parameter plot, regardless of their peak discharge. Thus, once the model is run with the test storms, the data exist from which to plot the line of approximate constant peak for any given peak flow.

Another way in which the results in Figure 6.6 may be viewed is to recall equation 6.13 which showed that $q_p = \kappa (i_e L_S/V_S)^{5/3}$. In that equation, which was developed for flow on an inclined plane, the term κ represented the term $S^{1/2}/n$ and was assumed to be constant for a particular runoff surface. If the relationship in equation 6.13 is to hold true at the watershed scale as is indicated by Figure 6.6, then there should be a similar term to κ that would apply at the watershed scale. However, rather than being a simple expression of the slope and roughness of the inclined plane, the watershed scale term would account for the combined slope, roughness, and channel routing effects in the watershed. Calling this term κ_W, the following form of equation 6.13 is presented for the watershed scale:

$$Q_p = \kappa_w \left(\frac{i_e L_s}{V_s} \right)^{5/3} \tag{6.17}$$

If equation (6.17) holds true at the watershed scale, then equation (6.17) may be used in two ways. It may be used to estimate the storm parameters required for a given peak flow, and it may be used to estimate the maximum potential peak flow for a given set of storm parameters. For example, consider two storms. One storm has peak Q_1 and parameters L_1, i_1, and V_1 while the second storm has peak Q_2 and parameters L_2, i_2 and V_2. Equation (6.17) may be written for these storms as:

$$Q_1 = \kappa_w \left(\frac{L_1 i_1}{V_1} \right)^{5/3} \tag{6.18}$$

and

$$Q_2 = \kappa_w \left(\frac{L_2 i_2}{V_2} \right)^{5/3} \tag{6.19}$$

Dividing (6.19) by (6.18) gives

$$\frac{Q_2}{Q_1} = \frac{\kappa_w \left(L_2 i_2 / V_2 \right)^{5/3}}{\kappa_w \left(L_1 i_1 / V_1 \right)^{5/3}} \tag{6.20}$$

Since κ_w is constant for a watershed, equation (6.20) reduces to

$$\frac{Q_2}{Q_1} = \left(\frac{L_2 i_2 V_1}{L_1 i_1 V_2} \right)^{5/3} \tag{6.21}$$

As an example of how this equation may be applied, the storm data for Cave Creek will be used. For Cave Creek, the line of constant peak for Q_p = 20,000 cfs has been determined as shown in Figure 6.6. Assume then that the location of the line of constant peak for Q_p = 10,000 cfs is desired. This should be able to be determined using two known points from the line of constant peak for Q_p = 20000 cfs and equation (6.21).

From the line of constant peak for Q_p = 20,000 cfs in Figure 6.6, the following point can be identified:

$$L_s/L_p = 0.75,\ V_s/i_e = 0.4$$

The following can now be used in equation (6.21): Q_1 = 20000, Q_2 = 10000, L_1 = $0.75L_p$, V_1/i_1 = 0.4 to obtain

$$\frac{10000}{20000} = 0.5 = \left(\frac{0.4 L_2 i_2}{0.75 L_p V_2} \right)^{5/3} \tag{6.22}$$

Now, to determine where on the vertical axis the same size storm (L_2=L_1) would plot for a peak of 10,000 cfs, let $L_2 = L_1 = 0.75L_p$ and (6.22) can be reduced to

$$\frac{V_2}{i_2} = \frac{0.4}{0.5^{0.6}} = 0.61 \tag{6.23}$$

This now provides one point on the line of constant peak for Qp= 10,000 cfs as

$$L_s/L_p = 0.75,\ V_s/i_e = 0.61$$

This process is repeated using another point from the line of constant peak for 20,000 cfs. That second point is L_s/L_p = 1.75, V_s/i_e = 0.97. The corresponding point for the same size storm on the line of constant peak for 10,000 cfs is L_s/L_p = 1.75, V_s/i_e = 1.47.

In Figure 6.7, this theoretical line of constant peak for Q_p = 10,000 cfs is shown on the storm parameter plot for Cave Creek. Shown also are red symbols for storms from the test matrix that had peaks greater than 10,000 cfs and green symbols for those storms from the test matrix that had peak flows less than 10,000 cfs.

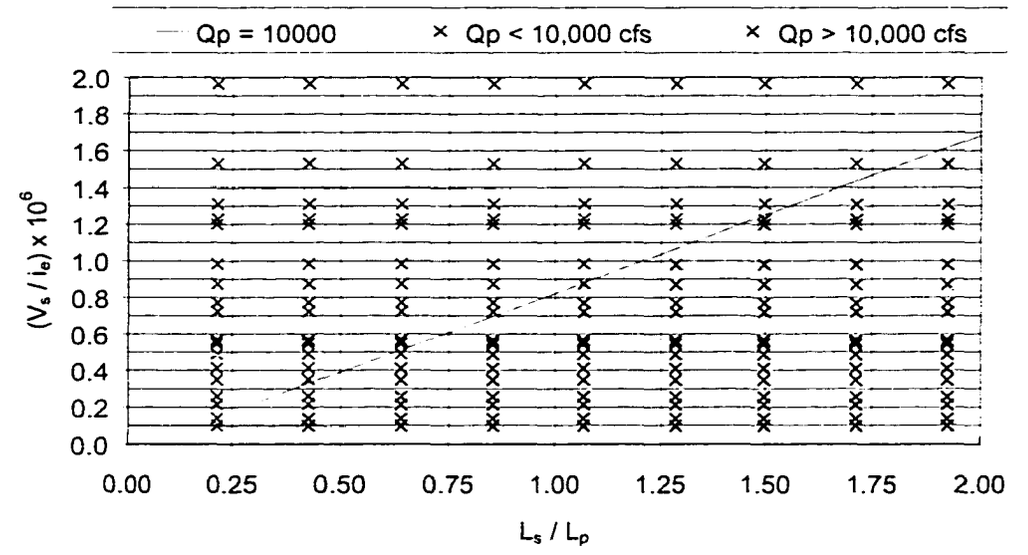

Figure 6.7 Line of Constant Peak for Qp=10,000 cfs for Cave Creek

Note that the theoretical line for Q_p = 10,000 cfs plots very well along the delineation between storms above and below Q_p = 10,000 cfs, except where the storm size becomes less than approximately $L_s/L_p \approx 0.5$ which represents storms with an area less than 1/4 the area of the watershed.

Using the peak flow results for all of the storms in the test matrix, the lines of constant peak for any peak discharge of interest can be plotted on the storm parameter plot. This can be done either from direct analysis of the model results, or via the method shown above for the line of constant peak for Q_p = 10,000 cfs. Figure 6.8 shows the lines of constant peak discharge for the Cave Creek watershed for various peak discharges ranging from 5,000 cfs to 30,000 cfs. Note that in Figure 6.8 the lines of constant peak have flatter slopes for higher peak discharges as expected.

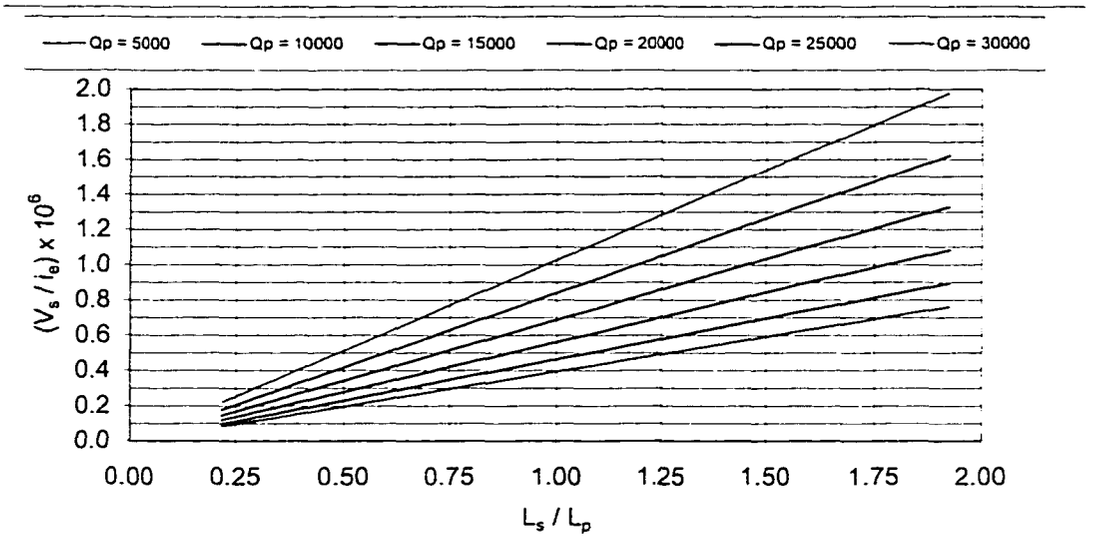

Figure 6.8 Lines of Constant Peak for Cave Creek, Qp = 5000 cfs → 30000 cfs

6.5.2 Storm Parameter Effects on Peak Runoff for Hassyampa River

These data show that the concept of linearity under partial equilibrium conditions between the length of a storm and the velocity divided by the intensity does approximately hold true for watershed scale applications. As further verification of this, the same parametric analysis was repeated using the CASC2D model of the Hassyampa River watershed. The exact same approach that was used for the Cave Creek model was followed for the Hassyampa River model. The only exception was that storm sizes up to 4,096 km^2 (64 x 64 km) were used in the test matrix for the Hassyampa River as opposed to the maximum storm size used for Cave Creek of 1,296 km^2. This was done to account for the fact that the Hassyampa Basin is approximately three times larger than the Cave Creek basin.

As with the Cave Creek parametric analysis, storms of each size from 16 km^2 to 4,096 km^2 were moved across the Hassyampa River basin along various paths to

determine the path for each storm size that resulted in the maximum peak discharge. Once the paths were determined, then the test matrix of storms was run with the model and the peak discharge from each of the 400 model runs was determined. It was expected that the same type of near-linear relationship would emerge from which lines of constant peak discharge can be identified on a plot of L_s/L_p vs. V_s/i_e. It was not expected that the lines for the Hassyampa River basin would be exactly the same as those for Cave Creek for given peak discharges. For example, the line for a peak of 20,000 cfs on Cave Creek would not be expected to be the same as the line for a peak of 20,000 cfs on the Hassyampa River. The concept of this linearity was predicated on the assumption that the slope and surface roughness parameters remain constant, and this assumption will not necessarily be valid from one watershed to another. Shown in Figure 6.9 is the storm parameter plot for the results of the Hassyampa River parametric analysis with the line of constant peak for 20,000 cfs shown.

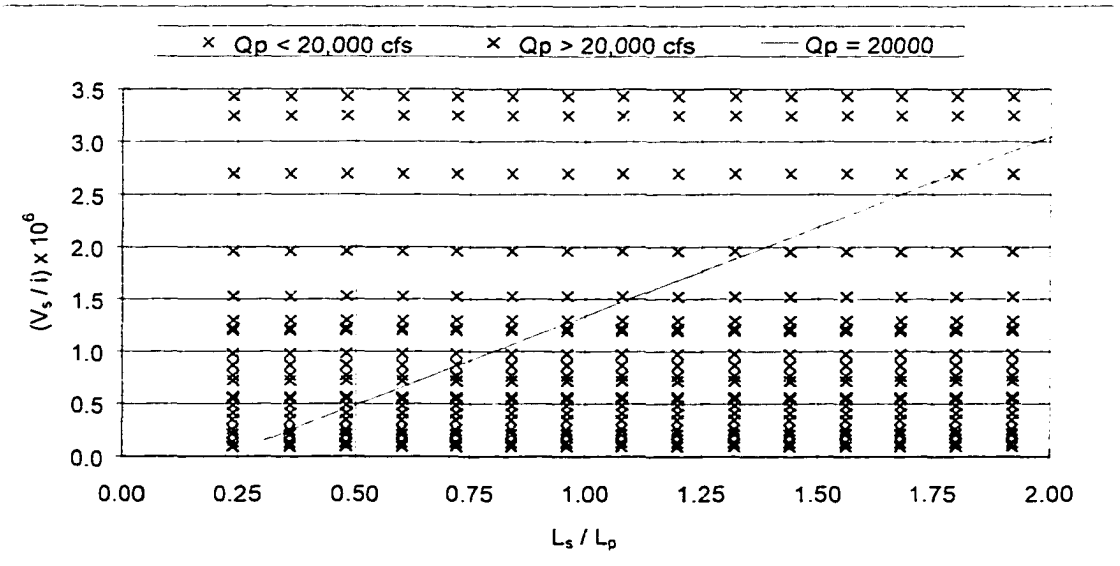

Figure 6.9 Storm Parameter Plot for Hassyampa River - Qp = 20000 cfs

As with the Cave Creek data, there is a delineation on the storm parameter plot shown in Figure 6.9 between storms with peak flow less than 20,000 cfs and those greater than 20,000 cfs. These results serve to confirm the results from the Cave Creek watershed that showed a generally linear relationship between L_S and V_S/i_e for constant values of peak discharge. As indicated earlier, the lines of constant peak discharge on the storm parameter plot will not be the same for the two watersheds. Figure 6.10 shows the lines of constant peak discharge for 20,000 cfs for both the Cave Creek and Hassyampa River watersheds.

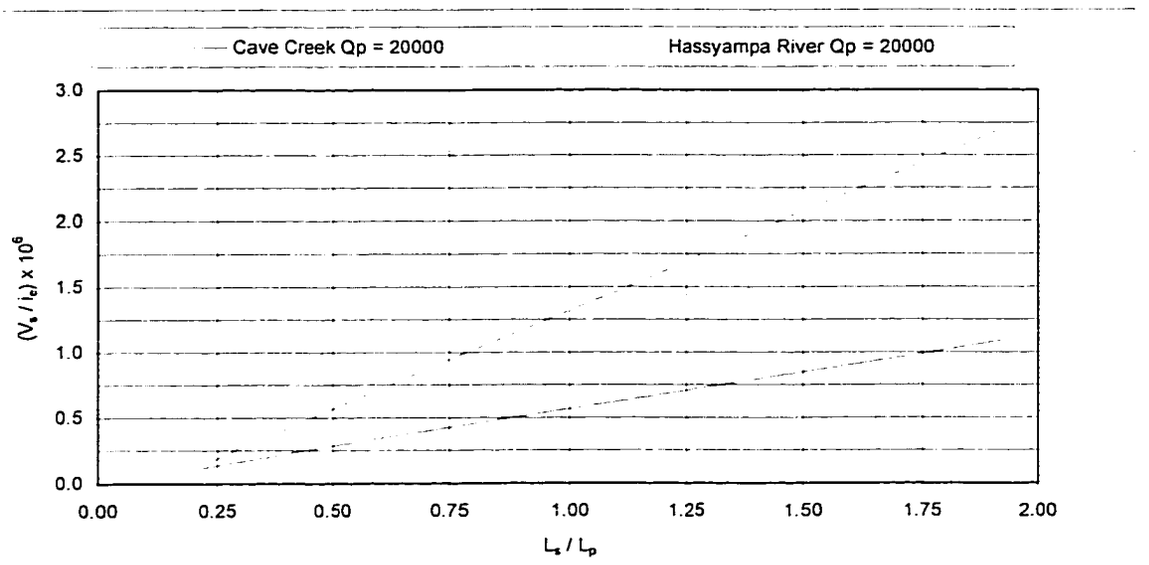

Figure 6.10 Hassyampa River and Cave Creek Lines of Constant Peak (Qp = 20000 cfs)

The slope of the line for Q_p = 20,000 cfs for Cave Creek is not as steep as the line for constant Q_p = 20000 cfs for the Hassyampa River. This steeper slope for the Hassyampa River was expected because it is a larger basin than the Cave Creek

watershed. Thus, if the same storm passes over each of these two basins, that storm will drop a larger amount of precipitation on the Hassyampa River basin because the Hassyampa basin is larger and therefore the storm is over that basin for a longer duration. Similarly, for a storm with the same size and rainfall intensity to produce equal peak flow from each of these two basins, that storm must travel slower over the Cave Creek basin and faster over the Hassyampa River basin in order to drop equal amounts of precipitation on each basin. Thus, on the storm parameter plot the storm that produces a certain peak flow on Cave Creek will have lower velocity and will plot lower on the vertical axis than a storm of equal size and intensity that produces the same peak flow on the Hassyampa River.

6.5.3 Effects of Soil Moisture Conditions

One other parameter that will influence the runoff from a watershed for a given rainfall event is the initial soil moisture condition of the basin. If the basin is very dry at the onset of a rainfall event, then typically there will be greater initial losses due to infiltration and thus a lower peak runoff. Conversely, if the basin is nearly saturated at the beginning of an event, then the initial infiltration losses should be less and the resultant peak flow greater. The influence of initial soil moisture conditions on peak runoff was analyzed by running the entire test matrix of 225 storms over the Cave Creek watershed using the CASC2D model of the basin with wet, medium and dry initial soil moisture conditions. For wet conditions, the initial soil moisture deficit (SMD) in the model was set to 5%, for medium conditions the SMD was 50%, and for dry conditions the initial SMD was 95%. It would be expected that for a storm of a given size and intensity to produce the same peak runoff, that storm would have to move more slowly

across the basin under dry conditions than under wet conditions. Thus, on the storm parameter plot, the line of constant peak for dry conditions would be the lowest line, the line of constant peak for medium conditions would be in the middle, and the line of constant peak for wet conditions would be the highest of these three. The results from the model runs on Cave Creek are shown in Figure 6.11 where the lines of constant peak for 20,000 cfs are shown for initial soil moisture deficits of 5%, 50%, and 95%. The results shown in Figure 6.11 confirm that the line for dry conditions is the loest on the plot and the line for wet conditions is the highest.

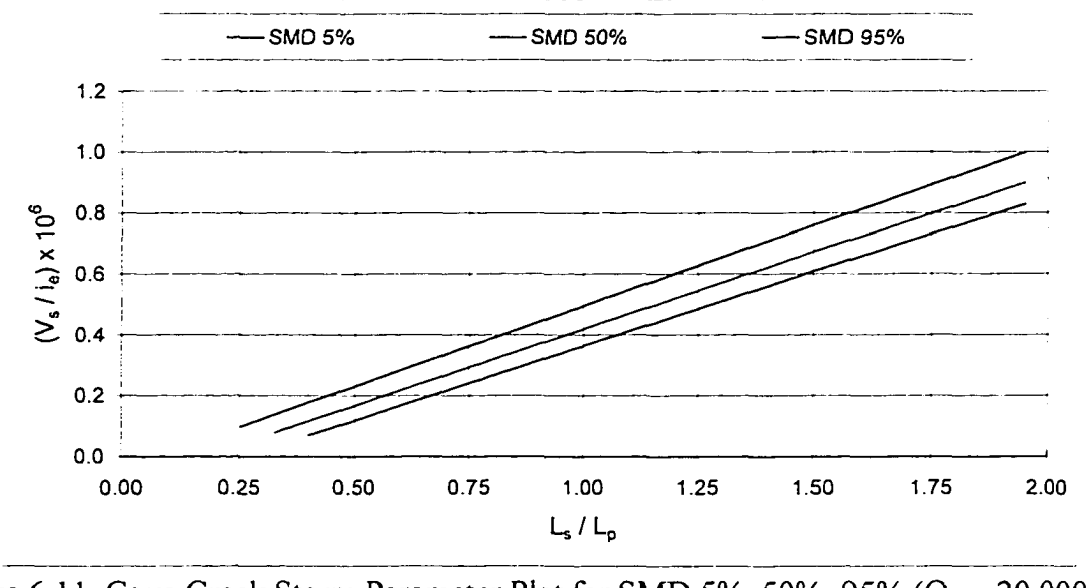

Figure 6.11 Cave Creek Storm Parameter Plot for SMD 5%, 50%, 95% (Q_p = 20,000 cfs)

6.6 SUMMARY

In this Chapter, the relationship between storm size, velocity and intensity and peak runoff was investigated. Starting with the concept of flow on a simple plane, a theoretical relationship was proposed that indicated the existence of a linear relationship

between the storm length L_S and the storm velocity divided by the storm intensity V_S/i_e for constant values of peak discharge. Based on these concepts it was surmised that this linear relationship would reveal lines with flatter slopes for higher values of peak discharge and steeper slopes for lower values of peak discharge on a given watershed. It was also indicated that this linear relationship would differ from one watershed to another.

To investigate the existence of this relationship at the watershed scale, a test matrix of storms was formulated that encompassed the range of reasonable values for storm size, velocity and intensity that might exist over central Arizona. This test matrix of storms was then passed over the Cave Creek CASC2D model that was developed and described in Chapter 4. For the Cave Creek basin, a total of 225 model runs were performed, and the peak discharge from each model run was determined. The peak discharge values were then summarized in the form of a storm parameter plot of L_S/L_D vs V_S/i_e. Using this concept of a linear relationship, it was shown that a line of constant peak for one peak discharge could be used to determined the line of constant peak for any other peak discharge in that watershed. Storms that produced peak discharges ranging from 5,000 to 30,000 cfs were then plotted on this graph, and in each case the existence of the near-linear relationship between L_S and V_S/i_e was shown. Also, the storms that resulted in higher peak discharges had lines with flatter slopes as was expected. This process was then repeated for the Hassyampa River basin using a test matrix of 400 storms, and the results verified the expected relationship and verified that the lines of constant peak discharge do vary from one watershed to another. Finally, the effects of initial soil moisture conditions on peak runoff were studied by running the 225 storms in

the Cave Creek test matrix with initial SMD of 5%, 50%, and 95%. Results of this showed that for a given peak flow the line of constant peak will be lower for dry conditions and higher for wet conditions.

Chapter 7

PRECIPITATION FORECASTING AND PEAK FLOW PREDICTION

7.1 INTRODUCTION

In the field of hydrology, the term forecasting refers to the estimation of conditions at some specific future time. For example, estimation of the discharge in a river at a specific time tomorrow would be a forecast. Forecasts may be classified based on the forecast lead-time, where lead-time refers to the time interval into the future for which the forecast is made. Forecasts with lead-times less then 7 days may be referred to as short-term forecasts and long-term forecasts are those with longer lead-times that may extend up to several months into the future. Short-term forecasts are generally used for flood warning, real-time operation of water control structures, and for military operations.

When choosing a conceptual or deterministic model with which to perform forecasting, the basic choices include models based on channel routing, those based on rainfall-runoff processes, or some combination thereof. In determining which class of model best fits the forecasting application, one primary criterion is the relationship between the required forecast lead-time and the hydrologic response time of the basin, which is often measured as the time of travel from the most remote point in the basin to the forecast point. If the required forecast lead-time is greater than the hydrologic response time of the basin, then it is necessary to incorporate forecast of future

precipitation into the model. If the forecast lead-time is shorter than the response time of the basin and that response time is dominated by routing of the flood through the channel system, then flow forecasts may be based on flow observations made upstream of the forecast point using channel routing models. This situation will exist for larger river systems such as the Mississippi. If the forecast lead-time is shorter than the response time and the response time is dominated by the overland flow or time of concentration in the basin, then a rainfall-runoff model may be used to generate forecasts using observed rainfall from the basin. This will typically be the case in smaller watersheds. Another criterion to consider is the ratio of the spatial scale of the precipitation event to the spatial scale of the basin. If the areal extent of the precipitation event is much smaller than the size of the watershed, then a model that assumes uniform precipitation over the entire basin may prove to be inaccurate. In such cases the watershed must be subdivided into smaller sub-basins in order to capture the spatial distribution of the rainfall event adequately (Lettenmaier and Wood, 1993).

Each of the above scenarios could conceivably lead a forecaster to select a different model, i.e., a rainfall-runoff model, a channel routing model, or some combination of both. However, the CASC2D model simulates both the rainfall-runoff and channel routing processes in a basin such that it could theoretically function in any of the scenarios discussed in the previous paragraph. The grid-based structure of the model also lends itself ideally to capturing the spatial distribution of even the smallest precipitation events. It is from this foundation that an investigation of the feasibility and applicability of the CASC2D model for flow forecasting has been pursued and is presented in this chapter. First, an application is presented where precipitation forecasts

from radar data are used to extend the lead-time for which the peak flow can be predicted. This is followed by a practical application of the parametric analysis wherein storm parameters are estimated from radar images and the peak flow is estimated based on those parameters.

7.2 MODELING PROCEDURE

The procedure followed for using the CASC2D model to predict peak flow using radar data consisted of the using the calibrated CASC2D model of the Hassyampa River basin with calibrated radar rainfall data as the precipitation input. The response time of the Hassyampa River watershed is less then 24 hours, and for this work the assumption was made that the required forecast lead-time is greater than 24 hours. Thus, it was desirable to incorporate forecasts of future precipitation into the modeling process. These precipitation forecasts were generated from the radar rainfall images and were combined with observed precipitation to create the rainfall input file for the model at each forecast time increment. The forecast procedure was started when the first rainfall was forecast to fall over the basin, and the input data were updated at 30-minute intervals as new observed data became available through the end of the event. The following sections describe the process that was followed for generating precipitation forecasts, how those forecasts were combined with observed precipitation, and how the procedure was conducted to use updated precipitation information throughout each of the events.

7.2.1 Precipitation Forecasts

The approach that was used to generate precipitation forecasts involved extrapolation of precipitation patterns based on estimated velocity data from radar images. In this approach, observations of a storm from two successive radar images at

30-minute time intervals were inspected, and the centroid of the rainfall pattern from each observation was determined. Then, based on the movement of the centroid over the 30-minute time interval between the two observations, an estimate of the velocity of the storm was generated. For example, if during a particular 30-minute time interval the centroid of a rainfall pattern moved 10 km in an easterly direction, then the velocity of the storm was estimated as 20 km/hr to the East. The assumptions were then made that this estimated velocity would remain constant into the future and that the spatial rainfall pattern would remain constant. Based on these assumptions, the most recent rainfall pattern was simply extrapolated into the future. This is illustrated in Figures 7.1 and 7.2 that show the rainfall pattern at two points in time. In Figure 7.1, the location of the centroid is shown as 354900 (meters East), 3785050 (meters North). Figure 7.2 shows this same storm 30 minutes later when the centroid of the rainfall pattern is 362850, 3785000. So, during this 30 minute time interval the centroid of the storm moved 7.95 km East and 0.05 km South. To generate the forecast of future precipitation, the assumption was made that the rainfall pattern would remain constant and would continue to move over the watershed at a constant velocity. Thus, the rainfall pattern in Figure 7.2 was moved in space at a constant velocity of 15.9 km/hr East and 0.1 km/hr South until it passed over the watershed.

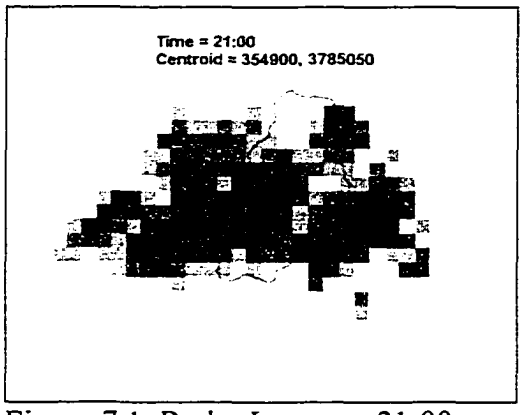

Figure 7.1 Radar Image at 21:00

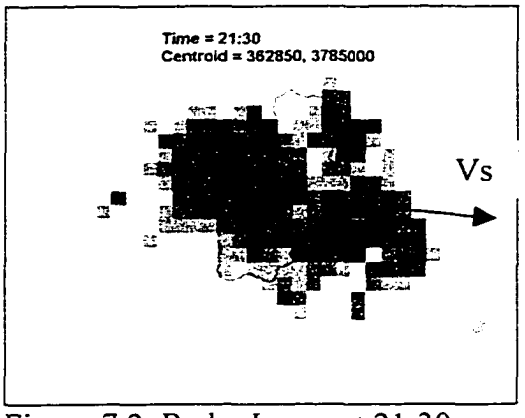

Figure 7.2 Radar Image at 21:30

It is apparent from viewing Figures 7.1 and 7.2 that at this point in the rainfall event precipitation is already falling on the watershed. At the point in the forecast process when the first precipitation was observed to actually fall on the watershed, that observed precipitation was used as the rainfall input to the model up to that point in time and the extrapolated rainfall as described above was used as the forecast precipitation. Again, this procedure was repeated every 30 minutes using updated radar observations through the end of the event.

There are certainly other methods of generating precipitation forecasts from radar observations, several of which were outlined in Chapter 2. This method is but one approach that does have the advantage of simplicity and ease of application, and for short term forecasts the accuracy of this approach has been shown to be reasonably close to that of more complex methods.

7.2.2 Peak Flow Prediction

Using the precipitation forecasts discussed in the previous section, predictions of peak flow were generated with the CASC2D model of the Hassyampa River basin for the

February and March events. The approach followed in this process was to run the model starting with the first observable precipitation that was forecast to proceed over the basin. This first forecast step occurred before any precipitation actually hit the watershed and was repeated with updated radar rainfall data at 30-minute intervals until the precipitation event stopped and runoff from the basin receded. Prior to any rainfall actually falling on the basin, only forecast precipitation was used in the models. Once precipitation actually fell over the watershed, the model was run with the observed radar rainfall data as input up through the time at which the forecast was being generated. From that point forward in time, the precipitation input was generated from the precipitation forecasts as detailed in the previous section. This process was repeated using updated data every 30 minutes throughout each of the two events.

7.3 RESULTS

First, the precipitation forecasts were analyzed to determine how well the forecast precipitation compared to the actual precipitation over the watershed at the end of the event. The two important factors considered for the precipitation forecasts were how well the forecast precipitation compared with the observed precipitation and how far in advance accurate precipitation forecasts were generated. Following a summary of the precipitation forecasts, a similar analysis of the peak flow predictions is presented.

7.3.1 Precipitation Forecast Results

The quality of the precipitation forecasts that were generated was measured by comparing the total volume of precipitation on the watershed at each forecast time with the actual volume of precipitation over the watershed as measured from the observed radar data. Figures 7.3 and 7.4 provide summaries of these data for the February and

March events, respectively. Each of these graphs shows how the total precipitation volume evolved over time from the beginning of each event through the time at which the peak occurs. The lines that are labeled as "Obs Event Total" reflect the actual observed total precipitation volume at each point in time. Prior to any rainfall hitting the basin, these lines show zero precipitation volume, and they steadily increase over time until the rainfall event ends from which point forward the observed total equals the final event total. Also shown on each graph are lines labeled "Fcst Event Total", and these lines represent the combination of observed precipitation up to each point in time plus the forecast precipitation forward in time for the remainder of the event. Since these lines reflect both observed and forecast precipitation, they increase more quickly from zero and reflect precipitation totals that are close to the final event total several hours earlier. For the February event, incorporation of the precipitation forecast increased the lead-time for the total rainfall volume by at least 6 hours, while the lead-time for the March event was increased by approximately 4 hours with the precipitation forecast included. Shown for reference purposes in Figures 7.3 and 7.4 are lines showing the final event total precipitation volume and precipitation totals 25% above and below that amount.

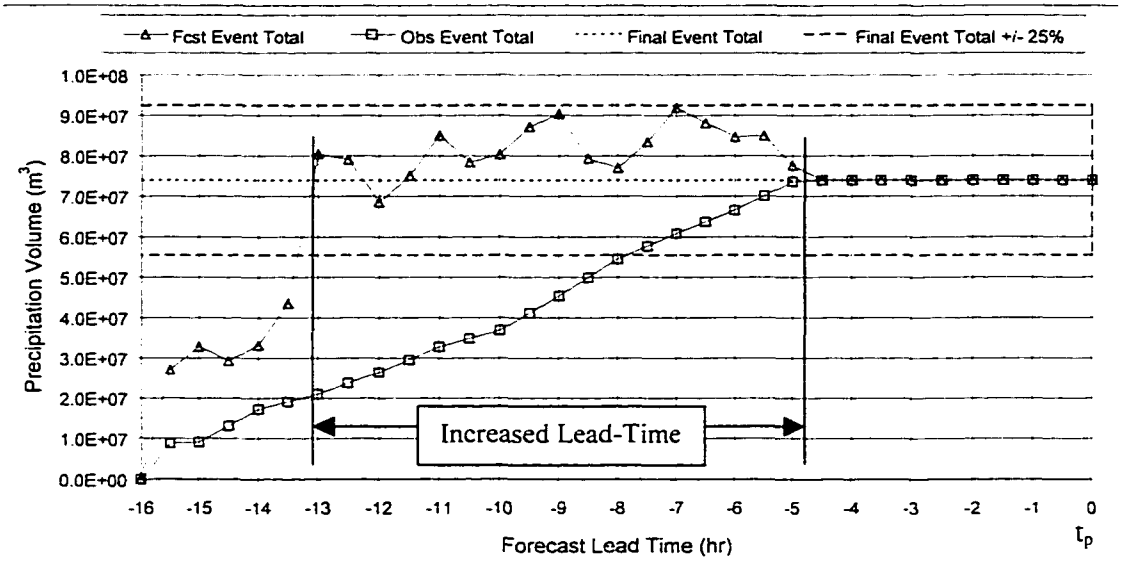

Figure 7.3 Forecast and Observed Precipitation Volumes (February Event)

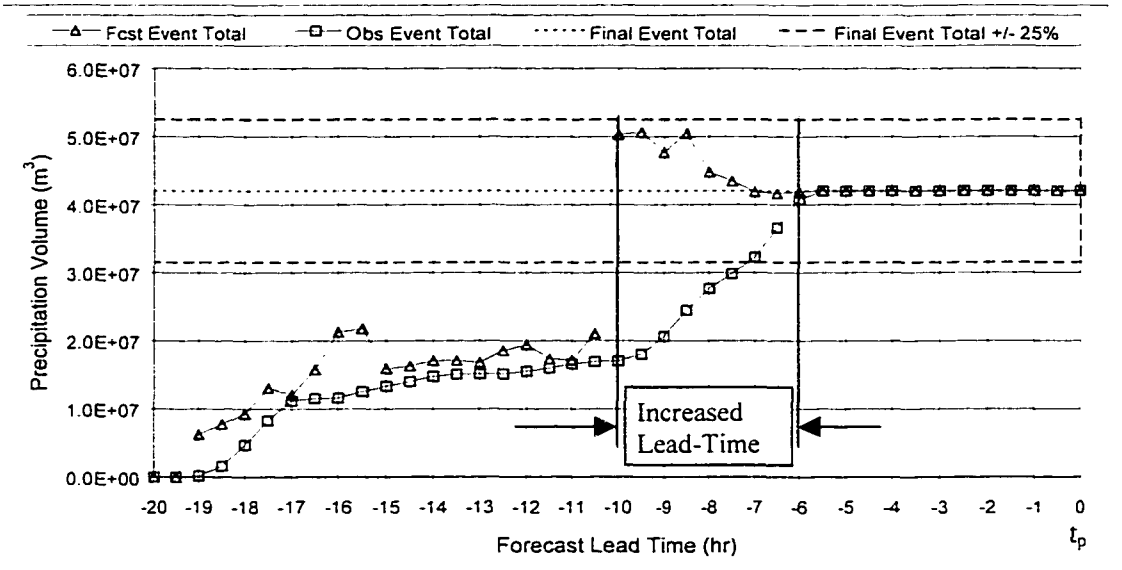

Figure 7.4 Forecast and Observed Precipitation Volumes (March Event)

7.3.2 Peak Flow Results

At each 30-minute time interval throughout both of the precipitation events, the CASC2D model of the Hassyampa River was run two times. One run used only observed

precipitation up to that point in time, and the other run used observed precipitation up to that point in time and forecast precipitation forward in time. The CASC2D program was modified for this purpose to accept two rainfall input files. The first input file contained the observed precipitation data, and the second input file contained the most recent radar image and the projected velocity with which that rainfall pattern should proceed across the watershed. Using that velocity data, the rainfall pattern was moved the appropriate distance at each 30-second model time step to simulate the movement of that storm over the watershed. The model used the observed rainfall data up to the point in time at which the forecast was being made, and from that point in time forward the model switched to the forecast data. Updated information was incorporated at 30-minute time intervals to generate new input files for the observed and forecast precipitation and the model was rerun using these updated data.

The following results depict the model output for both model runs at each 30-minute time interval throughout the forecast process. Incorporation of the precipitation forecasts did increase the lead-time at which the total precipitation for each event was estimated, so flow forecasts using the observed and forecast precipitation should be able to predict the peak discharge for each event several hours earlier than using the observed precipitation alone. Figures 7.5 and 7.6 show the forecast model results for the February rainfall event that were made at lead-times of -13, -11, -9, -7, and -5 hours along with the observed hydrograph for the event.

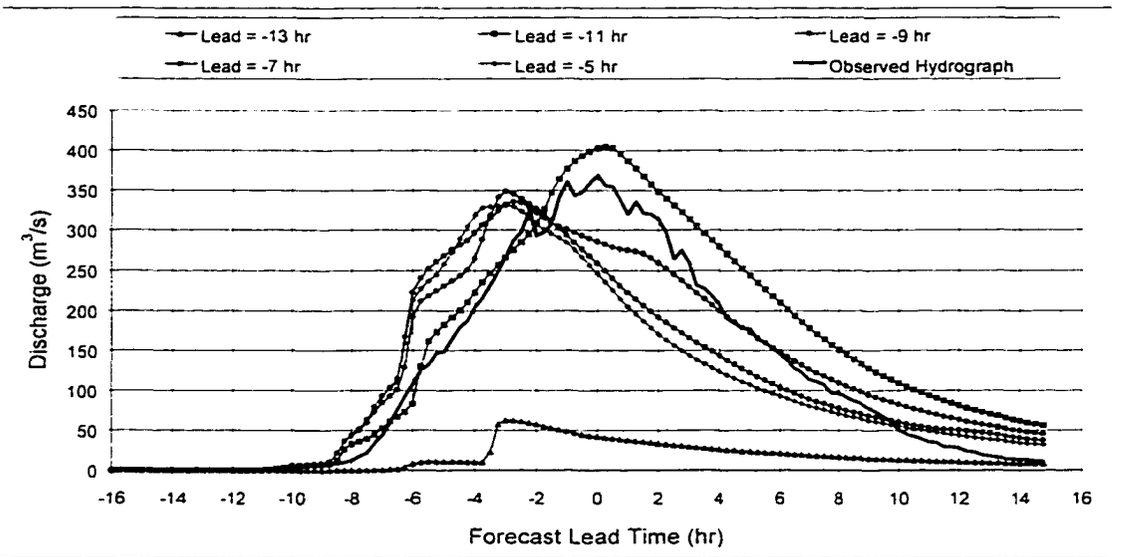

Figure 7.5 Forecast Model Results with Precipitation Forecasts (February Event)

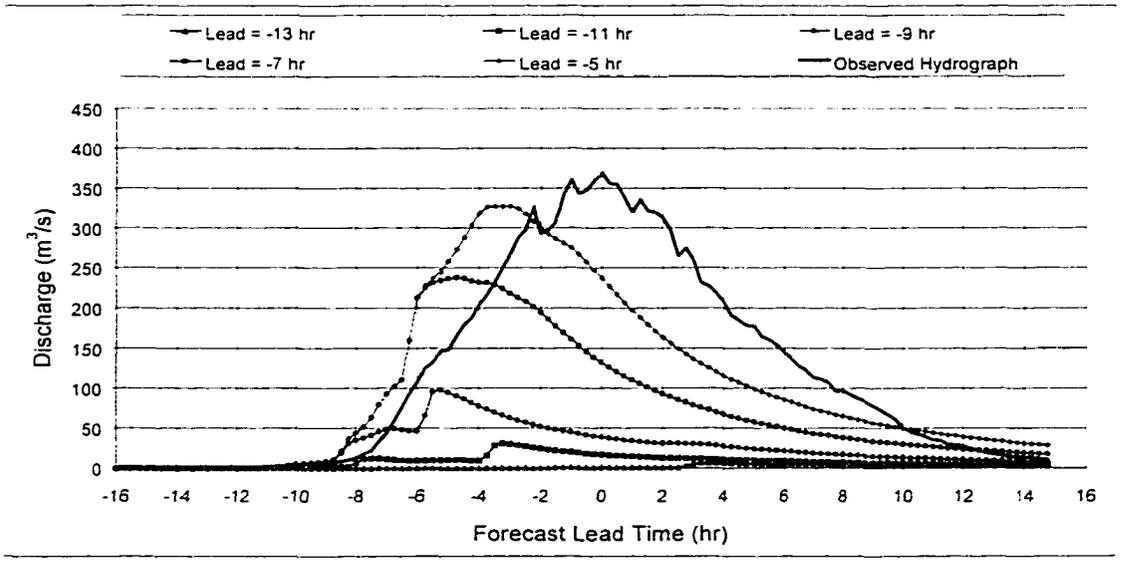

Figure 7.6 Forecast Model Results without Precipitation Forecasts (February Event)

Figure 7.5 contains results for the model runs with precipitation forecasts included, and Figure 7.6 includes model results with only observed precipitation accounted for. Figure 7.5 shows that 11 hours prior to the occurrence of the peak for this event, the inclusion of the precipitation forecasts enabled the model to forecast the event

peak within about 10%. Figure 7.6, on the other hand, shows that when only observed precipitation was accounted for, the event peak was not forecast to that level of accuracy until about 5 hours prior to the occurrence of the peak. Thus, incorporation of the precipitation forecasts increased the forecast lead-time by 6 hours for this event. Figure 7.7 provides a graph of the forecast peak vs. forecast lead-time for the model runs with and without precipitation forecasts. As with Figures 7.5 and 7.6, this shows that the event peak was forecast fairly well using the precipitation forecast at least 6 hours earlier than without the precipitation forecast.

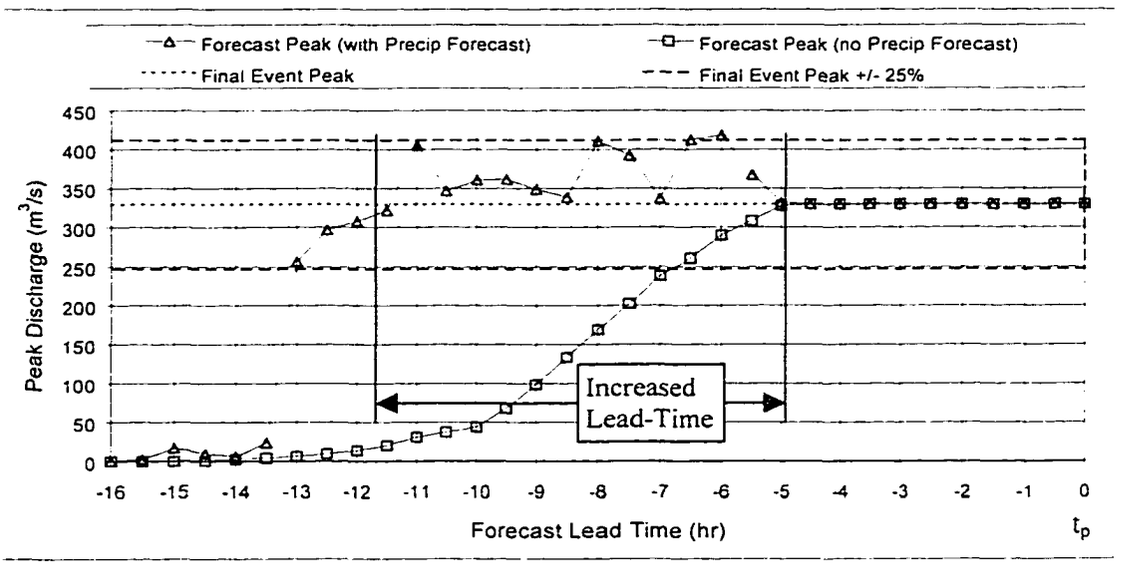

Figure 7.7 Forecast Peaks With and Without Precipitation Forecast (February Event)

This same procedure was used for the March event on the Hassyampa River. Figures 7.8 and 7.9 show the model results for the March event made at lead-times ranging from -11 to -5 hours along with the observed hydrograph for the event.

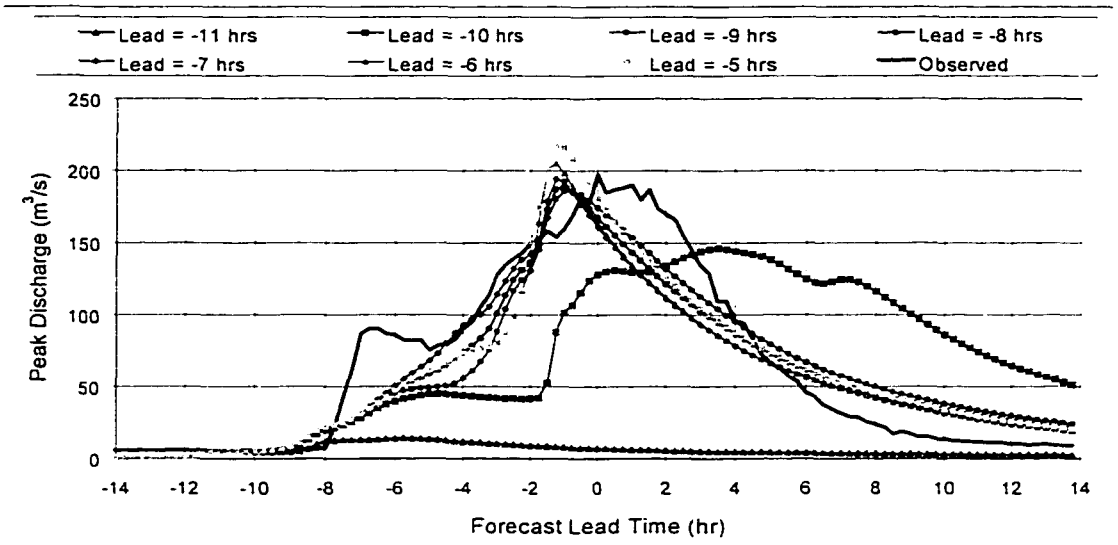

Figure 7.8 Forecast Model Results with Precipitation Forecasts (March Event)

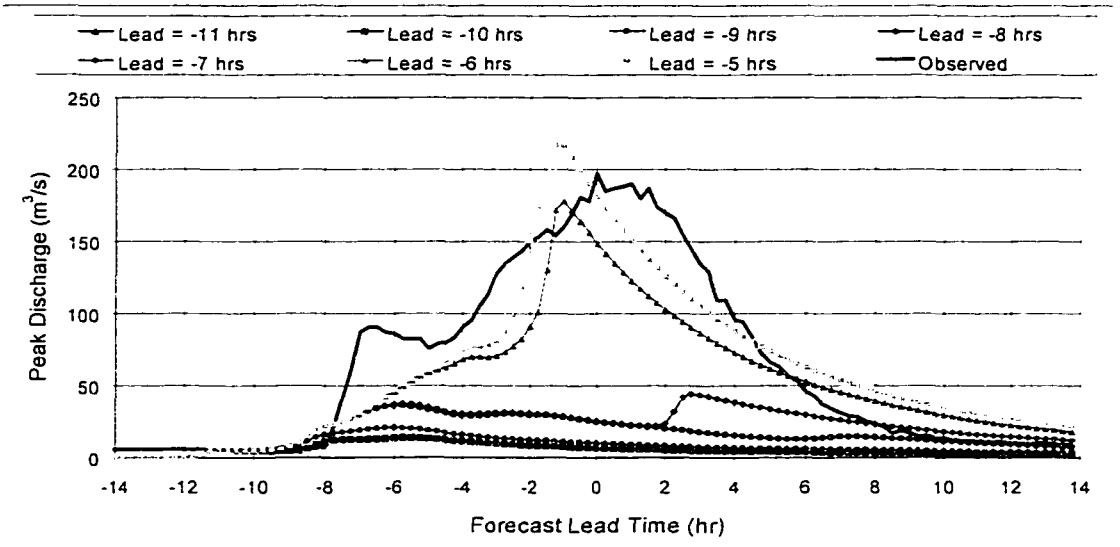

Figure 7.9 Forecast Model Results without Precipitation Forecasts (March Event)

Figure 7.8 provides results for the model runs with precipitation forecasts included, and Figure 7.9 includes those with only observed precipitation. Figure 7.8 shows that 9 hours prior to the peak for this event the model with precipitation forecasts was able to forecast the peak within 10%, while the model with only observed

precipitation, as shown in Figure 7.9, forecast the peak reasonably well about 6 hours prior to the peak. Incorporation of the precipitation forecasts increased the forecast lead time by 3 hours for this event. Figure 7.10 includes a graph of the forecast peak vs. forecast lead time for the model runs with and without precipitation forecasts. As with Figures 7.8 and 7.9, this shows that the event peak was forecast fairly well using the precipitation forecast at least 3 hours earlier than without the precipitation forecast.

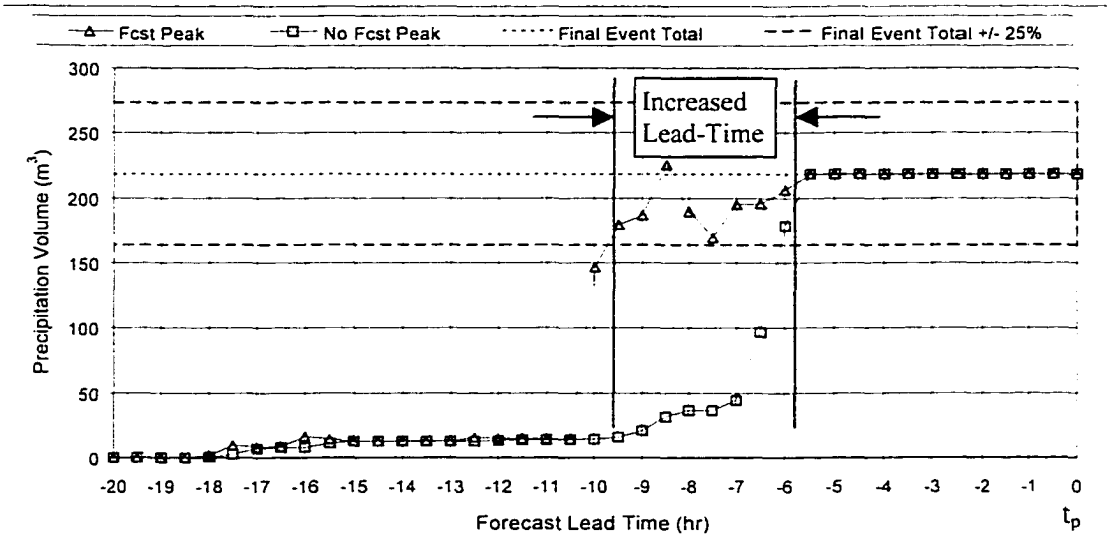

Figure 7.10 Forecast Peaks With and Without Precipitation Forecast (March Event)

7.4 PEAK FLOW ESTIMATES USING STORM PARAMETERS

The parametric analysis presented in Chapter 6 showed how various physical storm characteristics may be related to peak runoff from a watershed. Those storm characteristics, or parameters, included the size of the storm, the average rainfall intensity in the storm, and the velocity with which a storm moves across the watershed. The storms used in that parametric analysis were hypothetical storms that were square in size,

had uniform rainfall intensity over the spatial extent of the storm, and moved with uniform velocity across the basin. A series of such storms were passed over the Cave Creek an Hassyampa River basins using the CASC2D model, and the resultant peak flows from those model runs were summarized by means of a dimensionless plot using the storm velocity, storm intensity, storm size, and watershed size. From those plots, a linear relationship developed which delineated the combinations of these parameters that resulted in peak runoff either above or below a selected threshold. For a selected peak flow, a line could be determined above which peak flow would be expected to be less than the selected peak flow and below which the peak flow would be expected to be above the selected peak flow. The location of that line varied depending on the value of the threshold peak flow and the watershed. For higher threshold peaks and smaller watersheds, the slope of the line decreases. For lower threshold peak flows and larger watersheds, the slope of the line increases.

The final phase of this research was to extend the results of the parametric analysis using actual radar rainfall data to estimate potential peak flows. This was accomplished by using the same radar data from which the precipitation forecasts were generated as described in the previous section. At each 30-minute forecast point during each of the precipitation events, a radar rainfall image was analyzed to determine the velocity of the storm so that the storm could be extrapolated forward in time. Using those same radar rainfall images at each 30-minute interval, they were then analyzed to determine not only the velocity but also the size and average intensity. Thus, at each 30-minute interval the most recent radar image was analyzed to estimate the size, intensity, and velocity of the storm cell crossing the Hassyampa River basin. Those parameters

were then used to plot a data point on the storm parameter plot. To take into account observed rainfall on the basin as each event progressed, average values of the parameters were computed starting from the beginning of the event. So, for each 30-minute interval, the size, intensity and velocity from the current and all previous observations were averaged to determine a "storm average" for each parameter. In this manner the observed rainfall that had already hit the basin was taken into account for the forecasts which were done later in the event.

Figures 7.11 and 7.12 show the results of this process on the storm parameter plot for the Hassyampa River basin for the February and March events, respectively. The actual peak flow observed for the February event was 6,974 cfs and for the March event 13,016 cfs. For reference purposes, the lines of constant peak flow for Q_p = 20,000, Q_p = 10,00 and Q_p = 5,000 cfs are shown on these two plots. Since the parametric analysis was done using the assumption that a storm will cross the basin along the path that will result in the maximum peak, these lines of constant peak should indicate the maximum peak discharge that might result from a storm. The actual path that a storm follows will likely never be exactly along that path, so the resultant actual peak should be less than that indicated on the storm parameter plot.

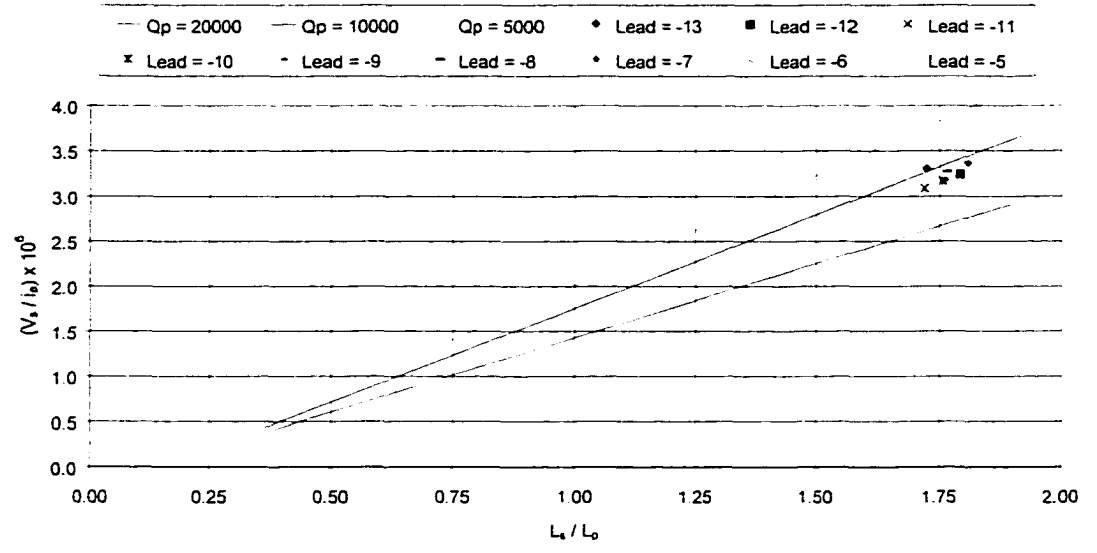

Figure 7.11 Storm Parameter Plots from Radar Data (February Event)

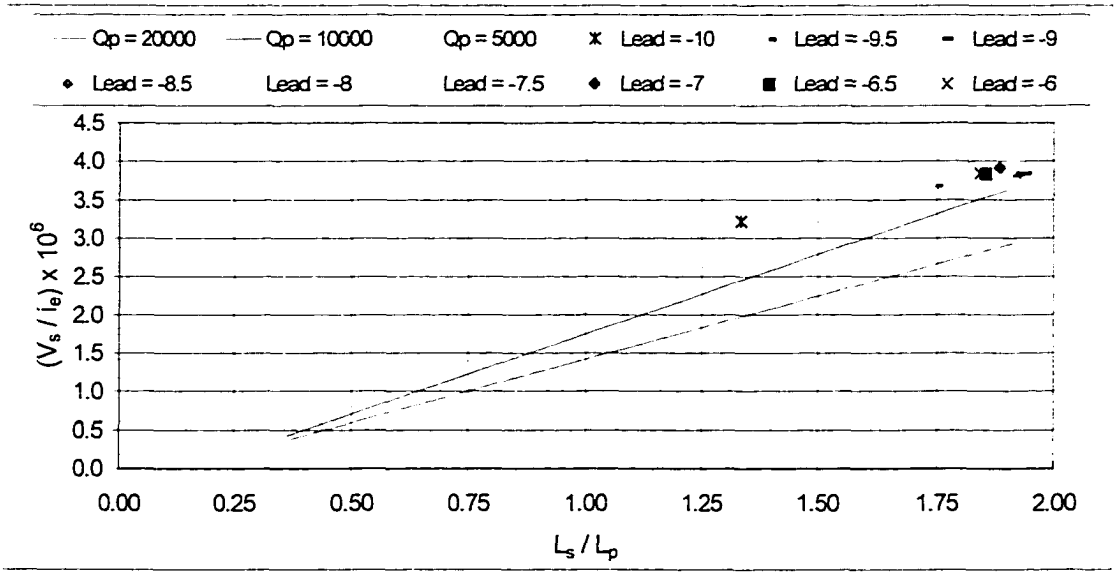

Figure 7.12 Storm Parameter Plots from Radar Data (March Event)

In Figures 7.11 and 7.12 it can be seen that the approach of using the storm parameters as estimated from radar images does result in reasonable estimates of the maximum peak flow for these two events. The use of the storm parameter plots is not

necessarily to provide a prediction of the exact peak flow for a storm. They should more appropriately be used as a tool to estimate the maximum potential peak that might result from a storm. For the two events studied here, the data points plotted on the storm parameter plots from the actual radar rainfall data did mostly fall within the region of the storm parameter plot for the actual peak flow of each event. The peak flow for the February event was just over 13,000 cfs, and the points on the storm parameter plot generally fell between the lines of constant peak for Q_p = 10,000 cfs and Q_p = 20,000 cfs. Similarly for the March event, the actual peak was just less than 7,000 cfs and the points on the storm parameter plot generally fell between the Q_p = 5,000 and Q_p = 10,000 lines of constant peak. The exceptions to this were very early in the precipitation event when the observed rainfall from the radar was not indicative of the final storm parameters. The storm parameter plots have thus been effectively used to establish estimated peak flows for each event.

7.5 SUMMARY

In this chapter an approach was described by which precipitation forecasts from radar rainfall data were be incorporated into the CASC2D rainfall-runoff model for the purpose of extending the forecast lead-time at which the peak flow for an event can be estimated. This precipitation forecasting method involved an analysis of sequential radar rainfall images to generate an estimate of the velocity of a storm. That velocity and the rainfall spatial pattern were then assumed to remain constant over time such that the most recent radar image could be extrapolated into the future at it moved across the watershed. This process was performed using radar data for two rainfall events over the Hassyampa River watershed in Arizona with the CASC2D model. The forecast process was

performed and updated at 30-minute intervals throughout each of these two rainfall events. Results indicated that incorporation of the precipitation forecasts extended the forecast lead-time by 6 hours for the February event and by 3 hours for the March event.

Also detailed in this chapter was a practical application of the results from the parametric analysis that was described in Chapter 6. The parametric analysis in Chapter 6 was performed using hypothetical block storms with uniform intensity and velocity moving across the watershed along a trajectory that results in the maximum peak discharge. The parametric analysis verified the existence of a generally linear relationship between the storm parameters of length, velocity and intensity for a given peak flow on a watershed. In this practical application of those results, the actual radar rainfall data were used as the moving storms across the basin. These data were from two actual events and did not have block shape, did not have uniform spatial precipitation intensity, and did not necessarily move across the watershed along the path of maximum peak. The actual size, average intensity, and actual path of movement for each storm were used as the parameters. For each of the precipitation events, these parameters were determined from the radar rainfall images at 30-minute intervals and running averages for each parameter were tabulated as each event progressed. These parameters of velocity, average intensity, and size were then plotted on the storm parameter plot for the Hassyampa River watershed. This revealed that the storm parameter plot did effectively enable estimates of the peak flow to be made for each of the two events. Given this type of information, decision makers for such things as emergency flood response or military operations have a simple tool with which to evaluate the potential for a given storm to result in a peak flow that might require response.

Chapter 8

SUMMARY AND CONCLUSIONS

8.1 SUMMARY

The CASC2D distributed watershed model was used in this research to simulate a number of rainfall-runoff events in two watersheds located in Central Arizona. The Cave Creek watershed covers approximately 349 km^2 and the Hassyampa River basin covers an area of slightly more than 1,110 km^2. The CASC2D model was calibrated first for the Cave Creek basin using observed rainfall data from 5 rain gauges and observed stream flow data for an event that occurred in February, 1995. The Hassyampa River basin was then calibrated using rain and streamflow data for the same event. Each calibrated model reproduced the peak flow for that event within 6% of the observed peak and the time to peak within 5% of the observed. The Cave Creek model was then verified with two additional rainfall events and the Hassyampa River model using one additional rainfall events. By changing only the parameter in the models for the initial soil moisture conditions, both models were able to reproduce the peak flow from these verification events within 4% of the observed peaks, and the time to peak within 10% of the observed. The ability of these models to reproduce these observed events without changing any model parameters other then the initial soil moisture conditions indicates that the models do provide a good simulation of the watershed response to precipitation input.

Precipitation data from the WSR-88D weather radar in Phoenix was analyzed for four rainfall events. The precipitation intensity measurements from the radar were compared with those from rain gauges for the same events, and the conclusion was reached that the radar data in its original form did not provide accurate intensity values. The reason for this was presumed to be related to the Z-R relationship that was used to derive the precipitation data from the radar reflectivity measurements. The probability density functions for the rain gauge and radar data were compared and a new Z-R relationship was adopted that provided a much higher level of correlation between the radar and the rain gauge data for these events. Comparison between the calibrated radar data and the rain gauge data at the gauge locations confirmed that the calibrated radar rainfall data produced precipitation values over the watershed that closely matched the rain gauge measurements. The calibrated radar data was then used as input to the CASC2D model of the Hassyampa River for two events, and the resultant hydrographs from the model matched the observed hydrographs well. A series of 100 moving rain cells were also analyzed from the radar data on four rainfall events. The cumulative distribution of the size, intensity, velocity, and duration of these 100 rain cells were determined that provided an estimate of the range of values that these storm parameters might have.

A parametric analysis was conducted to analyze the relationship between peak runoff and the storm parameters of size, velocity, and intensity. To provide a theoretical basis for the parametric analysis, a review of peak runoff under partial equilibrium conditions on a simple inclined plane was presented. The conclusion was reached that there exists a linear relationship between storm length L_S and storm velocity divided by

intensity V_S/i_e for constant peak on a given runoff surface. A test matrix of storms was then proposed to extend the parametric analysis and investigate the existence of this linear relationship at the watershed scale. A test matrix of moving storms with velocities ranging from 10 to 70 km/hr, size ranging from 16 to 4,096 km^2, and intensity ranging from 12.7 to 101.6 mm/hr was established. This test matrix of storms was then used on the Cave Creek watershed model to determine the peak runoff from the watershed for each storm. The process was also repeated for the Hassyampa River model. These results were plotted in the form of a "storm parameter" plot of L_S/L_p vs V_S/i_e with L_S the square root of the storm size, L_p the square root of the watershed size, V_S the velocity of the storm, and i_e the excess precipitation intensity. On this plot, it was shown that for a given constant peak flow, there does exist a near-linear relationship between L_S/L_p and V_S/i_e. This relationship resulted in lines of constant peak discharge, such that for a given value of peak flow the storms plotting above that line would be expected to have peaks less than that value and storms plotting below the line would be expected to have peaks higher than that value. These lines of constant peak were shown to be different for different watersheds and for different initial soil moisture conditions in the same basin.

An application of the use of radar rainfall data as input to the CASC2D model was then presented. In this application, radar images were used to produce precipitation forecasts based on a method of linear extrapolation of the precipitation pattern. The CASC2D model for the Hassyampa River was used with radar data from two precipitation events. For each event, the model was run with precipitation forecasts and without precipitation forecasts at 30-minute updates. The intent of this approach was to establish that the CASC2D model could be used with WSR-88D radar data and that the

use of precipitation forecasts from the radar data could increase the lead-time at which the peak runoff for an event might be predicted. Results indicated that the forecast lead-time was increased by 6 hours for one event and by 3 hours for the other event on the Hassyampa River with the precipitation forecasts.

A practical application of the parametric analysis results was finally presented. In this application, actual radar observations were used to estimate the storm size, velocity, and intensity at 30-minute updates through two precipitation events. These parameters were then plotted on the storm parameter plot for the Hassyampa River, and the plotted points did provide reasonable estimates of the actual peak runoff for these events.

8.2 CONCLUSIONS

The following conclusions have been reached as a result of the research presented in this dissertation:

1. Adjustment of the radar Z-R relationship based on ground observations resulted in improved radar rainfall intensity estimates for the storms studied in this research.
2. The CASC2D model was successfully used with calibrated radar data to reproduce two observed runoff events on the Hassyampa River watershed with peak flows for both events within 11% of the observed peak and the time to peak for both events within 7% of the observed.
3. For a constant value of peak flow on an inclined plane under partial equilibrium conditions, the length of a moving storm L_S is linearly related to the velocity of the storm divided by the excess intensity of the storm V_S / i_e.

4. Approximate linearity between L_S and V_S / i_e for a constant value of peak discharge was shown to exist at the watershed scale for moving storms crossing a watershed in the same direction along paths that produce maximum peak flow.
5. Short-term precipitation forecasts from radar via linear extrapolation of the rainfall pattern, when coupled with observed radar rainfall estimates, provide increased lead-time in predicting peak flow with the CASC2D model. Lead-times were increased for two events on the Hassyampa River by 6 hours and 3 hours, respectively.
6. Once the approximate linear relationship between L_S and V_S / i_e is established for a watershed, then storm size, velocity and intensity estimates derived from radar can be used to provide reasonable estimates of maximum peak flow for that watershed.

The objectives of this research were to demonstrate the coupling of radar precipitation data with the CASC2D model; to analyze the conditions of storm size, velocity and intensity required to produce peak discharge from a watershed exceeding a specified threshold; and to examine the potential for increasing forecast lead-time in predicting peak runoff through the combined use of radar and distributed modeling technologies. The research documented in this dissertation has clearly shown that the CASC2D model can successfully be used with radar rainfall data, that there does exist a relationship between storm size, velocity and intensity such that the storm conditions required to produce peak flow exceeding a specified threshold can be analyzed, and that increased lead-time can be obtained in peak flow forecasts with the CASC2D model through the use of precipitation forecasts generated from radar data. Therefore, the objectives of this research have been successfully met.

REFERENCES

Austin, G.L. and Bellon, A. 1974. "The Use of Digital Weather Radar Records for Short-Term Precipitation Forecasting," *Quarterly Journal of the Royal Meteorological Society*, Vol. 100, 658-664.

Anagnostou, E.N. and Krajewski, A.F. 1999a. "Real-Time Radar Rainfall Estimation: 1. Algorithm Formulation," *Journal of Atmospheric and Oceanic Technology*, Vol. 16 (2), 189-197.

Anagnostou, E.N. and Krajewski, A.F. 1999b. "Real-Time Radar Rainfall Estimation: 2. Melbourne, Florida WSR-88D Case Study," *Journal of Atmospheric and Oceanic Technology*, Vol. 16 (2), 198-205.

Anagnostou, E.N., Krajewski, W.F., and Smith, J.A. 1999. "Quantification of Radar Rainfall Uncertainty," *Journal of Atmospheric and Oceanic Technology*, Vol. 16 (2), 206-215.

Bell, J.F. and James, W.P. 1985. "Radar for Flood Forecasting-Reservoir Operation," *Proceedings of the Specialty Conference on Hydraulics and Hydrology in the Small Computer Age*, ASCE, Lake Buena Vista, FL, 295-299.

Bell, J.J., Robinson, C.G., and James, W.P. 1989. "Streamflow Forecasting with Weather Radar," *Texas Civil Engineering*, Vol. 59 (3), 10-15.

Beven, K. 1985. "Distributed Models," in *Hydrological Forecasting*, Anderson and Burt (Eds), John Wiley and Sons, Chichester, UK, ch. 13.

Black, P.E. 1972. "Hydrograph Response to Geomorphic Model Watershed Characteristics and Precipitation Variables," *Journal of Hydrology*, Vol. 17, 309-329.

Bond, J.E., Browning, K.A. and Collier, C.G. 1981. "Estimates of Surface Gust Speeds using Radar Observation of Showers," *Meteorology Magazine*, Vol. 110, 29-40.

Bras, R.L. 1990. *Hydrology - An Introduction to Hydrologic Science*, Addison-Wesley Publishing Co., Reading, MA, pp. 643.

Brigham Young University. 1998. *WMS Reference Manual*, Engineering Computer Graphics Laboratory, Provo, UT, pp. 466.

Browning, K.A. and Collier, C.G. 1989. "Nowcasting of Precipitation Systems," *Reviews of Geophysics*, Vol. 27 (3), 345-370.

CH2M Hill. 1990. *Final hydrologic and Hydraulic Report for Cave Creek / Carefree Flood Delineation Study*, prepared for Flood Control District of Maricopa County, Phoenix, AZ.

Charley, W.J. 1987. "Estimation of Rainfall for Flood Forecasting using Radar and Rain Gage Data," *Engineering Hydrology, Proceedings of the Symposium*, ASCE, Williamsburg, VA, 103-108.

Ciach, G.J. and Krajewski, W.F. 1999. "On the Estimation of Radar Rainfall Error Variance," *Advances in Water Resources*, Vol. 22 (6), 585-595.

Ciach, G.J., Krajewski, W.F., Anagnostou, E.N., McCollum, J.R., Baeck, M.L., Smith, J.A., and Kruger, A. 1997. "Radar Rainfall Estimation for Ground Validation Studies of the Tropical Rainfall Measuring Mission," *Journal of Applied Meteorology*, Vol. 36 (6), 735-747.

Dempsey, C. and Skindlov, J. 1998. Personal Correspondence, Meteorologists, Salt River Project, Phoenix, AZ.

Duda, R.O. and Blackmer, R.H. 1972. *Application of Pattern Recognition Techniques to Digitised Weather Radar, Final Report Covering the Period May 25, 1971 to March 31, 1972*, Contract 1-36072, Project 1287, Stanford Research Institute, Menlo Park, CA, pp. 135.

Eagleson, P.S. 1978. "Climate, Soil and Vegetation, 2. The Distribution of Annual Precipitation Derived from Observed Storm Sequence, *Water Resources Research*, Vol. 14 (5), 713-721.

Ebert, E. 1987. "A Pattern Recognition Technique for Distinguishing Surface and Cloud Types in Polar Regions," *Journal of Climate and Applied Meteorology*, Vol. 26, 1412-1425.

Engman, Edwin T. (1986). "Roughness Coefficients for Routing Surface Runoff," *Journal of Irrigation and Drainage Engineering*, Vol 112 (1), ASCE, 39-52.

Finnerty, B. and Johnson, D. 1997. "Comparison of Mean Areal Precipitation Estimates Derived from NEXRAD Radar vs. Rain Gage Networks," *Proceedings of the 1997 27th Congress of the International Association of Hydraulic Research (IAHR), Part A*, 601-606.

Finnerty, B., Smith, M., Seo, D., Koren, V, and Moglen, G. 1995. *Sensitivity of the Sacramento Soil Moisture Accounting Model to Space-Time Scale Precipitation Inputs from NEXRAD*, Office of Hydrology, National Weather Service, Silver Spring, MD.

Foroud, N., Broughton, R.S., and Austin, G.L. 1984. "The Effects of Moving Rainstorm on Direct Runoff Properties," *Water Resources Bulletin*, Vol. 20 (1), 87-91.

Garrote, L. and Bras, R.L. 1995. "A Distributed Model for Real-Time Flood Forecasting using Digital Elevation Models," *Journal of Hydrology*, Vol. 167, 279-306.

Georgakakos, K.P. 1986. "Generalized Stochastic Hydrometeorological Model for Flood and Flash-Flood Forecasting: 1. Formulation," *Water Resources Research*, Vol. 22 (13), 2083-2095.

Georgakakos, K.P. and Bras, R.L. 1984. "A Hydrologically Useful Station Precipitation Model 1. Formulation," *Water Resources Research*, Vol. 20 (11), 1585-1596.

George V. Sabol Consulting Engineers, Inc. 1997a. *Cave Creek above Carefree Highway Floodplain Delineation Study - Technical Data Notebook Hydrology - Existing Condition*, prepared for Flood Control District of Maricopa County, Scottsdale, AZ.

George V. Sabol Consulting Engineers, Inc. 1997b. *Cave Creek above Carefree Highway Floodplain Delineation Study - Technical Data Notebook Hydraulics - 100-Year Floodplain and Floodway (Natural) Delineation*, prepared for Flood Control District of Maricopa County, Scottsdale, AZ.

Glaudemans, M. 1997. "A Local Headwater Model for Operational Use in the Modernized National Weather Service," *Proceedings of the 13th International Conference on Interactive Information Processing Systems for Meteorology, Oceanography, and Hydrology*, American Meteorological Society, Long Beach, CA, February 1997.

Green, W.H. and Ampt, G.A. 1911. "Studies on Soil Physics, The Flow of Air and Water through Soils," *Journal of Agricultural Sciences*, Vol. 4, 1-24.

Haralick, R.M. and Kelly, G.L. 1969. "Pattern Recognition with Measurement Space and Spatial Clustering for Multiple Images," *Proceedings IEEE*, Vol. 57, 654-665.

Harrison, D.L., Newcomb, P.D. and Stone, D.J. 1995. "NIMROD: A Fully Automated System for Analysing and Forecasting Precipitation," *Proceedings of the 27th Conference on Radar Meteorology*, Vail, Colorado, USA, October 9-13, 600-602.

Howes, S. 1988. "Use of Satellite and Radar Images in Operational Precipitation Nowcasting," *Journal of the British Interplanetary Society*, Vol. 41 (10), 455-460.

Hudlow, M.D. 1988. "Technological Developments in Real-Time Operational Hydrological Forecasting in the United States," *Journal of Hydrology*, Vol. 102 (1-4), 69-92.

James, W.P. and Kim, K.W. 1990. "A Distributed Dynamic Watershed Model," *Water Resources Research*, Vol. 26 (4), 587-596.

Johnson, B.E. 1997. *Development of a Storm Event Based Two-Dimensional Upland Erosion Model*, PhD Dissertation, Colorado State University, Fort Collins, CO, pp. 254.

Johnson, E.R. and Bras, R.L. 1980. "Multivariate Short-Term Rainfall Prediction," *Water Resources Research*, Vol. 16 (1), 173-185.

Johnson, L.E. 1986. "Hydrologic Modeling using Radar-Rainfall Imagery," *Proceedings of the 4th Conference on Computing in Civil Engineering*, ASCE, Boston, MA, 53-63.

Johnson, L.E. 1995. "Flood Warning System Product Usage Patterns," *Proceedings 22nd Annual Conference on Integrated Water Resources Planning for the 21st Century*, ASCE, Cambridge, MA, 779-781.

Julien, P.Y. 1982. *Prediction d'apport solide pluvial et nival dans les cours d'eau nordiques a partir du ruissellement superficiel*, PhD Dissertation, Laval University, Quebec, Canada.

Julien, P.Y. 1996. "Transforms for Runoff and Sediment Transport," *Journal of Hydrologic Engineering*, ASCE, Vol. 1 (3), 114-122.

Julien, P.Y. and Frenette, M. 1985. "Modeling of Rainfall Erosion," *Journal of Hydraulic Engineering*, ASCE, Vol. 111 (10), 1344-1359.

Julien, P.Y. and Moglen G.E. 1990. "Similarity and Length Scale for Spatially Varied Overland Flow," *Water Resources Research*, Vol. 26 (8), 1819-1832.

Julien, P.Y and Saghafian, B. 1991. *A Two-Dimensional Watershed Rainfall-Runoff Model*, Civil Engineering Report CER90-91PYJ-BS-12, Department of Civil Engineering, Colorado State University, Fort Collins, CO, 63 pp.

Julien, P.Y., Saghafian, B and Ogden, F.L. 1995. "Raster-Based Hydrologic Modeling of Spatially-Varied Surface Runoff," *Water Resources Bulletin*, Vol. 31 (3), 523-536.

Klazura, G.E., and D.A. Imy, 1993, A Description of the initial Set of Analysis Products Available from the NEXRAD WSR-88D System, *Bulletin of the American Meteorological Society*, Vol. 74 (7), 1293-1311.

Krajewski, W.F. 1987. "Co-Kriging of Radar-Rainfall and Rain Gauge Data," Journal of Geophysical Research, Vol. 92 (D8), 9571-9580.

Krajewski, W.F. 1997. "Rainfall Estimation Using Weather Radar and Ground Stations," in *Weather Radar Technology for Water Resources Management*, Graga and Massambani, eds., UNESCO Press.

Krzysztofowicz, R. 1993. *Probabilistic Hydrometeorological Forecasting System: A Conceptual Design*, NOAA Technical Memorandum NWS ER-87, National Weather Service, Silver Spring, MD.

Krzysztofowicz, R. 1996. "Probabilistic Flood Forecast-Warning System," *Proceedings of the Conference on Natural Disaster Reduction*, ASCE, Washington, DC, 231-232.

Krzysztofowicz, R., Drzal, W.J., Drake, T.R., Weyman, J.C., and Giordano, L.A. "Probabilistic Quantitative Precipitation Forecasts for River Basins," *Weather and Forecasting*, Vol. 8 (4), American Meteorological Society, 424-439.

Kuchment, L.S. 1980. "A Two-Dimensional Rainfall-Runoff Model: Identification of Parameters and Possible use for Hydrological Forecasts," *Proceedings of Hydrological Forecasting Symposium*, Oxford, UK, 215-219.

Kull, D.W. and Feldman, A.D. 1995. "Clark's Unit Hydrograph Method - 50th Anniversary," *Proceedings of the 1st International Conference on Water Resources*, ASCE, 1683-1687.

Lattermann, A. and Ubald, K. 1981. "Flood Forecast Improvement by Stochastic Estimation of the Rainfall Depth," *Proceedings - International Symposium on Real-Time Operation of Hydrosystems*, Ontario, Canada, 694-706.

Lettenmaier, D.P. and Wood, E.F. 1993. "Hydrologic Forecasting," Chapter 26 in *Handbook of Hydrology*, Maidment, D.R., ed., McGraw-Hill, New York, NY.

Lovell, T.L., Killen, J.R., and Eichert, B.S. 1993. "Reservoir Regulation and Real-Time Models for Trinity River Flood Prevention and Control," in *Engineering Hydrology*, Kuo, C.Y., ed., ASCE, 778-783.

Mimikou, M.A. and Baltas, E.A. 1996. "Flood Forecasting Based on Radar Rainfall Measurements," *ASCE Journal of Water Resources Planning and Management*, Vol. 122 (3), 151-156.

Mimikou, M.A., Baltas, E.A., and Borga, M. 1993. "Flash-Flood Forecasting by Using the HEC1F Model," in *Engineering Hydrology*, Kuo, C.Y., ed., ASCE, 85-90.

Molnar, D.K. 1997. *Grid Size Selection for 2-D Hydrologic Modeling of Large Watersheds*, PhD Dissertation, Colorado State University, Fort Collins, CO, pp. 201.

National Weather Service. 1996. *National Weather Service River Forecast System (NWSRFS) User's Manual*, Hydrologic Research Laboratory, Silver spring, MD.

Nguyen, V.T.V. and Rouselle, J. 1981. "A Stochastic Model for the Time Distribution of Hourly Rainfall Depth," *Water Resources Research*, Vol. 17 (2), 399-409.

Niemczynowicz, J. 1984. "Investigation of the Influence of Rainfall Movement on Runoff Hydrographs, II, Simulation on Real Catchments in the City of Lund," *Nordic Hydrology*, Vol. 15 (2), 71-84.

Oganesyan, V.V. and Snitkovskii, A.I. 1987. "Scheme for Operational Short-Term Forecast of Temperature and Precipitation Using Statistical Models," *Journal of Soviet Meteorology and Hydrology*, Vol. 3, 10-14.

Ogden, F.L. 1992. *Two-Dimensional Runoff Modeling with Weather Radar Data*, PhD Dissertation, Colorado State University, Fort Collins, CO, pp. 211.

Ogden, F.L. 1994. "de-St. Venant Channel Routing in Distributed Hydrologic Modeling," *Proceedings of Hydraulic Engineering '94*, ASCE Specialty Conference, G.V Cotroneo and R.R Rumer, eds., Vol. 1, 492-496.

Ogden, F.L. 1997. *CASC2D Reference Manual*, Department of Civil and Environmental Engineering, University of Connecticut, Storrs, CT.

Ogden, F.L. and Julien, P.Y. 1993. "Runoff Sensitivity to Temporal and Spatial Rainfall Variability at Runoff Plane and Small Basin Scales," *Water Resources Research*, Vol. 29, No. 8, 2589-2597.

Ogden, F.L. and Julien, P.Y. 1994. "Runoff Model Sensitivity to Radar Rainfall Resolution," *Journal of Hydrology*, Vol. 158, 1-18.

Ogden, F.L., Richardson, J.R. and Julien, P.Y. 1995. "Similarity I Catchment Response 2. Moving Rainstorms," *Water Resources Research*, Vol. 31 (6), 1543-1547.

Peters, J.C. and Ely, P.B. 1985. "Flood-Runoff Forecasting with HEC1F," *Water Resources Bulletin*, Vol. 21 (1), 7-13.

Rawls, W.J., Brakensiek, D.L. and Miller, N. 1983. "Green-Ampt Infiltration Parameters from Soil Data," *Journal of Hydraulic Engineering*, American Society of Civil Engineers, Vol. 109 (1), 62-70.

Rhea, O.J. and Hartzell, C.L. 1993. "Combining Orographic Precipitation and Runoff Models for Improving Reservoir Operations," *Proceedings of the Symposium on Engineering Hydrology*, ASCE, San Francisco, CA, 103-108.

Roberts, M.C. and Klingeman, P.C. 1970. "The Influence of Landform and Precipitation Parameters on Flood Hydrographs," *Journal of Hydrology*, Vol. 11, 393-411.

Saghafian, B. 1992. *Hydrologic Analysis of Watershed Response to Spatially Varied Infiltration*, PhD Dissertation, Department of Civil Engineering, Colorado State University, Fort Collins, CO.

Schultz, G. 1987. "Flood Forecasting Based on Rainfall Radar Measurement and Stochastic Rainfall Forecasting in the Federal Republic of Germany," Chapter 13 in *Weather Radar and Flood Forecasting*, Collinge and Kirby, eds., John Wiley & Sons Ltd., 191-207.

Seliga, T. and Chen, C. 1996. "Factors Affecting NEXRAD-Based Point Rainfall Estimation in the Seattle Area," *Proceedings of the 1996 International Geoscience and Remote Sensing Symposium, Part 1*, May 28-31 196, Lincoln, NE.

Seo, D.J., Krajewski, W.F., and Bowles, D.S. 1990. "Stochastic Interpolation Methods Used for Multiple Sensor Rainfall Estimation, Experimental Design, 1," *Water Resources Research*, Vol. 26 (3), 469-478.

Shedd, R.C., Peterlin, A. and Fox, L.E. 1992. "WSR-88D and Water Management." *Proceedings of Managing Water Resources During Global Change*, American Water Resources Association.

Singh, V.P. 1997. "Effect of Spatial and Temporal Variability in rainfall and Watershed Characteristics on Stream Flow Hydrograph," *Hydrological Processes*, Vol. 11, 1649-1669.

Singh, V.P. 1998. "Effect of the Direction of Storm Movement on Planar Flow," *Hydrological Processes*, Vol. 12, 147-170.

Smith, M.B., Seo, D., Finnerty, B., and Koren, V. 1996. "Distributed Parameter Hydrologic Modeling and NEXRAD for River Forecasting: Scale Issues Facing the National Weather Service," *Proceedings of the North American Water and Environment Congress '96*, ASCE, Anaheim, CA, June 1996.

Taylor, C., Al-Mashidani, G, and Davis, J.M. 1974. "A Finite Element Approach to Watershed Runoff," *Journal of Hydrology*, Vol. 21, 231-246.

U.S. Army Corps of Engineers. 1991. *GRASS Version 4.0 User's Reference Manual*, Construction Engineering Research Laboratory, Champaign, IL, pp. 513.

U.S. Army Corps of Engineers. 1996. *Runoff Simulation using Radar Data*, Hydrologic Engineering Center, Technical Paper 155, Davis, CA, pp. 88.

U.S. Department of Agriculture (USDA). 1994. *State Soil Geographic (STATSGO) Data Base - Data Use Information*, Soil Conservation Service, Miscellaneous Publication Number 1492, Fort Worth, TX, pp. 106.

U.S. Department of Commerce. 1961. *Rainfall Frequency Atlas of the United States for Durations from 30 Minutes to 24 Hours and Return Periods from 1 Hour to 100 Years*, National Weather Service, Technical Paper 40 (TP-40), Washington, D.C.

U.S. Geological Survey (USGS). 1987. *Digital Elevation Models - Data Users Guide 5*, U.S. Department of the Interior, Reston, VA, pp. 39.

U.S. Geological Survey (USGS). 1990. *Land Use and Land Cover Digital Data from 1:250000 and 1:100000 Scale Maps - Data Users Guide 4*, U.S. Department of the Interior, Reston, VA. 1990, pp. 54.

Vieux, B.E. and Gaur, N. 1994. "Finite Element Modeling of Storm Water Runoff Using GRASS GIS," *Microcomputers in Civil Engineering*, Vol. 9(4), 263-270.

Vieux, B. and Jones, A.T. 1997. "Flood Forecasting Using WSR-88D Rainfall Estimates: Distributed Hydrologic Simulation of Two River Basins in Oklahoma," *Proceedings of the 77th Annual Meeting of the American Meteorological Society*, February 2-7, 1997, Long Beach, CA, J83-J86.

Wall, D.J. and Shedd, R.C. 1989. "Radar Rainfall Measurements and Runoff Forecasting," *Proceedings of the 1989 National Conference on Hydraulic Engineering*, ASCE, New Orleans, LA, 565-570.

Watts, L.G. and Calver, A. 1991. "Effects of Spatially-Distributed Rainfall on Runoff for a Conceptual Catchment," *Nordic Hydrology*, Vol. 22, 1-14.

Wilson, J.W. 1966. *Movement and Predictability of Radar Echoes*, Report, U.S. Weather Bureau Contract CWB-11093, Travellers Weather Research Center, Hartford, CT.

Yen, B.C. and Chow, V.T. 1969. "A Laboratory Study of Surface Runoff Due to Moving Rainstorms," *Water Resources Research*, Vol. 5 (5), 989-1006.

Zawadski, I.I. 1973. "Statistical Properties of Precipitation Patterns," *Journal of Applied Meteorology*, Vol. 12, 459-472.

Appendix A

CASC2D SOURCE CODE

```
C     CASC2D SOURCE MODIFIED BY JEFF JORGESON
C     ISHP = WATERSHED MASK
C     IMAN = Manning's roughness grid
C     ISOIL = Soil index grid
C     E = Elevation grid (from the file ELAVG.DAT)
C     H = Overland depth
C     RINT = Rainfall intensity
C     VINF = Infiltration depth
C     DQOV = Overland flow rate
C     DQCH = Channel flow rate
C     HCH = Channel depth
C     XRGF = Column position of rainfall gage for forecast data
C     YRGF = Row position of rainfall gage for forecast data
C     RRGF = Rainfall intensities of forecast rainfall data
C     XRG = Column position of each rainfall gage
C     YRG = Row position of each rainfall gage
C     RRG = Rainfall intensities at recorded gages
C     PMAN = Manning's roughness coefficients corresponding to each roughness group
C     PINF = Infilt. parameters (Hyd. Conductivity, Cap. Head, Soil Moisture Deficit)
C     ICHN = Channel element addresses
C     CHP = Channel parameters (width, depth, and Manning's 'n')
C
      CHARACTER dname*20,tname*20,rname*20,qname*20,
      CHARACTER headline(6)*80,vinfname*20,susname*20
      INTEGER ISHP(273,173),IMAN(273,173),ISOIL(273,173)
      DIMENSION E(273,173),H(273,173),RINT(273,173),
     +VINF(273,173),DQOV(273,173),DQCH(273,173),
     +HCH(273,173),RTOT(273,173),XRGF(1000),YRGF(1000),
     +RRGF(1000),PMAN(10),PINF(12,7),ICHN(100,100,2),
     +CHP(100,4),IQ(20,2),Q(20),XRG(1000),YRG(1000),RRG(1000)
C     ---------------------------------------------------------
C     OPENING FILES
C     ---------------------------------------------------------
      OPEN(UNIT=21,FILE='SHAP.DAT',status='unknown')
      OPEN(UNIT=22,FILE='ELAVG.DAT',status='unknown')
```

```
      OPEN(UNIT=23,FILE='RAIN.DAT',status='unknown')
      OPEN(UNIT=24,FILE='SOIL.DAT',status='unknown')
      OPEN(UNIT=25,FILE='DATA1.JJ',status='unknown')
      OPEN(UNIT=26,FILE='CHN.DAT',status='unknown')
      OPEN(UNIT=27,FILE='OUT.PRN',status='unknown')
      OPEN(UNIT=28,FILE='IMAN.DAT',status='unknown')
      OPEN(UNIT=29,FILE='DISCHARGE.OUT',status='unknown')
      OPEN(UNIT=36,FILE='DEPTH.OUT',status='unknown')
      OPEN(UNIT=37,FILE='PLOT.OUT',status='UNKNOWN')
      OPEN(UNIT=54,FILE='WARN.OUT',status='UNKNOWN')
      OPEN(UNIT=32,FILE='RAINFCST.DAT',status='UNKNOWN')
C
C     "head" file contains header data for output maps in GRASS format
C     "region" file contains boundaries of watershed and rows / cols for grid
C
      open(unit=38,file='head',status='unknown')
      do 1500 i=1,6
      read(38,1501) headline(i)
1501  format(a80)
1500  continue
      close(38)
      open(unit=46,file='region',status='unknown')
      read(46,*) north,south,east,west,rows,cols
      close(46)
C
C     M = Maximum number of rows
C     N = Maximum number of columns
C     W = Grid Cell Resolution
C     NMAN = Total number of Manning 'n' values in the overland plane
C     SDEP = Storage deposition
C     DT = Computational time step
C     NITER = Total number of time intervals for the runoff simulation
C     NITRN = Total number of time intervals for the rainfall
C     NPRN = Number of time steps to write the output
C     NPLT = Number of time steps to update graphics display
C     JOUT = Row number for the outlet cell
C     KOUT = Column number for the outlet cell
C     SOUT = Bed Slope for the channel at the outlet
C     qmax = Maximum discharge at the outlet (for plotting purposes)
C     WCHOUT = Width of the outlet channel
C     DCHOUT = Depth of the outlet channel
C     RMANOUT = Manning's 'n' for the outlet channel
C     SOVOUT = Slope of the Outlet Cell
C     INDEXINF = Infiltration index (1 for infiltration or 0 for none)
C     NSOIL = Number of soils with different infiltration parameters
C     NCHN = Total number of channel links
```

```
C     MAXCHN = Maximum number of channel elements plus one
C     IRAIN = Rainfall index (1 for raingages and 0 for uniform rain)
C     CRAIN = Uniform rainfall intensity (IRAIN=0)
C     NRG = Number of rainfall gages (IRAIN=1)
C     NREAD = Ratio between raingage rainfall time step and DT
C
      READ(25,*) M,N,W,NMAN,SDEP
      write(27,9000) m,n,w,nman,sdep
9000  format('INPUT DATA'//'No. of Rows = ',i5,
     &/'No. of Columns = ',i5,/'Grid Cell Width = ',
     &f10.3,/'No. of Roughness Categories = ',i5,/'sdep = ',f10.2)
      READ(25,*) DT,NITER,NITRN,NPRN,NPLT,elconv,chancheck
      write(27,9001) dt,niter,nitrn,nprn,nplt,elconv,chancheck
9001  format('Computational Time Step (seconds) = ',f10.2,
     &/'NITER = ',i10,/'NITRN = ',i10/'NPRN = ',i10,
     &/'NPLT = ',i10,
     &/'Elevation Conversion Factor = ',f10.2,
     &/'Channel Routing Option = ',f10.2)
      READ(25,*) JOUT,KOUT,SOUT,qmax,WCHOUT,DCHOUT
     &RMANOUT,SOVOUT
      write(27,9002) jout,kout,sout,qmax,wchout,dchout,rmanout,
     &sovout
9002  format('Outlet Row = ',i5,/'Outlet Column = ',i5,
     &/'Outlet Channel Slope = ',f10.4,/'QMAX = ',f10.3,
     &/'Outlet Channel Width = ',f10.3,/'Outlet Channel Depth = ',f10.3,
     &/'Outlet Channel Roughness Coeff. = ',f10.3,
     &/'Outlet Overland Slope = ',f10.4)
      READ(25,*) INDEXINF,NSOIL
      write(27,9003) indexinf,nsoil
9003  format('INDEXINF = ',i5,/'NSOIL = ',i5)
      READ(25,*) NCHN,MAXCHN
      write(27,9004) nchn,maxchn
9004  format('No. of Channel Links = ',i5,
     &/'Max. No. of Channel Nodes = ',i5)
      READ(25,*) IRAIN
      write(27,9005) irain
9005  format('IRAIN = ',i5)
      IF(IRAIN.EQ.0) READ(25,*) CRAIN
      if (irain .eq. 0) write(27,9006) crain
9006  format('Uniform Rainfall (cm/hr) = ',f10.4)
      IF(IRAIN.EQ.1) READ(25,*) NRG,NREAD
      if (irain .eq. 1) write(27,9007) nrg,nread
9007  format('No. of Raingages = ',i10,/'NREAD = ',i10)
      IF(IRAIN.EQ.1) READ(25,*) (XRG(L),YRG(L),L=1,NRG)
      if (irain .eq. 1) then
      write(27,9008)
```

```
      write(27,9009) (xrg(l),yrg(l),l=1,nrg)
9008  format(//'     Raingage Locations',
     +/'     Column        Row'/)
9009  format(f10.2,5x,f10.2)
      endif
C     Reading rainfall forecast file which contains storm velocity
C     north, south, east, and west boundaries, number of rows and
C     columns, and uncalibrated radar precipitation values in
C     mm/hr * 1000 with data values on a 4000 meter grid.
      READ(32,*) RAINVELX,RAINVELY
      READ(32,*) NTH
      READ(32,*) STH
      READ(32,*) EST
      READ(32,*) WST
      READ(32,*) INTRWS
      READ(32,*) INTCLS
      NRGF=INTRWS*INTCLS
      write(27,9018)
9018  format(//'    RAINGAGE LOCATIONS',/'    COLUMN   ROW'/)
      KOUNTROW=0
      WST1=WST
      do 9021 K=1,INTRWS
      do 9020 L=1,INTCLS
      XRGF(L+KOUNTROW)=(WST1-west)/W
      YRGF(L+KOUNTROW)=(north-NTH)/W
      READ(32,*) RRGF(L+KOUNTROW)
      WST1=WST1+4000.0
      write(27,9019)
      XRGF(L+KOUNTROW),YRGF(L+KOUNTROW),RRGF(L+KOUNTROW)
9019  format(f10.2,5x,f10.2)
9020  continue
      KOUNTROW=KOUNTROW+INTCLS
      WST1=WST
      NTH=NTH-4000.0
9021  continue
      CLOSE(32)
C     Converting precipitation values to inches per hour and applying radar
C     calibration for new Z-R
      do 9017 LL=1,NRGF
      RRGF(LL)=RRGF(LL)/1000.
      RRGF(LL)=RRGF(LL)/300.
      RRGF(LL)=RRGF(LL)**(1.0/1.4)
      RRGF(LL)=RRGF(LL)**1.00
      RRGF(LL)=RRGF(LL)*150.
      RRGF(LL)=RRGF(LL)/25.4
9017  continue
```

```
C
      READ(25,*) (PMAN(J),J=1,NMAN)
      write(27,9010)
      write(27,9011) (pman(j),j=1,NMAN)
9010 format(//' Roughness Coeff.'/)
9011 format(f10.2)
      IF(INDEXINF.EQ.1) READ(25,*) ((PINF(J,K),K=1,3),J=1,NSOIL)
      if (indexinf .eq. 1) then
      write(27,9012)
      write(27,9013)((pinf(j,k),k=1,3),j=1,nsoil)
9012 format(//'                    INFILTRATION PARAMETERS',
     +//'Hyd. Cond.  Cap. Head    SMD'/)
9013 format(f10.9,f10.5,f10.3)
      endif
      READ(25,*) INDEXDIS,NDIS
      write(27,9014) indexdis,ndis
9014 format(//'INDEXDIS = ',i10,/'NDIS = ',i10)
      IF(INDEXDIS.EQ.1) READ(25,*) ((IQ(J,K),K=1,2),J=1,NDIS)
      if (indexdis .eq. 1) then
      write(27,9015)
      write(27,9016) ((iq(j,k),k=1,2),j=1,ndis)
9015 format(//' Discharge Gage Locations'/'      Column    Row',/)
9016 format(2i10)
      endif
      CLOSE(25)
      if (chancheck .eq. 1.0) then
      IF(NCHN.NE.0) READ(26,*) ((CHP(L,K),K=1,4),L=1,NCHN)
      IF(NCHN.NE.0) READ(26,*) (((ICHN(L,J,K),J=1,MAXCHN),
     +K=1,2),L=1,NCHN)
      CLOSE(26)
      WRITE(29,229) ((IQ(J,K),K=1,2),J=1,NDIS)
      endif
C     READING SHAP MATRIX, ELEVATIONS, INITIALIZATIONS
      DO 150 J=1,M
      DO 150 K=1,N
      READ(21,*) ISHP(J,K)
      READ(22,*) E(J,K)
      E(J,K)=E(J,K)/elconv
      IF(NSOIL.NE.0) THEN
      IF(NSOIL.EQ.1) THEN
      ISOIL(J,K)=1
      ELSE
      READ(24,*) ISOIL(J,K)
      ENDIF
      ENDIF
      IF(NMAN.EQ.1) THEN
```

```
      IMAN(J,K)=1
      ELSE
      READ(28,*) IMAN(J,K)
      ENDIF
      H(J,K)=0.
      HCH(J,K)=0.
      DQOV(J,K)=0.
      DQCH(J,K)=0.
      VINF(J,K)=0.
      RTOT(j,k)=0.
150   CONTINUE
      CLOSE(21)
      CLOSE(22)
      CLOSE(24)
      CLOSE(28)
C     Note : IC is the Link number and L is the Node number.
C     J is the row location and K is the column location.
      DO 160 IC=1,NCHN,1
      DO 175 L=1,MAXCHN,1
      J=ICHN(IC,L,1)
      K=ICHN(IC,L,2)
      IF(J.LE.0) GO TO 160
C     When ISHP is equal to 2, then the program knows that this grid
C     cell has a channel going through it.
      if (chancheck .eq. 1.0) then
      ISHP(J,K)=2
      endif
175   CONTINUE
160   CONTINUE
      VIN=0.
      VOUT=0.
      VSUR=0.
      VINFTOT=0.
      RINDEX=1.
      IFCOUNT=1
      ICOUNT=1
      IPCOUNT=1
C     TIME LOOP
      DELX=((RAINVELX*1000.*DT)/(W*3600.))
      DELY=((RAINVELY*1000.*DT)/(W*3600.))
      DO 10 I=1,NITER
      RT=(DT*I)/60.0
      RAINTOTAL=0.0
      ICALL=0
      IF(I.LE.NITRN.AND.IRAIN.EQ.1)  THEN
      IF(((I-1)/NREAD)*NREAD.EQ.(I-1))  THEN
```

```
      ICALL=1
      READ(23,*) (RRG(L),L=1,NRG)
      DO 2702 L=1,NRG
      RAINTOTAL=RAINTOTAL+RRG(L)
2702  CONTINUE
      WRITE(54,*) I,RAINTOTAL
      ENDIF
      ENDIF
      IF(I.GT.NITRN.AND.IRAIN.EQ.1)  THEN
      ICALL=1
      NRG=NRGF
      do 1504 L=1,NRG
      XRGF(L)=XRGF(L)+DELX
      YRGF(L)=YRGF(L)-DELY
      XRG(L)=XRGF(L)
      YRG(L)=YRGF(L)
      RRG(L)=RRGF(L)
1504  continue
      ENDIF
C     Applying the rainfall to each grid cell within the watershed.
      DO 1 J=1,M
      DO 1 K=1,N
      IF(ISHP(J,K).EQ.0) GO TO 1
      IF(IRAIN.EQ.0) THEN
C     Uniform rainfall
      RINT(J,K)=CRAIN
      ELSE
C     Spatially distributing the rainfall
      IF(ICALL.EQ.1) CALL RAIN(J,K,NRG,XRG,YRG,RRG,RINT)
      ENDIF
      IF(I.GT.NITRN) RINT(J,K)=0.
C     Determining the Total Rainfall Depth
      RTOT(J,K)=RTOT(J,K)+RINT(J,K)*DT
C     Computing the portion of the overland depth due to the overland flow.
      HOV=DQOV(J,K)*DT/(W*W)
C     Computing the Total Overland Depth due to the overland flow,
C     previous overland depth, and the addition due to rainfall.
      HOV=HOV+H(J,K)+RINDEX*RINT(J,K)*DT
C     When HOV is less than zero, then a negative depth situation occurs.
      IF(HOV.LT.0) THEN
      WRITE(54,9997) I,j,k,HOV
9997  FORMAT(i6,i6,i6,f7.3)
      print*,'Negative Depth in the Overland Plane'
      print*,'Grid Cell ',j,k,HOV
      stop
      endif
```

```
C     Calling the Infiltration subroutine. HOV will be modified by subtracting the
C     infiltration losses. NOTE : if the infiltration volume that can be lossed for DT is
C     greater than the amount of surface volume present, then HOV will reduce to zero.
      IF(INDEXINF.EQ.1)CALL INFILT(J,K,DT,ISOIL,VINF,PINF,HOV)
      H(J,K)=HOV
      DQOV(J,K)=0.
C     Keeping track of the Total Volume of Rainfall and the Total Volume of Infiltration.
      IF(I.EQ.NITER) THEN
      VIN=VIN+RTOT(J,K)*W*W
      vinftot=vinftot+vinf(j,k)*w*w
      endif
1     CONTINUE
C     Overland Flow Routing
11    DO 20 J=1,M
      DO 30 K=1,N
      IF(ISHP(J,K).EQ.0) GO TO 30
      DO 40 L=-1,0,1
      JJ=J+L+1
      KK=K-L
      IF(JJ.GT.M.OR.KK.GT.N.OR.ISHP(JJ,KK).EQ.0) GO TO 40
      CALL OVRL(W,IMAN,PMAN,SDEP,J,K,JJ,KK,E,H,DQOV,DT,I,
     +ISOIL,PINF,IFCOUNT,ISHP)
40    CONTINUE
30    CONTINUE
20    CONTINUE
      if (chancheck .eq. 1.0) then
C     Updating the Channel Depths
      DO 2 IC=1,NCHN,1
      DO 3 L=1,MAXCHN,1
      J=ICHN(IC,L,1)
      K=ICHN(IC,L,2)
      JJ=ICHN(IC,L+1,1)
      IF(J.LE.0) GO TO 2
      IF(JJ.LT.0) GO TO 2
      WCH=CHP(IC,1)
      DCH=CHP(IC,2)
      SFACTOR=CHP(IC,4)
      DHCH=DQCH(J,K)*DT/(W*SFACTOR*WCH)
      HCH(J,K)=HCH(J,K)+DHCH
      IF(H(J,K).GT.SDEP) THEN
C     Adding the volume of water in the overland cell into the channel.
      HCH(J,K)=HCH(J,K)+(H(J,K)-SDEP)*W/WCH
      H(J,K)=SDEP
      ENDIF
      HTOP=DCH+H(J,K)
C     In the case where the watersurface in the channel is greater than the watersurface in
```

```
C     the overland cell, then the volume of water needs to be redistributed.
      IF(HCH(J,K).GT.HTOP) THEN
      DH=(HCH(J,K)-HTOP)*WCH/(W*SFACTOR)
      H(J,K)=H(J,K)+DH
      HCH(J,K)=HTOP+DH
      ENDIF
C     Negative depths in the channel
      IF(HCH(J,K).LT.0) then
      print*,'Negative Depth in the Channel'
      print*,'j,k = ',j,k
      goto 170
      else
      endif
      DQCH(J,K)=0.
      IF(I.EQ.NITER) VSUR=VSUR+HCH(J,K)*W*WCH+H(J,K)*W*W
3     CONTINUE
2     CONTINUE
C     Channel Routing
      DO 50 IC=1,NCHN,1
      WCH=CHP(IC,1)
      DCH=CHP(IC,2)
      RMANCH=CHP(IC,3)
      SFACTOR=CHP(IC,4)
      DO 60 L=1,MAXCHN-1,1
      J=ICHN(IC,L,1)
      K=ICHN(IC,L,2)
      JJ=ICHN(IC,L+1,1)
      KK=ICHN(IC,L+1,2)
C     JJJ is a check to see when the end of a channel link has been reached.
      JJJ=ICHN(IC,L+2,1)
C     When JJ < 0, channel routing for the current link is complete.
      IF(JJ.LE.0) GO TO 50
      CALL CHNCHN(NCHN,W,WCH,DCH,RMANCH,SFACTOR,
     +J,K,JJ,KK,JJJ,E,HCH,ICHN,CHP,DQCH,NDIS,IQ,Q,
     +pman,dt,i,qsmaxout,pinf,ifcount)
60    CONTINUE
50    CONTINUE
      endif
C     Determining the Outflow Discharge
      HOUT=H(JOUT,KOUT)
      ALFA=SQRT(SOVOUT)/PMAN(IMAN(JOUT,KOUT))
      QOUTOV=0.
      QOUTCH=0.0
      IF(HOUT.GT.SDEP) QOUTOV=W*ALFA*((HOUT-SDEP)**1.667)
      H(JOUT,KOUT)=HOUT-QOUTOV*DT/(W*W)
      if (chancheck .eq. 1.0) then
```

```
      HOUT=HCH(JOUT,KOUT)
      WPOUT=WCHOUT+2.*HOUT
      IF(HOUT.GT.DCHOUT) WPOUT=WCHOUT+2.*DCHOUT
      AREAOUT=WCHOUT*HOUT
      ALFA=SQRT(SOUT)/RMANOUT
      QOUTCH=ALFA*(AREAOUT**1.6667)/(WPOUT**0.6667)
      HCH(JOUT,KOUT)=HOUT-QOUTCH*DT/(W*WCHOUT)
      endif
      QOUT=QOUTOV+QOUTCH
      if (qout .gt. qpeak) then
      qpeak=qout
      tpeak=real(i)*dt/60.
      endif
      write(6,5000) i,real(i)*dt/60.0,qout*3.28**3.0
5000  FORMAT(1x,'Iteration = ',i7,'  Time (Min) = ',f15.4,
     +'  Outflow (cfs) = ',f15.4)
C     Keeping track of the total outflow volume
      VOUT=VOUT+QOUT*DT
C     UNIT CHANGE FROM m3/s TO cfs
      IF (ICOUNT .EQ. NPRN .OR. I .EQ. 1) THEN
      WRITE(27,111) I*DT/60.,QOUT*(3.28)**3
      WRITE(29,112) I*DT/60.,(Q(ILL)*(3.28)**3,ILL=1,NDIS)
      IF (I .EQ. 1) ICOUNT=ICOUNT+1
      IF (I .NE. 1) ICOUNT=1
      ELSE
      ICOUNT=ICOUNT+1
      ENDIF
C     WRITING OUTPUT GRIDS
      IF (IPCOUNT .EQ. NPLT .OR. I .EQ. 1) THEN
      print*,'Writing Output Grids, IFCOUNT = ',IFCOUNT
      OPEN(UNIT=38,FILE='JUNK',STATUS='UNKNOWN')
      IF (IFCOUNT .LE. 9) THEN
      WRITE(38,1701) IFCOUNT
      WRITE(38,1703) IFCOUNT
      WRITE(38,1706) IFCOUNT
1701  FORMAT('depth.',i1)
1703  FORMAT('rain.',i1)
1706  FORMAT('vinf.',i1)
      else
      endif
      IF (IFCOUNT .GT. 9 .AND.IFCOUNT .LE. 99) THEN
      WRITE(38,1001) IFCOUNT
      WRITE(38,1003) IFCOUNT
      WRITE(38,1007) IFCOUNT
1001  FORMAT('depth.',i2)
1003  FORMAT('rain.',i2)
```

```
1007 FORMAT('vinf.',i2)
     else
     endif
     if (IFCOUNT .gt. 99 .and. IFCOUNT .le. 999) then
     WRITE(38,1601) IFCOUNT
     WRITE(38,1603) IFCOUNT
     WRITE(38,1606) IFCOUNT
1601 FORMAT('depth.',i3)
1603 FORMAT('rain.',i3)
1606 FORMAT('vinf.',i3)
     else
     endif
     rewind(38)
     read(38,1006) dname
     read(38,1006) rname
     read(38,1006) vinfname
1006 format(a20)
     close(38)
C    Writing the Output Grids (Depth, Rain and Infiltration )
     open(unit=39,file=dname,status='unknown')
     open(unit=42,file=rname,status='unknown')
     open(unit=45,file=vinfname,status='unknown')
     do 1010 j1=1,6
     write(39,1020) headline(j1)
     write(42,1020) headline(j1)
     write(45,1020) headline(j1)
1020 format(a80)
1010 continue
     do 1030 j1=1,M
     do 1040 k1=1,N
     if (ISHP(j1,k1) .eq. 2) then
     write(39,*) HCH(j1,k1)*1e3
     else
     write(39,*) H(j1,k1)*1e3
     endif
C    Note : The rainfall intensity is being written in in/hr * 1000
     write(42,*) RINT(j1,k1)*1000*3600/.0254
     write(45,*) VINF(j1,k1)*1e6
1040 continue
1030 continue
     close(39)
     close(42)
     close(45)
     IFCOUNT=IFCOUNT+1
     IF (I .EQ. 1) IPCOUNT=IPCOUNT+1
     IF (I .NE. 1) IPCOUNT=1
```

```
      ELSE
      IPCOUNT=IPCOUNT+1
      ENDIF
10    CONTINUE
C     Writing the Final Output Information
      WRITE(36,898)
      DO 899 J=1,M
      DO 899 K=1,N
      IF(ISHP(J,K).EQ.0) GO TO 899
      WRITE(36,891) J,K,1000.*H(J,K),1000.*VINF(J,K)
899   CONTINUE
C     UNIT CHANGE FROM m3 TO ft3
      WRITE(27,113) qpeak*(3.28**3),tpeak,VIN*(3.28**3),
     +VOUT*(3.28**3),100.*VOUT/VIN,VSUR*(3.28**3),
     +100.*VSUR/VIN,VINFTOT*(3.28**3),100.*VINFTOT/VIN
     +,100.*(VOUT+VSUR+VINFTOT)/VIN
      GO TO 172
170   WRITE(27,171) J,K,I*DT,HOV
172   CONTINUE
      WRITE(27,'(" Stopped at ",I2,":",I2,":",I2)')IHR,IMIN,ISEC
222   FORMAT(//' TIME(MIN)  DISCHARGE(CFS)'/)
229   FORMAT('DISCHARGE AT: ',20(2I3,'   '))
111   FORMAT(2X,F7.2,F14.3)
112   FORMAT(2X,F7.2,20F10.3)
113   FORMAT(//' PEAK DISCHARGE in CFS=',F15.3/' TIME TO PEAK in MIN=',
     +  F15.1/' VOLUME IN in FT3=',F20.1/' VOLUME OUT in FT3=',2F25.3
     + /' SURFACE VOLUME in FT3=',2F25.3/' VOLUME INFILTRATED IN FT3='
     + ,2F25.3/'PERCENT MASS BALANCE=',F25.3/)
171   FORMAT(/'PROGRAM STOPPED FOR NEGATIVE DEPTH',2I4,2F15.6)
1054  FORMAT(I10)
550   FORMAT(i4)
898   FORMAT(' ROW  COLUMN  DEPTH(MM)  INILTRATION(MM)')
891   FORMAT(2I6,2F10.0)
      STOP
      END
C     ================================================
      SUBROUTINE RAIN(J,K,NRG,XRG,YRG,RRG,RINT)
C     ================================================
      DIMENSION XRG(NRG),YRG(NRG),RINT(273,173),RRG(NRG)
      RINT(J,K)=0.
      TOTDIST=0.
      TOTRAIN=0.
      SMALLEST=1000000.
      CLOSEST=1
C     If there is only one rain gage, then the rainfall intensity at cell j,k "rint(j,k)" is set
C     equal to the rainfall intensity for that single gage.
```

```
      if (nrg .eq. 1) then
      rint(j,k)=rrg(1)
      else
C     If there are more than one rain gage (if nrg > 1), then the distance from cell J,K to
C     rain gage is computed below as DIST.
      DO 1 L=1,NRG
      REALJ=J
      REALK=K
      DIST=SQRT((REALJ-YRG(L))**2+(REALK-XRG(L))**2)
C     Finding gage closet to the cell (Thiessen Polygon)
      IF(DIST.LT.SMALLEST) THEN
      SMALLEST=DIST
      CLOSEST=L
      ENDIF
1     CONTINUE
      RINT(J,K)=RRG(CLOSEST)
      ENDIF
C     UNIT CHANGE FROM in/hr TO m/s
2     RINT(J,K)=RINT(J,K)*0.0254/3600.
      RETURN
      END
C     ==========================================================
      SUBROUTINE INFILT(J,K,DT,ISOIL,VINF,PINF,HOV)
C     ==========================================================
      INTEGER  ISOIL(273,173)
      DIMENSION  VINF(273,173),PINF(12,7)
C     Setting the Infiltration Parameters
      IINF=ISOIL(J,K)
      HYDCON=PINF(IINF,1)
      CS=PINF(IINF,2)
      SMD=PINF(IINF,3)
C     Computing the Rate of Infiltration
      P1=HYDCON*DT-2.*VINF(J,K)
      P2=HYDCON*(VINF(J,K)+CS*SMD)
      RINF=(P1+SQRT(P1**2+8.*P2*DT))/(2.*DT)
C     When the rate of infiltration is greater than HOV/DT, then all the water on the
C     overland cell is assumed to be infiltrated and the overland depth is reduced to zero
      IF((HOV/DT).LE.RINF) THEN
      RINF=HOV/DT
      HOV=0
      ELSE
      HOV=HOV-RINF*DT
      ENDIF
C     Accumulated volume of water infiltrated for the grid cell (J,K)
      VINF(J,K)=VINF(J,K)+RINF*DT
      RETURN
```

```
      END
C     ==========================================================
      SUBROUTINE OVRL(W,IMAN,PMAN,SDEP,J,K,JJ,KK,E,H,DQOV,DT,
     +I,ISOIL,PINF,IFCOUNT,ISHP)
C     ==========================================================
      DIMENSION  E(273,173),H(273,173),DQOV(273,173),PMAN(10),
     +PINF(12,7), ISHP(273,173)
      INTEGER  IMAN(273,173),ISOIL(273,173)
      DATA     A/1./
      S0=(E(J,K)-E(JJ,KK))/W
      DHDX=(H(JJ,KK)-H(J,K))/W
      SF=S0-DHDX+1E-30
      HH=H(J,K)
      RMAN=PMAN(IMAN(J,K))
      IF(SF.LT.0) HH=H(JJ,KK)
      IF(SF.LT.0) RMAN=PMAN(IMAN(JJ,KK))
      IF(HH.LT.SDEP) RETURN
      ALFA=(ABS(SF)**0.5)/RMAN
C     Computing Overland Flow
      DQQ=SIGN(A,SF)*W*ALFA*((HH-SDEP)**1.667)
      DQOV(J,K)=DQOV(J,K)-DQQ
      DQOV(JJ,KK)=DQOV(JJ,KK)+DQQ
      RETURN
      END
C     ==========================================================
      SUBROUTINE CHNCHN(NCHN,W,WCH,DCH,RMANCH,SFACTOR,
     +J,K,JJ,KK,JJJ,E,HCH,ICHN,CHP,DQCH,NDIS,IQ,Q,
     +pman,dt,i,qsmaxout,pinf,ifcount)
C     ==========================================================
      DIMENSION E(273,173),HCH(273,173),ICHN(100,100,2),CHP(100,3),
     +DQCH(273,173),IQ(20,2),Q(20),pman(10),
     +qsmaxout(273,173),pinf(12,7)
      DATA     A/1./
      S0=(E(J,K)-DCH-E(JJ,KK)+DCH)/(W*SFACTOR)
C     If JJJ less than zero, end of the channel link has been reached.
      IF(JJJ.LT.0) THEN
      DO 5 IIC=1,NCHN,1
      IF(JJ.EQ.ICHN(IIC,1,1).AND.KK.EQ.ICHN(IIC,1,2)) THEN
      S0=(E(J,K)-DCH-E(JJ,KK)+CHP(IIC,2))/(W*SFACTOR)
      IJUN=IIC
      GO TO 7
      ENDIF
5     CONTINUE
      ENDIF
7     DHDX=(HCH(JJ,KK)-HCH(J,K))/(W*SFACTOR)
      SF=S0-DHDX+1E-30
```

```
      IF(ABS(SF).LT.1E-20) SF=1E-20
      HH=HCH(J,K)
      IF (SF .LT. 0 .AND. JJJ .LT. 0) THEN
      WCH=CHP(IJUN,1)
      DCH=CHP(IJUN,2)
      RMANCH=CHP(IJUN,3)
      SFACTOR=CHP(IJUN,4)
      HH=HCH(JJ,KK)
      ENDIF
      WP=WCH+2.*HH
      IF(HH.GT.DCH) WP=WCH+2.*DCH
      AREA=WCH*HH
      DQ=SIGN(A,SF)*(SQRT(ABS(SF))/RMANCH)*(AREA**1.6667)/(WP**0.667)
      DQCH(J,K)=DQCH(J,K)-DQ
      DQCH(JJ,KK)=DQCH(JJ,KK)+DQ
      DO 367 ILL=1,NDIS
      IF(J.EQ.IQ(ILL,1).AND.K.EQ.IQ(ILL,2)) Q(ILL)=DQ
367   CONTINUE
2600  RETURN
      END
```

Appendix B

SOURCE CODE FOR WSR-88D RADAR PROCESSING PROGRAM

```
#include <stdio.h>
#include <sys/types.h>
#include <sys/stat.h>
#include <math.h>

/*  This program reads in a list of binary WSR-88D radar files and generates a    */
/*  precipitation input file for either the HEC-1 or CASC2D models.                */

FILE *input;
float xw,xe,y_n,ys;
double x_coord[15000],y_coord[15000];
float incr_precip[15000][500];
int fl=0,pt_ct,num_files,yes_old,units,num_hr_files,zone;
unsigned char val_keep[15000][500];
unsigned short int rainfall_end_time[500],hr_end_time[100];

/*  This function starts with the latitude and longitude of the  radar site and    */
/*  determines the LFM grid coordinates where the radar site is.  Then the upper   */
/*  left LFM grid for that radar file is computed, the precipitation values are read, */
/*  the coordinates are converted to UTM and those radar data points falling       */
/*  within the area of  interest are written to an array which later used to create */
/*  the desired output file(s) for either HEC-1 or CASC2D use.                     */

void lfm_convert (lat,lon)

{
 double mesh_len,xpole,ypole,re,latit,latrad,longit,lonrad;
 double r,lfmx_site,lfmy_site,deg_per_rad,earth_rad,Mesh_len;
 double lfmx_nw,lfmy_nw,Xpole,Ypole,Stdlon,Stdlat,fraction;
 double lfmx_cell,lfmy_cell,ang,lon_cell,lat_cell,gi,x,y,rr;
 double longitude,latitude,zone_radar,conval;
 double zone2,a=6378206.4,ecc=0.006768658,k0=0.9996;
 double a0=.998305682,a1=.002542556,a2=.000002698,a3=.000000004;
 double centmer,lprime,r2,lrad,lnrad,lprad,t,sphi;
```

```
  double eye,p2,p4,a6,ivp,vp3,b5,n2,easting,northing;
  double conval1,conval2,conval3,conval4;
  double lat_cell_rad,lon_cell_rad,sin_phi,cos_phi,tan_phi;
  double maxrain;
  unsigned short num_bytes_in_row;
  unsigned char num_values;
  unsigned char value;
  int i,j,k,l,m,n,zone1,zone_rad,west_lon_radar;
  int nbytes_raw,nwords,wordsread;
  maxrain = 0.0;

/*  The UTM zone where the radar site is located is determined, and later only    */
/*  those precipitation values which fall in the same UTM zone are saved.        */

  zone_radar = (648000. - (lon/-1000. * 3600.)) / 21600.;
  zone_rad = floor(zone_radar) + 1;
  west_lon_radar = (((180 - (zone_rad * 6)) + 3) * 3600) + (3 * 3600);

/* The following are constants for use in converting lat-lon to LFM.             */

  deg_per_rad = 57.2957795131;
  earth_rad = 6371.2;
  Mesh_len = 190.5;
  Xpole = 11.0;
  Ypole = 41.0;
  Stdlon = 105.0;
  Stdlat = 60.0 / deg_per_rad;
  fraction = 40.;

/* These do the actual conversion from lat-lon to lfm grid.                      */

  mesh_len = Mesh_len / fraction;
  xpole = (fraction * (Xpole - 1.0)) + 1.0;
  ypole = (fraction * (Ypole - 1.0)) + 1.0;
  re = (earth_rad * (1.0 + sin (Stdlat))) / mesh_len;
  latit = lat/1000.;
  latrad = latit / deg_per_rad;
  longit = (lon * -1.0) / 1000.;
  lonrad = (longit + 180.0 - Stdlon) / deg_per_rad;
  r = re * cos(latrad) / (1.0 + sin(latrad));
  lfmx_site = (r * sin(lonrad)) + xpole;
  lfmy_site = (r * cos(lonrad)) + ypole;

/*  Now from that center grid, the center of northwest corner LFM grid cell is   */
/*  found.  This is the starting point of the actual data in the radar file. From this,  */
/*  the data values move one lfm grid cell at a time across to the east for 131  */
```

```
/*  values, then back to the west edge and down one row to go across for the next  */
/*  131 values, etc.                                                                */

  lfmx_nw = floor(lfmx_site) - 64.5;
  lfmy_nw = floor(lfmy_site) + 65.5;
  lfmy_cell = lfmy_nw + 1.0;

/* The values for the 131x131 grid are now read and converted to proper units.     */

  pt_ct = 0;

  for (i=0; i<131; i++)
   {
    lfmx_cell = lfmx_nw;
    lfmy_cell = lfmy_cell - 1.0;
    fread(&num_bytes_in_row,1,2,input);

    for (j=0; j<num_bytes_in_row/2; j++)
     {
      fread(&num_values,1,1,input);
      fread(&value,1,1,input);
      if(i==0&&j==0&&value==157)
       yes_old=1;
        printf("%d \n",yes_old);
      for (k=0; k<num_values; k++)
       {
        if (yes_old == 1)          /* Old format is different */
         {
          if (value ==  157)
           conval = -10.0;
          else if (value == 0)
           conval = 0.0;
          else
           {
            conval1 = value;
            conval2 = log(10.0);
            conval3 = ((0.5 * conval1) -17.0) / 10.0;
            conval4 = conval2 * conval3;
            conval = (exp(conval4));
           }
         }
        else
         {
          if (value ==  255)
           conval = -10.0;
          else if (value == 0)
```

```
    conval = 0.0;
   else
    {
     conval1 = value;
     conval2 = log(10.0);
     conval3 = ((0.125 * conval1) - 6.0) / 10.0;
     conval4 = conval2 * conval3;
     conval = (exp(conval4));
    }
   }

  gi = re * re;
  x = lfmx_cell - xpole;
  y = lfmy_cell - ypole;
  rr = x*x + y*y;
  lat_cell = asin((gi - rr) / (gi + rr)) * deg_per_rad;
  ang = atan2(y,x) * deg_per_rad;
  if (ang < 0)
   ang = ang + 360.0;
  lon_cell = 270.0 + Stdlon - ang;
  if (lon_cell < 0)
   lon_cell = lon_cell + 360.0;
  if (lon_cell > 360)
   lon_cell = lon_cell - 360.0;

/*  Here the lat and lon are converted to UTM coordinates                    */

    latitude = lat_cell * 3600.;
    longitude = lon_cell * 3600.;
    centmer = ((180 - (zone_rad * 6)) + 3) * 3600;
    lprime =  centmer - longitude;
    lrad = (latitude / 3600.) * (3.1415927 / 180.);
    lnrad = (longitude / 3600.) * (3.1415927 / 180.);
    r2 = a / pow((1.-((ecc)*(pow(sin(lrad),2.)))),.5);
    lprad = lprime * (3.1415927 / 648000.);
    t = sin(lrad) / cos(lrad);
    n2 = (ecc) * pow(cos(lrad),2.) / (1 - ecc);
    sphi=a*((a0*lrad)-(a1*sin(2.*lrad))+(a2*sin(4.*lrad))-
      (a3*sin(6.*lrad)));
    eye = sphi * k0;
    p2 = r2*(pow(lprad,2.)) *.5 * sin(lrad) * cos(lrad) * k0;
    p4 = (r2/24.) * (pow(lprad,4.)) * sin(lrad) * cos(lrad) * k0;
    a6=(r2/720.)*(pow(lprad,6.))*sin(lrad)*cos(lrad)*(61.-(58.*pow(t,2.))+
       pow(t,4.)+(270.*pow(n2,.5))-(330.*n2*pow(t,2.))+(445.*n2*n2))*k0;
    ivp=r2*lprad*cos(lrad)*k0;
    vp3=(r2/6.)*pow(lprad,3.)*pow(cos(lrad),3.)*(1.-(t*t)+n2)*k0;
```

```
        b5=(r2/120.)*pow(lprad,5.)*(5.-(18.*t*t)+pow(t,4.)+(14.*n2)-
          (58.*n2*t*t)+(13.*n2*n2))*k0;
        easting=500000.+ivp+vp3+b5;
        northing=eye+p2+p4+a6;

/*  UTM conversion complete with easting and northing as coords.          */

/*  Saving the x and y coordinates and the precipitation value.           */

        x_coord[pt_ct] = easting;
        y_coord[pt_ct] = northing;
        val_keep[pt_ct][fl] = value;
        incr_precip[pt_ct][fl] = conval;
        pt_ct++;
        if (conval > maxrain)
         maxrain = conval;

/*  At this point, you have an array of values called incr_precip[pt_ct][fl].  */
/*  The values in this array represent the incremental precipitation at each time  */
/*  for each location in the radar grid which falls within the N-S-E-W limits  */
/*  entered earlier.  The first array index, [pt_ct], refers to the location in space,  */
/*  while the second array index, [fl], relates to the time.              */

/*  Move to next LFM cell                                                 */

        lfmx_cell = lfmx_cell + 1.0;
        }
       }
      }

/*  Counter for number of data files read.                                */

 fl++;
 printf("   %10.2f\n",maxrain);
}

/*  This function prints two files, a scattered data file and an ASCII scalar data  */
/*  set file.  These two files are used by WMS to interpolate basin average  */
/*  precipitation values over each subbasin in a TIN.                     */

void print_hec1()

{

 FILE *hec_xyf,*hec_scl;
```

```
 char file_hec[20],file_xyf[20],file_scl[20];
 int l1,l2,l3;
 printf("\n\nEnter the name of the output files:\n\n");
 scanf("%s", file_hec);
 strcpy(file_xyf,file_hec);
 strcat(file_xyf,".xyf");
 hec_xyf=fopen(file_xyf,"w");
 strcpy(file_scl,file_hec);
 strcat(file_scl,".scl");
 hec_scl=fopen(file_scl,"w");

/*  Print out the 2D scattered point file.                                  */

 fprintf(hec_xyf,"SCAT2D\n");
 fprintf(hec_xyf,"DELEV 0.000000000000000e+00\n");
 fprintf(hec_xyf,"XY %d %s %d\n",pt_ct,file_xyf,f1);
 for(l1=0; l1<pt_ct; l1++)
  fprintf(hec_xyf,"%7.2f  %7.2f\n",x_coord[l1],y_coord[l1]);

/*  Print out the ASCII scalar data set file.                               */

 fprintf(hec_scl,"SCALAR\n");
 fprintf(hec_scl,"ND %d\n",pt_ct);
 fprintf(hec_scl,"STAT 0\n");
 for (l2=0; l2<num_files; l2++)
  {
   fprintf(hec_scl,"TS %5d\n",hr_end_time[l2]);
    for (l3=0; l3<pt_ct; l3++)
     fprintf(hec_scl,"%5.2f\n",incr_precip[l3][l2]);
  }
}

/*  This function prints a CASC2D gage file with the precipitation values in mm.  */

void print_casc2d()
{
 FILE *gage;
 char file_casc2d[20],gage_file[20];
 int l4,l5,l6;
 printf("\n\nEnter the name of the CASC2D gage file:\n\n");
 scanf("%s", file_casc2d);
 strcpy(gage_file,file_casc2d);
 strcat(gage_file,".gag");
 gage=fopen(gage_file,"w");
 for(l4=0; l4<pt_ct; l4++)
  fprintf(gage,"%7.2f  %7.2f\n",x_coord[l4],y_coord[l4]);
```

```
 for (l5=0; l5<num_hr_files; l5++)
  {
   for (l6=0; l6<pt_ct; l6++)
    fprintf(gage,"%5.2f ",incr_precip[l6][l5]);
   fprintf(gage,"\n");
  }
}

main()

{
 FILE *out_head,*data_list;

 char file_list[20],file_head[20];
 char input_file[500][20],data_files[20],file_in[20];
 struct stat status_buffer;
 int filesize,eocheck,junk,f,model,hr;

/*  These variables are the header information in the radar files.                */

 unsigned short int msg_code,msg_code_test,msg_date,msg_date_test;
 long int msg_time,msg_length;
 unsigned short int source_id,dest_id,num_block,dummy;
 short int block_divide;
 long int lat_radar;
 long int long_radar;
 unsigned short int height_radar;
 unsigned short int prod_code;
 unsigned short int op_mode;
 unsigned short int vol_cov_pat;
 unsigned short int seq_num;
 unsigned short int vol_scan_num;
 unsigned short int vol_scan_date;
 unsigned short int vol_scan_time;
 unsigned short int prod_gen_date;
 unsigned long int prod_gen_time;
 long int not_used_1;
 unsigned short int el_num;
 short int not_used_2;
 unsigned short int max_rain_accum;
 unsigned short int rate_bias;
 unsigned short int err_var_bias;
 unsigned short int rainfall_end_date;
 short int not_used_3;
 unsigned short int num_maps;
 long int offset_to_symb;
```

```
long int offset_to_graph;
long int offset_to_tab;
short int packet_flags;
unsigned short int i_coord_start;
unsigned short int j_coord_start;
unsigned short int x_scale_int;
unsigned short int x_scale_fract;
unsigned short int y_scale_int;
unsigned short int y_scale_fract;
unsigned short int num_row;
unsigned short int packing_desc;
unsigned short int row_width;
unsigned short int num_rows;
float first_time,last_time,time_incr,hour,end_time;

/*  The input files are read from file called "data_files".                    */

printf("\n\n  NOTE:  You must have a list of the radar data\n");
printf("         files to be processed in a file called\n");
printf("         'data_files'.  Enter 1 to continue or 2 to quit => \n\n");
scanf("%d",&junk);
if (junk == 2)
 exit(0);
printf("\nDo you want to create input for HEC-1 or CASC2D?\n");
printf("\n  Enter 1 for HEC-1 or 2 for CASC2D:\n");
scanf("%d",&model);

strcpy (file_list,"data_files");
data_list=fopen(file_list,"r");

eocheck - 4;
num_files = 0;
num_hr_files = 0;
while (eocheck != EOF)
 {
  eocheck=fscanf(data_list,"%s",input_file[num_files]);
  num_files ++;
 }
num_files --;
fclose(data_list);

printf("\n\nfile          rain end time    time incr.   max rain\n");
printf("name            (min)        (min)      (mm)\n");
printf("====          ============   ==========  ========\n");

for (f=0; f<num_files; f++)
```

```
{
 strcpy(file_in,input_file[f]);
 strcpy(file_head,input_file[f]);
 strcat(file_head,".head");

 input=fopen(file_in,"rb");
 out_head=fopen(file_head, "w");

 if (input == NULL)
  printf("Error opening file called: %s\n\n", file_in);

/*  This gets the file size.                                          */

 stat(file_in, &status_buffer);
 filesize = status_buffer.st_size;
 fprintf(out_head,"\nThe file size is: %d\n",filesize);

/*  The following statements read and write the header information.   */

 fread(&msg_code,1,2,input);
 fprintf(out_head,"\nmessage code: %d",msg_code);

 fread(&msg_date,1,2,input);
 fprintf(out_head,"\nmessage date: %d",msg_date);

 fread(&msg_time,1,4,input);
 fprintf(out_head,"\nmessage time: %d",msg_time);

 fread(&msg_length,1,4,input);
 fprintf(out_head,"\nmessage length: %d",msg_length);

 fread(&source_id,1,2,input);
 fprintf(out_head,"\nsource id: %d",source_id);

 fread(&dest_id,1,2,input);
 fprintf(out_head,"\ndestination id: %d",dest_id);

 fread(&num_block,1,2,input);
 fprintf(out_head,"\nnumber of blocks: %d",num_block);
 fread(&block_divide,1,2,input);
 fprintf(out_head,"\nblock divider: %d",block_divide);

 fread(&lat_radar,1,4,input);
 fprintf(out_head,"\nlatitude of radar: %d",lat_radar);

 fread(&long_radar,1,4,input);
```

```
fprintf(out_head,"\nlongitude of radar: %d",long_radar);

fread(&height_radar,1,2,input);
fprintf(out_head,"\nheight of radar: %d",height_radar);

fread(&prod_code,1,2,input);
fprintf(out_head,"\nproduct code: %d",prod_code);

fread(&op_mode,1,2,input);
fprintf(out_head,"\noperational mode: %d",op_mode);

fread(&vol_cov_pat,1,2,input);
fprintf(out_head,"\nvolume coverage pattern: %d",vol_cov_pat);

fread(&seq_num,1,2,input);
fprintf(out_head,"\nsequence number: %d",seq_num);

fread(&vol_scan_num,1,2,input);
fprintf(out_head,"\nvolume scan number: %d",vol_scan_num);

fread(&vol_scan_date,1,2,input);
fprintf(out_head,"\nvolume scan date: %d",vol_scan_date);

fread(&vol_scan_time,1,4,input);
fprintf(out_head,"\nvolume scan time: %d",vol_scan_time);

fread(&prod_gen_date,1,2,input);
fprintf(out_head,"\nproduct generation date: %d",prod_gen_date);

fread(&prod_gen_time,1,4,input);
fprintf(out_head,"\nproduct generation time: %d",prod_gen_time);

fread(&not_used_1,1,4,input);

fread(&el_num,1,2,input);
fprintf(out_head,"\nelevation number: %d",el_num);

fread(&not_used_2,1,34,input);

fread(&max_rain_accum,1,2,input);
fprintf(out_head,"\nmax rainfall accumulation: %d",max_rain_accum);

fread(&rate_bias,1,2,input);
fprintf(out_head,"\nrate bias: %d",rate_bias);

fread(&err_var_bias,1,2,input);
```

```
fprintf(out_head,"\nerror variatin of bias: %d",err_var_bias);

fread(&rainfall_end_date,1,2,input);
fprintf(out_head,"\nrainfall end date: %d",rainfall_end_date);

fread(&rainfall_end_time[f],1,2,input);
fprintf(out_head,"\nrainfall end time: %d",rainfall_end_time[f]);

printf("%s     %7d",file_in,rainfall_end_time[f]);

if (f == 0)
 printf("              ");
else
 {
 time_incr = rainfall_end_time[f] - rainfall_end_time[f-1];
 printf("         %5.0f",time_incr);
 }

fread(&not_used_3,1,4,input);

fread(&num_maps,1,2,input);
fprintf(out_head,"\nnumber of maps: %d",num_maps);

fread(&offset_to_symb,1,4,input);

fread(&offset_to_graph,1,4,input);

fread(&offset_to_tab,1,4,input);

fread(&packet_flags,1,6,input);
fprintf(out_head,"\npacket flags: %d",packet_flags);

fread(&i_coord_start,1,2,input);
fprintf(out_head,"\ni coordinate start: %d",i_coord_start);

fread(&j_coord_start,1,2,input);
fprintf(out_head,"\nj coordinate start: %d",j_coord_start);

fread(&x_scale_int,1,2,input);
fprintf(out_head,"\nx scale integer: %d",x_scale_int);

fread(&x_scale_fract,1,2,input);
fprintf(out_head,"\nx scale fractional: %d",x_scale_fract);

fread(&y_scale_int,1,2,input);
fprintf(out_head,"\ny scale integer: %d",y_scale_int);
```

```
  fread(&y_scale_fract,1,2,input);
  fprintf(out_head,"\ny_scale fractional: %d",y_scale_fract);

  fread(&num_row,1,2,input);
  fprintf(out_head,"\nnumber of rows: %d",num_row);

  fread(&packing_desc,1,2,input);
  fprintf(out_head,"\npacking descriptor: %d",packing_desc);

  fread(&row_width,1,2,input);
  fprintf(out_head,"\nwidth of row: %d",row_width);

  fread(&num_rows,1,2,input);
  fprintf(out_head,"\nnumber of rows: %d\n\n",num_rows);

/*  The function lfm_convert is called.  This function takes the latitude and   */
/*  longitude of the radar site, determines which lfm cell it is in, and        */
/*  georeferences the radar data to the Universal Transverse Mercatur (UTM)     */
/*  coordinate system.                                                          */

 lfm_convert(lat_radar,long_radar);

 fclose(input);
 fclose(out_head);
}

 printf("\n\nThe number of files processed is: %d\n",num_files);

 if (model == 1)
  print_hec1();
 else
  print_casc2d();

 printf("\n\nDONE\n\n");

}
```

Appendix C

CASC2D INPUT DATA

This appendix provides a brief summary of the input data required for the CASC2D model with sample input files from the calibration runs for the Cave Creek and Hassyampa River watersheds.

The CASC2D model requires four basic raster maps:

1. SHAPE - Defines the watershed "mask" or shape of the watershed.
2. ELEVATION - Provides the elevation value for each grid cell in the watershed.
3. SOIL - Provides a soil index number for each grid cell. The infiltration parameters for each soil index are then provided in the input data file. These parameters include hydraulic conductivity, wetted front suction head, and initial soil moisture deficit.
4. IMAN - Provides a roughness index for each grid cell. The Manning n value for each index is then provided in the input data file.

The SHAPE map provides a simple map consisting of "0" and "1" values. Cells with value "1" are inside the watershed and cells with value "0" are outside the watershed boundary. Infiltration parameters are generally initially estimated based on the soil texture of the soil in each grid cell. The data in Table C.1 from Rawls et al. (1983) are commonly used to relate these infiltration parameters to soil texture.

Soil Texture	Total Porosity	Effective Porosity	Wetted Front Capillary Head (m)	Hydraulic Conductivity (m/s)
sand	0.437	0.417	0.0495	3.27E-5
loamy sand	0.437	0.401	0.0613	8.31E-6
sandy loam	0.453	0.412	0.1101	3.03E-6
loam	0.463	0.434	0.0889	9.44E-7
silt loam	0.501	0.486	0.1668	1.81E-6
sandy clay loam	0.398	0.330	0.2185	4.17E-7
clay loam	0.464	0.309	0.2088	2.78E-7
silty clay loam	0.471	0.432	0.2730	2.78E-7
sandy clay	0.430	0.321	0.2390	1.67E-7
silty clay	0.479	0.423	0.2922	1.39E-7
clay	0.475	0.385	0.3163	8.33E-8

Table C.1 Green-Ampt Parameters by Soil Texture (after Rawls and Brakensiek, 1983)

The input data and channel data files for the Cave Creek and Hassyampa River models are provided below with some descriptive comments to clarify some of the variable names and input data. Descriptions of most variables are provided in the comment lines of the CASC2D source code in Appendix A.

CAVE CREEK INPUT FILE - FEBRUARY CALIBRATION EVENT

```
160  110  200.0  4  0.          > M, N, W, NMAN, SDEP
10.  30000  27810  30           > DT, NITER, NITRN, NPRN
240  10.0  1.0                  > NPLT, ELCONV, CHANCHECK
154  6  0.0025  15000.  200.0   > JOUT, KOUT, SOUT, QMAX, WCHOUT
3.0  0.05  0.0025               > DCHOUT, RMANOUT, SOVOUT
1  9                           > INDEXINF, NSOIL
35  31                         > NCHN, MAXCHN
1                              > IRAIN
8  30                          > NRG, NREAD
75.5    10.0                   > XRG(L), YRG(L) for L = 1, NRG
101.0   50.0
77.0    112.0
28.5    102.0
9.0     153.0
-14.3   195.0
```

```
-23.8   97.0
31.0    5.2
0.015                          > PMAN(J) for J = 1, NMAN
0.065
0.04
0.03
3.29E-7  0.146  0.095          > PINF(J,K) for K = 1, 3 and J = 1, NSOIL
2.44E-7  0.131  0.072
5.02E-7  0.200  0.051
2.58E-7  0.173  0.089
3.38E-7  0.161  0.097
8.40E-7  0.200  0.037
1.18E-6  0.110  0.082
1.29E-6  0.200  0.072
2.33E-6  0.110  0.121
1   1                          > INDEXDIS, NDIS
154   6                        > IQ(J,K) for K = 1, 2 and J = 1, NDIS
```

CAVE CREEK CHANNEL DATA FILE

```
20.0   2.5  0.037  1.0         > Width (m), Depth (m), Manning n, Sinuosity
10.0   2.0  0.037  1.0         >  Same format for Links 1 through 35
10.0   2.0  0.037  1.0
10.0   2.0  0.037  1.0
10.0   2.5  0.037  1.0
10.0   2.5  0.037  1.0
10.0   2.5  0.037  1.0
15.0   2.5  0.037  1.0
20.0   3.0  0.037  1.0
8.0    2.0  0.037  1.0
20.0   2.5  0.037  1.0
30.0   3.0  0.037  1.0
30.0   3.0  0.037  1.0
40.0   3.0  0.037  1.0
60.0   3.5  0.037  1.0
50.0   4.0  0.047  1.0
40.0   4.0  0.027  1.0
40.0   4.0  0.027  1.0
70.0   4.0  0.027  1.0
50.0   4.0  0.037  1.0
75.0   3.5  0.037  1.0
150.0  3.5  0.037  1.0
150.0  4.0  0.037  1.0
150.0  3.0  0.037  1.0
```

```
150.0  4.0  0.037  1.0
100.0  3.5  0.037  1.0
100.0  2.5  0.027  1.0
150.0  2.5  0.027  1.0
200.0  3.0  0.027  1.0
8.0    2.0  0.027  1.0
200.0  3.0  0.027  1.0
200.0  3.0  0.027  1.0
5.0    2.0  0.027  1.0
200.0  3.0  0.027  1.0
25.0   1.5  0.037  1.0

62 61 60 60 59 59 58 58 57 -1  0 0 0 0 0 0 0 0 0 0 0 0 0 0 0 0 0 0 0 0 0 0 0 0 0 Link1
72 72 72 71 71 70 70 69 69 -1  0 0 0 0 0 0 0 0 0 0 0 0 0 0 0 0 0 0 0 0 0 0 0 0 0

78 77 77 76 75 74 73 72 71 70 69 68 67 67 66 65 64 63 62 -1 0 0 0 0 0 0 0 0 0 0 0 Link 2
74 74 73 73 73 73 73 73 73 73 73 73 73 72 72 72 72 72 72 -1 0 0 0 0 0 0 0 0 0 0 0
```

Etc. through Link 35

HASSYAMPA RIVER INPUT FILE - FEBRUARY CALIBRATION EVENT

```
273   173   200.0   4   0.          > M, N, NMAN, SDEP
30.   8000  7200    30              > DT, NITER, NITRN, NRPN
30    1.0   1.0                     > NPLT, ELCONV, CHANCHECK
248   2   0.0025   15000.   200.0   > JOUT, KOUT, SOUT, QMAX, WCHOUT
5.0   0.04   0.0025                 > DCHOUT, RMANOUT, SOVOUT
1  12                               > INDEXINF, NSOIL
89  33                              > NCHN, MAXCHN
1                                   > IRAIN
7  30                               > NRG, NREAD
252.0     5.0                       > XRG(L), YRG(L), for l = 1, NRG
187.0   146.0
146.0   166.0
106.0    72.0
41.0     65.0
50.0    143.0
161.0   170.0
0.015                               > PMAN(J), for J = 1, NMAN
0.085
0.06
0.04
2.78E-7    0.209    0.0927          > PINF(J,K) for K = 1, 3 and J = 1, NSOIL
1.67E-7    0.239    0.0963
```

```
4.17E-7   0.219   0.0990
2.78E-7   0.209   0.0927
4.00E-7   0.209   0.0927
9.44E-7   0.089   0.1302
4.00E-7   0.209   0.0927
4.00E-7   0.209   0.0927
4.00E-7   0.209   0.0927
3.03E-6   0.110   0.1236
9.44E-7   0.089   0.1302
4.00E-7   0.209   0.0927
1   1                          > INDEXDIS, NDIS
248  2                         > IQ(J,K) for K = 1, 2 and J = 1, NDIS
```

HASSYAMPA RIVER CHANNEL DATA FILE

```
 5.0   2.0  0.04  1.0          > Width (m), Depth (m), Manning n, Sinuosity
 7.5   2.5  0.04  1.0          > Same format for Links 1 through 89
 5.0   2.0  0.04  1.0
 7.5   2.5  0.04  1.0
10.0   3.0  0.04  1.0
40.0   3.5  0.04  1.0
.
.
.
Etc. through Link 89


 41  40  40  39  39  38  38  38  38  39  39  40  40  41  41  41  41  41  (Link 1)
 41  40  40  39  38  38  37  37  36  36  35  -1   0   0   0

145 145 144 144 143 143 142 141 140 140 139 139 138 138 137 136 135 134
133 133 132 132 132 131 131 130 130 129 129  -1   0   0   0

 35  35  34  34  34  33  33  32  32  32  31  31  31  30  30  30  29  29  (Link 2)
 29  28  28  28  27  27  26  26  26  26  26  -1   0   0   0

129 128 128 127 126 126 125 125 124 123 123 122 121 121 120 119 119 118
117 116 116 115 115 114 114 113 112 111 110  -1   0   0   0
.
.
.
Etc. through Link 89
```

SAMPLE PRECIPITATION FORECAST INPUT FILE

```
13.5  20.0          > RAINVELX, RAINVELY (X and Y velocities of storm, km/hr)
3814000             > NTH (north boundary of storm, m)
3750000             > STH (south boundary of storm, m)
394000              > EST (east boundary of storm, m)
362000              > WST (west boundary of storm, m)
15                  > INTRWS (number of rows of precipitation values)
8                   > INTCLS (number of columns of precipitation values)
                    > INTRWS * INTCLS precipitation values in uncalibrated mm/hr
0   0   0   0   0   0   0   0   0   0   0   0 307   0   0
0   0   0   0   0   0   0   0   0   0   0   0   0   0   0
0   0   0   0   0   0   0   0   0   0   0   0   0   0   0
0   0   0   0   0   0   0   0   0 4466   0   0   0   0   0
0   0   0   0 1122 409 409   0   0 2206   0 707   0 613 307
0   0   0 501   0 613   0 501   0 409   0   0   0   0   0
0   0   0   0   0   0   0   0 307   0   0   0   0 409 307
0   0 307 307   0   0   0   0   0   0   0   0   0   0   0
```